BRITISH GEOLOGICAL SURVEY
Natural Environment Research Council

Fluid Processes Series

Technical Report WE/94/7

Migration of repository gases in an overconsolidated clay

by S. T. Horseman and J. Harrington

Fluid Processes Group, British Geological Survey

This report describes work carried out within the 4th Framework of the Commission of European Communities Programme on Radioactive Waste Management and Storage (1990 - 94).

CEC Contract No. F12W-CT91-0076

Keyworth, Nottingham (UK)
Tel: (0602) 363100

PREFACE

This work has been performed within the 4th Framework (1990 - 94) of the Commission of European Communities (CEC) Programme on Radioactive Waste Management and Storage under Contract No. F12W-CT91-0076. The research described represents the BGS component of the MEGAS Project (Modelling and Experiments on Gas Migration in Repository Rocks). Partners in this project were SCK/CEN (Mol, Belgium), INTERA Ltd (Henley-on-Thames, UK) and ISMES Spa (Bergamo, Italy). The project was coordinated by Dr G. Volckaert of SCK/CEN. Co–funding was provided by the UK Office of Science and Technology through the BGS R&D Programme. Funding for a number of technical exchange visits was made available by the British Council within the framework of the ALLIANCE Project.

The authors wish to thank Miss Cécile Javelle (formerly of the Ecoles des Mines de Paris) for her excellent study of the microfabric and mineralogy of the clay, Dr Paul Hooker for positive help in a number of areas of the research, Drs Dave Noy and John Barker for assistance in the analysis of transient hydraulic data, Mr Marcus Sen for help in the processing of gas flow data and Mr Keith Bateman for assistance in the construction of the testing apparatus. Components were manufactured by BGS workshop staff under the able supervision of Mr Martin Shenton. Special thanks are also due to Mr Robert Marsden of Imperial College, London, for his enthusiastic support of our research efforts and to Dr Jöel Billiotte and staff and students of the Ecoles des Mines de Paris for the interesting discussions on matters of mutual scientific interest. Finally, the authors would like to mention the valuable exchange of ideas with project partners at a number of MEGAS progress meetings.

EXECUTIVE SUMMARY

Prompted by the problem of the migration of repository gases in a clay host-medium, our study has aimed to provide a conceptual model for the entry and movement of a gaseous phase in an initially water-saturated low permeability clay. The type-material for the experimental component of this study was Boom Clay, which is an overconsolidated Oligo-Miocene (Tertiary) clay from Belgium. Undisturbed samples were supplied by SCK/CEN from the Hades underground laboratory at Mol.

We start from the fundamental soil science concept of the total potential of the soil water. In clay soils, the total potential has three main components, the first gravitational, the second osmotic (due to the presence of solutes) and the third associated with the pressure difference between the reference state and the pore water. If we attempt to displace pore water by an equivalent volume of gas, then the amount of work performed in this operation must be *at least* equal to the sum of the work expended in (a) raising the pressure of the gas relative to an appropriate reference pressure, (b) moving the water from its initial location to its new location and (c) creating an interface between the two phases.

The quantitative treatment of this problem is far from trivial. The complications arise when we examine the way in which a compact clay carries the load of the overlying sediments. There is broad agreement that the total stress in a clay is borne partly by mineral-mineral contacts, partly by water pressure and partly by physico-chemical forces acting between the clay particles. The physico-chemical forces have at least two components, the first a repulsion between particles and the second an attraction. One popular model for the repulsion is based on the interpenetration, at small interparticle separations, of the Gouy-Chapman adsorbed double layers. The repulsive stress is calculated as the difference between the osmotic pressure of the cation-dominated midplane solution and the osmotic pressure of an external solution which is in equilibrium with the medium.

The important point is that the aqueous phase between clay minerals actually transmits a very significant part of the total stress acting on the clay medium. We have shown experimentally that up to 75% of the total stress in Boom Clay is transmitted through this aqueous phase. Since a gas phase can neither develop nor transmit the physico-chemical forces of repulsion and attraction acting across water-filled interparticle spaces, then it is unable to occupy these spaces until its pressure is sufficient to overcome these local forces. We have derived a theoretical relationship for this pressure and quantified it in our experiments.

If the gas pressure exceeds this critical pressure at any point in the clay-medium, then there will be a local imbalance in the forces acting in the system. We suggest that there is a tendency for the volume of gas to increase by pushing back the clay particles and displacing water from adjacent interparticle spaces. This observation provides the basis of our explanation of gas entry. In order for gas to enter the clay, its pressure must exceed the

"local pore pressure" by an amount equal to the maximum pressure drop across the gas-water meniscus at the mouth of the largest pathway. We assume that gas entry would normally occur when the radius of curvature of the meniscus is equal to the half-thickness of the critical flow pathway. If the pore size distribution of the medium is such that excessively high gas pressures are necessary to overcome capillarity, then the gas pressure will simply force the clay minerals apart. We call this process "pathway dilation" but note that there are close similarities with the processes of microcrack initiation and propagation. Gas will enter a dilated pathway at a pressure which is lower than we might anticipate from the pore sizes and "local pore water pressures".

Provided that the gas pressure continues to rise then it is possible for additional dilated pathways to form. These will propagate through the medium following routes which lead to a continuous lowering of the pressure (free energy) of gas near the tip of the pathway. There are a number of possible controls on the direction of propagation: (a) anisotropy of the clay fabric, (b) aniotropy of the stress field, (c) pore water pressure gradients, (d) stress gradients, (e) lithological variability, and (d) fissuring. It is premature to say which of these will have the dominant effect.

When the stress field in the clay is both uniform and isotropic, as it is in our experiments, then the gas will probably move along the bedding planes. Or test results show that the excess gas pressure for gas entry $(p_g - p_w)_e$ is lower parallel to bedding than it is normal to bedding and that the effective gas permeability of the clay is significantly higher with flow along the bedding planes. Ease of pathway dilation provides a probable explanation.

The propagation of a gas pathway ceases when it encounters a medium with large pores that can accommodate normal 2-phase flow. An important experimental finding is that the gas pathways are inherently unstable. If they lose pressure they collapse and gas flow ceases. In the laboratory this leads to intermittent "burst-type" flow. The periodicity of the "bursts" depends on system variables and the properties of the clay.

Our tentative scoping calculations suggest that a dilated gas pathway in Boom Clay under typical *in situ* stress might have an aperture of around 20 μm. We are confident that we can refine this initial estimate. These thin gas films are so unstable that that they collapse when subject to only minor reductions in gas pressure, flow rate or temperature.

Based on our overall assessment of gas migration in Boom Clay, we define three zones of behaviour on the basis of the principal mechanism of gas transport in each zone. We relate these zones to the curve of total soil suction against water saturation for the clay. In **Zone 1** the gas pressure is less than the sum of the excess gas entry pressure and the external equilibrium water pressure ($P_g < p_e + p_{w0}$) so the only gas transport mechanisms that can operate in the clay are associated with movement of gas molecules in solution. Fickian diffusion will be the dominant gas transport mechanism in this zone. **Zone 2** is only present in material with lower than average clay content. Gas flow commences when the threshold

for gas entry into pores is exceeded. Only then is gas migration by 2–phase flow physically possible and accompanied by a small degree of desaturation. Based on our calculations of capillary number, stable displacement of water seems highly improbable. Depending on clay content, flow probably ranges from being fairly dispersed to being concentrated in a relatively small number of pathways. The relative permeability to water k_{rw} will be little affected by the gas phase and will be close to unity. The relative permeability to gas k_{rg} will be very small. Pathway dilation at high gas pressures may cause a sudden increase in gas permeability and the flow behaviour will then assume the main characteristics of Zone 3. This sudden change may correspond with a drop in pressure. We note that all our experiments show a post-breakthrough fall in gas pressure. **Zone 3** commences when the gas pressure exceeds the pressure necessary to cause pathway dilatancy. In material with high clay content, Zone 2 is absent and pathway dilatancy is a necessary pre-requisite for gas entry. Flow in this zone will occur predominantly along a small number of discrete pathways. Instability of these pathways leads to the intermittent behaviour seen in our experiments. Relative permeability to gas will rise dramatically ($k_{rg} > 1$) with increasing gas pressure as the aperture of the flow paths increase. We have quantified a relationship between gas permeability and net mean stress ($\sigma - p_g$).

It is physically impossible for the gas pressure to exceed the total stress σ. If gas pressures ever did approach this level, then the effective gas permeability of the medium would be enormous and flow would probably be focused in gas-induced macroscopic fractures. Since significantly large flows can be accommodated at much lower pressures, it is highly unlikely that this situation could ever arise.

Our experiments on hydraulic flow in Boom Clay were intended to provide intrinsic permeability data for the interpretation of gas flow. We have reached a number of interesting conclusions which have broad relevance to the modelling of transport processes in clays.

The key to a full understanding of water flow in clays lies in the complex interactions between the clay particles, water and solutes. If we consider the equilibrium state in a compact clay then we consider not only the equilibrium of the aqueous phase and its dissolved solutes but also the equilibrium of forces associated with the stress field. Based on our simple treatment of this problem, we conclude that the pore water pressure at any fixed height varies continuously from point to point within the clay medium and is the sum of a "hydrostatic term" p_w and an "osmotic term" Π. It is not actually necessary to invoke osmosis as the cause of this phenomenon. A more general explanation would be that the additional pressure Π arises because water molecules are drawn into interparticle spaces because of a lowering of the chemical potential of water in these regions.

In common with a number of other researchers, we believe that it is not possible to separate the p_w and Π terms when we consider the local water pressure in a compact clay. Furthermore, we must be very careful how we measure local water pressure. There is an

accumulating volume of evidence to suggest that hydraulic measurements in compact clays are sensitive to the chemistry of the test fluid.

Our experimental data exhibit a significant degree of nonlinearity between flow rate and hydraulic gradient. Departures from Darcy's law, in the form of nonlinearities and thresholds, have commonly been reported and have been attributed to a wide variety of possible causes. The nonlinearities seen in our tests can be largely explained in terms of the very pronounced sensitivity of hydraulic conductivity to effective stress. We are confident that this sensitivity is due, not to the minor changes in void ratio or porosity which are occasioned by changes in effective stress, but to changes in the fundamental forces acting on water molecules in the interparticle spaces.

We have quantified the relationships between hydraulic conductivity and effective stress for flow normal and parallel to bedding. Like gas permeability, hydraulic conductivity parallel to bedding is significantly larger than it is normal to bedding. If the results are extrapolated to *in situ* stress conditions, we find that out predicted "small-scale" hydraulic conductivity values are, in each case, substantially lower than the commonly reported values for Boom Clay. By the analysis of transient flow data we have also obtained reasonable values for the specific storage of Boom Clay. This parameter also varies with effective stress and we have quantified this relationship.

The stress-dependency of the hydraulic parameters has important consequences in field testing. If the testing procedure results in large excess water pressures being applied to a test section, then the effective stress in the clay will locally decrease and the measured hydraulic conductivity will be significantly larger than the true *in situ* value. In this context, we also draw attention to our comments regarding the chemistry of the test fluid since these are also pertinent to the specification of testing procedures. These considerations are likely to be most important when testing highly compacted clays, but may be far less of a problem when testing superficial deposits.

In mathematical modelling, it is a relatively simple matter to represent the functional dependency of hydraulic conductivity, intrinsic permeability and specific storage on effective stress, if the need arises.

KEYWORDS:

GAS MIGRATION, CLAY, MUDROCK, GAS PERMEABILITY, BREAKTHROUGH PRESSURE, BOOM CLAY, HYDRAULIC CONDUCTIVITY, SPECIFIC STORAGE, EFFECTIVE STRESS, SOIL SUCTION, OVERCONSOLIDATED, REPOSITORY

CONTENTS

LIST OF TABLES

LIST OF FIGURES

LIST OF PLATES

4. View of a microfissure (F) in Boom Clay. Uncoated material, not subjected to drying, examined using ESEM at a pressure of 6.6 torr. Aperture a = 30 μm.

5. View of the same microfissure at a pressure of 14 torr. Uncoated material, not subjected to drying, examined using ESEM. Aperture a = 25 μm.

6. View of the same microfissure at a pressure of 3.7 torr. Uncoated material, not subjected to drying, examined using ESEM. Aperture a = 33 μm.

1. INTRODUCTION

A range of gases will be produced in a radioactive waste repository after sealing and closure. Possible mechanisms of gas generation include the corrosion of metals, the chemical and microbial degradation of organic and inorganic materials, the radiolysis of water, the radioactive decay of the wastes and, if near-field temperatures are high enough, the production of a steam phase (Voinis et al., 1992; Agg et al., 1992). These gases are a matter of concern for a number of reasons: (a) the pressurisation of waste containers, (b) the effects of gas on the thermal and mass transport properties of repository backfilling, buffering and sealing materials, (c) the effects of gas migration on groundwater flow and host-rock properties and (d) the possible release of active gases to the surface environment.

In a repository for the disposal of high and intermediate level wastes, containing only a small amount of organic materials, the main gas production mechanism will probably be the anoxic corrosion of metals. Metals may be present as constituents of the waste, container materials, overpacks, gallery linings and other items of repository hardware. The anoxic corrosion of metals, and of ferrous metals in particular, represents a major potential source of hydrogen (Rees, 1989). The main chemical reactions are:

$$3\,Fe + 4\,H_2O \rightarrow Fe_3O_4 + 4\,H_2$$

$$Fe + 2\,H_2O \rightarrow Fe(OH)_2 + H_2$$

These reactions are specific to anoxic conditions, but do not occur simultaneously. Corrosion may be general or localised and will proceed at rates which depend on the nature of the ferrous metal, the availability of water, the chemical environment and on temperature. The rate of hydrogen production (moles per year) is directly proportional to the corrosion rate and the total surface area of metal subject to corrosion. Where groundwater flow-rates are very low, the availability of water may be a rate-limiting factor. If a gas phase develops in the near-field of a repository then it might temporarily affect the supply of water to support corrosion reactions, leading to some form of cyclical behaviour.

In an ideal situation, the gas generated in the near-field of a repository would dissolve in the groundwater to be transported away from the repository by the mechanisms of advection, diffusion and dispersion. Far-field chemical and, possibly, biological attenuation would then render the flux innocuous. There is an irony in the fact that the sought-after characteristic of the clay host-medium of very low permeability becomes somewhat problematic when one considers gas migration. Under normal circumstances, advection in a compact clay is likely to be a very slow process and Fickian diffusion is likely to be the main transport mechanism of gas in solution. Stenhouse and Grogan (1992) examined hydrogen attenuation in geological media and were unable to identify any mechanism capable of significantly depleting a significantly large flux of this gas.

Calculations of the probable maximum diffusive flux of gas in solution in a typical host-rock suggest that Fickian diffusion may be too slow a mechanism to accommodate the rate of gas production in the near-field of a repository (Lever and Rees, 1987). This conclusion is, of course, highly dependent on specific details of the waste inventory, the repository design and the host-rock. Nevertheless, there is a strong possibility that a gas phase will form within the void-space of a clay repository. If this is indeed the case, then some rise in near-field gas pressure is inevitable.

Our experimental study has focused on the criterion for the entry of a gas phase into an initially water-saturated clay, on the mechanisms of gas flow and on the relationship between the gas flux, the pressure gradient and other variables. Our type-material for the laboratory experiments is Boom Clay from Belgium. This overconsolidated clay is under investigation as a possible host-rock for the disposal of high and intermediate level wastes. An underground laboratory has been constructed at the SCK-CEN facility at Mol as part of the "Hades Project" to allow *in situ* experiments to be performed on the clay and to assist in the development of the disposal technology (Neerdael and Manfroy, 1985; Bonne et al, 1992).

The Boom Clay is the youngest argillaceous unit in a sequence of marine clays and sands deposited during the Middle Oligocene (Tertiary). The clay is present in the N.E. of Belgium, outcropping in the south of the area and dipping gently N.N.W. under a cover of Miocene and Pliocene sandy deposits. In the vicinity of Mol, the top of the clay lies at about 160 m below surface and the total thickness of the unit is around 110 m. With a typical plastic limit in the range 19 - 33% and water content 20 - 26%, the clay is reasonably plastic in its response to deformation. One-dimensional consolidation tests on material from a depth of 247 m suggests an overconsolidation ratio (OCR) of about 2.4. The undrained shear strength is around 1.1 MPa (Horseman et al., 1993). When seen at surface exposures, the clay has been described as a "stiff, fissured, layered and preconsolidated clay" (de Beer, 1967; Vanderberghe and van Echelpoel, 1987). As is the case for most overconsolidated clays, the fissuring may be a consequence of the stress-relief accompanying erosion or of minor tectonic deformation, with near-surface weathering mechanisms possibly playing a role. The intensity of fissuring would appear to decrease significantly with depth. At typical repository depths the fissures are probably "incipient features" of the material, with little or no aperture, which only become apparent to the naked eye when the clay is sheared, de-stressed or dessicated.

2 BASIC THEORY AND CONCEPTS

2.1 Scientific background to the problem

One of the difficulties in the quantitative treatment of gas migration in a clay host-rock is the very diverse range of approaches to this problem. The mathematical theories of multiphase flow in porous media (Bear, 1972; Aziz and Settari, 1979) are based on a semi-empirical generalisation of Darcy's Law and stem largely from oil industry interest in the movement

of gaseous and liquid hydrocarbons in geological media. These theories are widely applied to the problems and rock-types of concern to that industry. The studies of capillarity and gas flow in low permeability rocks by Thomas et al. (1968) are very pertinent, as are the observations on departures from Darcy's law at high flow-rates due to inertia (Hubbert, 1956) and turbulence (e.g. Cornell and Katz, 1953). More recent work on unstable displacement during 2-phase flow is also of considerable interest (Homsy, 1987; Lenormand et al., 1988). Many oil industry concepts have been adopted by hydrogeologists in examining unsaturated systems (Stallman, 1964) and the movement of immiscible liquid phase pollutants. Soil mechanics, as a discipline, has focused primarily on the engineering properties and responses of near-surface unconsolidated deposits, and has provided the concept of effective stress (Terzaghi, 1943) and a valuable theoretical framework for the analysis of hydrodynamic phenomena in saturated clay soils, including consolidation, swelling and seepage. A paper by Lambe (1960) provides an interesting re-examination of effective stress in saturated clay which acknowledges the physico-chemical interactions between clay particles. A number of definitions for the effective stress in unsaturated soils have been proposed by Croney et al. (1958), Bishop (1959), Richards (1966) and Aitchison (1973), amongst others. Studies of the movement of water and air in near-surface, unsaturated soils have been largely the province of the soil physicists and agronomists. The very early work of Buckingham (1907), Richards (1928) and Schofield (1935) on the capillary potential of soils laid the foundations for these studies. Some of the landmarks were Edlefsen and Anderson (1943) on the thermodynamics of soil moisture, Richards (1949) on the measurement of soil suction, Childs and Collis-George (1950) and Corey (1957) on permeability and Bolt and Miller (1955) on the total and component potentials of soil water. The very active research over the years on the nature of the clay-water interface (eg: Low, 1962; 1989; van Olphen, 1975; 1977) and the properties of adsorbed water (eg: Martin, 1962; Graham, 1964; Low, 1979; Sun et al, 1986; Skipper et al., 1991) is also very significant to the problem. There is currently an upsurge in interest in unsaturated soils, which is prompting an integration of concepts stemming from soil mechanics, soil physics and porous media theory and the emergence of "unsaturated soil mechanics" as a distinct sub-discipline (e.g. Fredlund and Rahardjo, 1993). The continuum mechanics concept of the "stress state variable" (Matyas and Radhakrishna, 1968; Fredlund and Morgenstern, 1977) is a cornerstone of modern theories of this branch of soil mechanics. Recent research papers on this topic are Alonso et al. (1990) and Gens and Alonso (1992). We must also note the work on gas transport in discontinuous geological media (e.g. Schrauf and Evans, 1986), since some of the findings in this area are pertinent to the problem of gas migration in initially water-saturated, overconsolidated and, possibly fissured, clays.

Studies which have addressed the migration of repository gases in clay include the experimental work of Lineham (1989) on natural clay samples and Pusch et al. (1985) on MX-80 bentonite buffer material. Pusch et al. (1987) examined models for the movement of water and gas in smectite clay. The overview of mechanisms and modelling of gas migration in repository rocks by Rodwell and Nash (1991) is also of interest, as are the literature reviews of Tomlinson (1988), Worgan et al. (1989) and Jones (1991).

Based on our appraisal of the published literature, it is our basic contention that compact clays do not behave as classic porous media and that excessive reliance on standard porous media theory, developed for other rock-types, is inadvisable. Distinguishing features of compact clays include the complex interaction between the mineral phase, water and solutes (Low, 1961; van Olphen; 1977), the sub-microscopic dimensions of the pore channels, the highly deformable matrix (Wroth, 1971) and the very low tensile strength. We regard these characteristics as being of paramount importance to the problem of gas transport in compact clays. We have therefore elected to follow an approach which is very specific to clays and is firmly grounded in the basic principles of soil physics and soil mechanics. We start by examining soil water potentials.

2.2 Total and component potentials of water in a clay soil

The International Committee on Soil Science (Bolt, 1976) define the total potential ψ_t of the constituent water at a point in a soil at temperature T_0 as the amount of useful work per unit mass of soil water in $J.kg^{-1}$ that must be done by externally applied forces to transfer reversibly and isothermally an infinitesimal amount of water from the standard state to the soil liquid phase at the point under consideration. The total potential is, in essence, the "free energy" per unit mass. The standard state comprises a pool of pure, free water at temperature T_0, height h_0 and atmospheric pressure p_0. The total potential may be then be written as the sum of a number of component potentials:

$$\psi_t = \psi_g + \psi_o + \psi_p \qquad (1)$$

where ψ_g is the gravitational (elevation) potential, ψ_o is the osmotic potential and ψ_p is the pressure potential. As Bolt (1976) shows, the total potential ψ_t at a height h_x in the soil is then given by

$$\psi_t = g\,\Delta h - \int_0^{\Pi} v_w\,dp + \int_0^{p} v_w\,dp \qquad (2)$$

where g is the acceleration due to gravity, $\Delta h = h_x - h_0$, v_w is the partial specific volume ($m^3.kg^{-1}$) of the constituent water in the soil solution, and Π is osmotic pressure of the soil solution (referenced to pure water). The limits of integration are as per the original paper. The precise meaning of pressure p requires careful consideration of the equilibrium condition. Bolt (1976) defined the pressure potential as the amount of useful work per unit mass of pure water that must be done to transfer reversibly and isothermally an infinitesimal quantity of aqueous solution from pool, having the same osmotic pressure Π and height h_x as the soil solution, but at temperature T_0 and pressure p_0. We shall denote the total potential of the constituent water in this pool by ψ_{te}. If the point under consideration in the soil is at reference height h_0, then $\Delta h = 0$. If we assume water to be incompressible, after integration, we obtain

$$\psi_t = v_w(p - \Pi) \qquad (3)$$

for the total potential of the constituent water in the soil solution and

$$\psi_{te} = v_w(p_0 - \Pi) \qquad (4)$$

for the pool. If we connect the point in the soil to the pool by a very small horizontal tube, then there will be a flow of water in the tube. An equilibrium condition can be obtained if we alter the pressure in the pool so that it is precisely equal to p. Thus p may be regarded as the pressure recorded by a perfect pressure measuring instrument, having negligible size and compliance (e.g. a tiny piezometer or tensiometer), installed at the specific point of interest in the soil, and containing a solution which has precisely the same osmotic pressure Π as the soil solution at the point of measurement. We note that there is some debate as to whether a instrument filled with pure water would register p or p - Π, in the absence of any obvious osmotic membrane. Fredlund and Rahardjo (1993) state that the osmotic component of soil suction is not measured by tensiometers since soluble salts are free to move through the porous cup. However, in very compact clays and clay-shales, there is clear evidence that pressure measurements using fresh water in packered-off test sections are influenced by the osmotic term (Horseman et al., 1991). One possibility is that the compact clay acts as its own osmotic membrane between the water in the instrument and the pore solution (Fritz, 1986). Alternatively, the osmotic term may be intimately linked to the swelling response of these compact clays (Chenevert, 1969; Horseman et al., 1991; Hale et al, 1993).

The definitions of the component potentials of the soil water outlined above are equally valid for saturated and unsaturated clays. Since Equation (1) makes no explicit reference to a gaseous phase, it is analytically convenient to split ψ_p into at least two subcomponents, the pneumatic potential ψ_a (associated with the gas pressure) and the matric potential ψ_m, where $\psi_p = \psi_a + \psi_m$. For soils with a rigid matrix, the two additional terms have a clear physical meaning (Bolt, 1976). However, for swelling clays, capable of substantial volume changes, the definition of these terms is substantially more complex and demands a clear understanding of the relationship between the total stress σ acting on a clay and the component potentials of the pore water.

2.3 Osmotic pressure

The osmotic pressure Π of a aqueous solution is the excess pressure that must be applied to the solution to prevent the osmotic movement of water molecules through an ideal semi-permeable membrane separating the solution from a reservoir of pure water. From basic physical chemistry (Atkins, 1986), the osmotic pressure is given by

$$\Pi = - \frac{RT}{v_w \omega_w} \log_e (a_w) \qquad (5)$$

where R is the gas constant, T is the absolute temperature, and v_m, ω_w and a_w are the partial specific volume, molecular mass (18 kg per kmol), and activity, respectively, of the constituent water in the solution. If the partial vapour pressure of the water in a solution is

p_{vw} and the vapour pressure of pure water, at the same temperature and pressure, is p_{vp}, then $a_w = p_{vw}/p_{vp}$. Based on the Gibbs-Duhem equation, the activity of the constituent water in a solution can be related to that of the solute by

$$55.5\ d(\log_e a_w) + m_s\ d(\log_e a_s) = 0 \qquad (6)$$

where m_s is the molality of the solute (mol.m^{-3}). This gives

$$\log_e a_w = -\frac{1}{55.5}\int_0^{m_s} m_s\, d(\log_e a_s) \qquad (7)$$

Substituting in Equation (5)

$$\Pi = \frac{RT}{55.5}\int_0^{m_s} m_s\, d(\log_e a_s) \qquad (8)$$

In dilute solution $a_s \approx m_s$ and $55.5\ v_w\ \omega_w \approx 1$ which gives the van der Waals relationship

$$\Pi = m_s RT \qquad (9)$$

In dilute electrolyte solutions, m_s can be replaced by $\Sigma\ m_i$ where the summation is over all the ions present.

2.4 Forces between clay particles

In a compacted clay, the clay mineral particles are forced into such close proximity that the adsorbed double layers associated with each particle interact producing a net force of repulsion between the mineral constituents of the material. There is no general consensus on the precise mechanism by which this force develops. In one model, this repulsion per unit area of the clay is equated with the osmotic pressure Π_m of the pore solution midway between two interacting clay particles less the osmotic pressure Π_e of the "external solution" (Langmuir, 1936; van Olphen, 1977). Alternatively, this repulsion is explained in terms of force associated with the hydration of the clay mineral surfaces or of cations in the interparticle space (Low, 1987). Whichever is correct, the repulsion between clay particles can be viewed simply in terms of water molecules being attracted into the interparticle space by the lowered chemical potential in this region, where they tend to force the particles apart. This net repulsion between particles is manifested in the swelling of clays and in the development of swelling pressures when volume changes are constrained.

In colloid science, it is widely recognised that an attractive force also acts between narrow, water-filled, interparticle spaces (see, for example, Hunter, 1991). This attraction probably arises from London – van der Waals' dispersion forces (Kallmann and Willstätter, 1932) and the forces associated with hydrogen bonding. These are the source of the cohesion between molecules in liquid water. By analogy with the theory of non-ideal gases, the pressure of a liquid may be separated into two parts, the first associated with the kinetic activity of the molecules and the second (negative) with the net attraction between the

molecules. The thermodynamic equation of state may be written in the form

$$P = T\left(\frac{\partial P}{\partial T}\right)_V - \left(\frac{\partial E}{\partial V}\right)_T \qquad (10)$$

The first term on the right is the "kinetic pressure" of the liquid and the second term is the "internal pressure" due to molecular attraction. At 25°C and atmospheric pressure, the internal pressure of water has been estimated to be around 2 GPa. Since the liquid phase in a compact clay resides in very narrow interparticle films, typically 80 - 800 molecular diameters across, molecules in the film are continually colliding with the solid surface. Some of the kinetic energy of the water is transferred to the mineral particle. This causes localised cooling of the water film and a spontaneous decrease in entropy in the affected region. The thermodynamics of the problem are highly complex and imperfectly understood. However, the net effect is that the water molecules of the film act "in concert" to produce a long-range attractive force between the mineral particles. Qualitatively, at least, any factor which influences the "kinetic pressure" of the thin film would also affect the magnitude of this interparticle attraction.

It is not totally clear whether we should treat the net interactive force per unit area between clay particles as a scalar (i.e. a pressure) or a tensor quantity (i.e. a stress). There are good reasons to believe that water in thin films has properties which are very different to those of "free water" (see Low, 1986). It is not unreasonable to assume that adsorbed water can sustain significant shear stresses. This would have important consequences if we were to digress from our main areas of concern and examine the shear strength of clay. For the time-being, we will simplify the problem by assuming that the total stress σ acting on a clay is isotropic (no shear components). We will refer to the repulsive force per unit cross-sectional area as R and the attractive force acting on the same area as $-A$. We will assume that these two quantities are actually stresses (tensor quantities), but we will equate them with scalar pressure-type quantities when it is convenient to do so. In mathematical terms, we are actually equating the trace of the tensor with the scalar quantity.

2.5 Effective stress in a compact clay

The repulsive stress R and the attractive stress $-A$ may be regarded as a components of the total stress σ acting on the clay. Lambe (1960), in an important early paper on this topic, proposed the following relationship

$$\sigma = \sigma_i + R - A + p_{w0} \qquad (11)$$

where σ_i is the so-called "interparticle stress" and p_{w0} is the pressure registered by our perfect measuring instrument, filled with pure water and at equilibrium with the soil water. Conventional effective stress σ_{eff} (Terzaghi, 1943; Terzaghi and Peck, 1967) for a saturated soil is defined as the difference between the total stress and the measurable pore pressure. Since pure (or fresh) water is almost invariably used in laboratory and field pore pressure measurements, we can write the relationship

molecules. The thermodynamic equation of state may be written in the form

$$P = T\left(\frac{\partial P}{\partial T}\right)_V - \left(\frac{\partial E}{\partial V}\right)_T \qquad (10)$$

The first term on the right is the "kinetic pressure" of the liquid and the second term is the "internal pressure" due to molecular attraction. At 25°C and atmospheric pressure, the internal pressure of water has been estimated to be around 2 GPa. Since the liquid phase in a compact clay resides in very narrow interparticle films, typically 80 - 800 molecular diameters across, molecules in the film are continually colliding with the solid surface. Some of the kinetic energy of the water is transferred to the mineral particle. This causes localised cooling of the water film and a spontaneous decrease in entropy in the affected region. The thermodynamics of the problem are highly complex and imperfectly understood. However, the net effect is that the water molecules of the film act "in concert" to produce a long-range attractive force between the mineral particles. Qualitatively, at least, any factor which influences the "kinetic pressure" of the thin film would also affect the magnitude of this interparticle attraction.

It is not totally clear whether we should treat the net interactive force per unit area between clay particles as a scalar (i.e. a pressure) or a tensor quantity (i.e. a stress). There are good reasons to believe that water in thin films has properties which are very different to those of "free water" (see Low, 1986). It is not unreasonable to assume that adsorbed water can sustain significant shear stresses. This would have important consequences if we were to digress from our main areas of concern and examine the shear strength of clay. For the time-being, we will simplify the problem by assuming that the total stress σ acting on a clay is isotropic (no shear components). We will refer to the repulsive force per unit cross-sectional area as R and the attractive force acting on the same area as $-A$. We will assume that these two quantities are actually stresses (tensor quantities), but we will equate them with scalar pressure-type quantities when it is convenient to do so. In mathematical terms, we are actually equating the trace of the tensor with the scalar quantity.

2.5 Effective stress in a compact clay

The repulsive stress R and the attractive stress $-A$ may be regarded as a components of the total stress σ acting on the clay. Lambe (1960), in an important early paper on this topic, proposed the following relationship

$$\sigma = \sigma_i + R - A + p_{w0} \qquad (11)$$

where σ_i is the so-called "interparticle stress" and p_{w0} is the pressure registered by our perfect measuring instrument, filled with pure water and at equilibrium with the soil water. Conventional effective stress σ_{eff} (Terzaghi, 1943; Terzaghi and Peck, 1967) for a saturated soil is defined as the difference between the total stress and the measurable pore pressure. Since pure (or fresh) water is almost invariably used in laboratory and field pore pressure measurements, we can write the relationship

$$\sigma_{eff} = \sigma - p_{w0} = \sigma_i + R - A \qquad (12)$$

If the soil behaved as a "perfect colloid", then the interparticle stress σ_i would be zero and the effective stress would be simply $R - A$..

Guided by Langmuir (1936), we will assume that the net repulsive stress R_m at the midplane can be directly equated with difference between the osmotic pressure Π_m at the midplane and the osmotic pressure Π_e of the external solution. Since Equation (10) was referenced to pure water, $\Pi_e = 0$ so we can use Equation (5) to write

$$R_m = \Pi_m = - \frac{RT}{v_w \omega_w} \log_e \left(\frac{p_{vw}}{p_{vp}} \right) \qquad (13)$$

where p_{vw} is the partial vapour pressure of constituent water in a pool of free solution having the same solute chemistry as the midplane solution and p_{vw} is the vapour pressure of pure free water at the reference temperature T_0. We note that it may be possible to treat the attractive stress $-A$ in a similar manner, considering its effect on partial vapour pressure, although the thermodynamic rationale for doing so remains obscure at the present time.

Using diffuse double layer theory, R_m can be also be estimated from basic properties of the clay-water-solute system (Verwey and Overbeek, 1948; van Olphen, 1977). Experiments and theory indicate that R decreases roughly exponentially with increasing particle half-spacing and is a function of the exchangeable cation species and valence, the electrical charge of the clay surface, the solution properties and temperature.

Equation (10) may be viewed as a simple implementation of DLVO theory (see Hunter, 1986) to an imperfect colloidal system exhibiting mineral-mineral contact. In highly compacted clays (clayshales and shales) with small interparticle spacings, an extra term S might be added to the right hand side of Equation (11) to represent the repulsive stress associated with "solute structure".

2.6 Spatial variability of the component soil water potentials

The concentration of solutes in the pore water of a clay soil is far from uniform, as we might surmise from the above discussion. With its negative charge, the clay mineral surface attracts cations. A large number are held close to the surface in the Stern layer and many more reside in the diffuse layer. The concentration of cations falls away roughly exponentially with distance beyond the Stern layer (van Olphen, 1977). In the larger pores, the electrostatic forces stemming from mineral surfaces will have minimum intensity and the soil solution in these pore will contain both cations and anions, in proportions which are commensurate with an approximate local charge balance.

It is apparent that both activity of the constituent water of the soil solution and the osmotic pressure Π of the solution must vary considerably from one point to another. The activity

of the water must be very low (<1) close to the clay surface and the corresponding osmotic pressure must be very high. Osmotic pressure will exhibit local minima at points that are midway between surfaces (i.e. points on the midplanes discussed above).

If we assume that the constituent water of the soil solution is in equilibrium with and external solution of total potential ψ_{te}, then the total potential of the soil water at the midplane ψ_{tm} must equal to ψ_{te}. provide the points under consideration are at the same height. Using Equation (1) we can write

$$\psi_{om} + \psi_{pm} = \psi_{oe} + \psi_{pe} = ... \quad (14)$$

which suggests that the sum of the osmotic potential ψ_o and the pressure potential ψ_p is constant for all points at the same elevation. This suggests that it is not possible to separate these two component potentials in a clay system. Mitchell (1976), in his examination of the equilibrium state of soil water, also reached this conclusion. Using Equation (2) we can rewrite this as

$$p_m - \Pi_m = p_{we} - \Pi_e = ... \quad (15)$$

where p_m and Π_m are the hydrostatic and osmotic pressures of soil water at the midplane and p_{we} and Π_e are the equivalent pressures of the external solution.

The actual pore water pressure p_w may vary continuously throughout the clay soil, with high values close to clay surfaces and low values at the centre of large pores. The quantity $p_w - \Pi$ should be constant for all points at the same height. Ravina and Zaslavsky (1972) estimated the water pressure within the double layer of an isolated montmorillonite particle to be around 10 MPa at a distance of 1.3 nm from the surface. Since the particles in a saturated clay soil are totally enclosed by adsorbed water, most of the forces generated by these high pressures are locally balanced. As we noted above, only the midplane pressures contribute to the force balance with the applied stress.

2.7 Midplane relationships

The midplanes between clay particles are significant regions, since gas entering the clay will tend to follow the routes of least resistance. Water in the midplane regions is least affected by the presence of the clay surface and there seems little doubt that the gas will move through these regions preferentially. Using Equations (13) and (15), we can express Equation (11) in terms of the midplane pore pressure p_m

$$\sigma = \sigma_i + p_m - A_m \quad (16)$$

where p_m is given by

$$p_m = p_{we} + \Pi_m - \Pi_e \quad (17)$$

Recapping, the terms p_{we} and Π_e are the hydrostatic pressure and osmotic pressure of an external solution in equilibrium with the clay. In the field situation, this external solution might be interpreted as the pore fluid of an interbedded sandy horizon or lens within the clay. Since the sand will have very large pores, its pore pressure and water chemistry are easily defined. In the laboratory, p_{we} and Π_e relate to the fluid used to back-pressure a test sample during consolidation. Ideally, the fluid used in laboratory testing should have a chemistry exactly matched to that of the sand horizon.

We note that it can be argued that the midplane water pressure is influenced by the attractive stress $-A_m$. From our discussions on the origins of this fundamental attraction between particles, we feel that A must be a subcomponent of the local water pressure related to the right hand term of Equation (10). If we include it in Equation (17), then we may actually be "double accounting". Our uncertainty in this matter emphasises the requirement for a thorough thermodynamic analysis of the attraction term.

2.8 Local variability of stress

Equation (11) gives the relationship between the total stress σ and it components for a volume of clay which is sufficiently large that the local forces acting across any prescribed cross-section can be averaged to give meaningful continuum parameters. Although we know that the total force acting across this section, divided by the area of the section, must be equal to the total stress, Equation (11) tells us nothing about the local variability of either the forces or the stress components. Average stress is probably only really meaningful if we think in terms of a square cross-section with sides at least 10 times the maximum grain size ($\approx$ 2 mm for Boom Clay). Since we are concerned with the pressures acting in channels which are perhaps 200 nm across, the use of average stress in any calculation will always be associated with considerable uncertainty.

During the compaction process, the clay will assume some form of "packing arrangement" which will be a very complex function of particle size distribution, the balance of forces between particles, the chemical environment and many other factors. At higher compaction levels, the platy clay minerals become reasonably aligned with the plane normal to the major principal stress. With a broad distribution of particle sizes, there is often a tendency for larger particles to arch over smaller particles, sheltering the smaller ones from some of the applied stress. Many compact clays also exhibit "fabric domains" (Moon, 1972) which are local assemblages of clay-particles of a similar mineralogical composition, orientation and size. It is possible that the stress carried by these domains differs somewhat from the average total stress σ.

2.9 Significance of interparticle stress

The quantity σ_i in Equation (11) is usually referred to as the interparticle stress. In simple terms it represents the fraction of the total stress σ which is carried by mineral-mineral contacts in the medium. In a granular soil this is easy to visualise. However, as observed

by Lambe (1960), the precise meaning of the σ_i term in a clay-rich medium is somewhat obscure. Clay particles are usually encapsulated in very strongly adsorbed water. As we already noted, the faces of these particles generally carry a large negative charge. These two facts may preclude face-to-face contact in anything but the most compact of materials. However, the ragged ends of these particles may carry a positive charge, which could allow particles to touch in an edge-to-face configuration. The introduction of natural cements (e.g. carbonates) may also give rise to mineral-mineral contacts. The total area of mineral-mineral contacts across any representative section may be less than 1% of the section area in a typical plastic clay (Rosenqvist, 1959).

There is very good reason to believe that, like the other components of total stress, the interparticle stress σ_i probably varies throughout the clay. In a fabric domain comprising small particles of hydrated smectite, we might anticipate the "local average" value of σ_i to be very small, given the very strong physico-chemical repulsion between smectite clay layers. In other parts of the clay, where illite might be a dominant clay mineral, we would expect σ_i to be significantly larger. The homogeneous gel networks filling the intergranular space of compacted Na bentonites (Pusch and Hökmark, 1990) are interesting in this context. Similar gel-like hydrated clays were observed in the environmental scanning electron microscope (ESEM) studies of the Boom Clay (see Appendix 1).

Local variability of the stress components and the associated forces suggests that we should be cautious in the application of Equations (10), (15) and (16) to very localised phenomena, such as the initial entry of a gaseous phase into an initially water-saturated clay. The above discussion suggests that the "local average values" of total stress σ and interparticle stress σ_i may be somewhat lower at the point of gas entry than the average "continuum values" of these parameters.

2.10 Interfacial tension and the Young-Laplace equation

The Young-Laplace equation forms the basis of most calculations of capillary effects in unsaturated porous media (Dullien, 1979). It states that the difference in pressure between a gas and a liquid, separated by a hemispherical meniscus, is

$$p_g - p_w = \frac{2\,\tau_{gw}}{a} \qquad (18)$$

where τ_{gw} is the interfacial tension ($N.m^{-1}$) between the two phases and a is the radius of curvature of the meniscus. If gas and water are at one point in contact with the flat surface of a solid, then equilibrium is only possible if the interface between the gas and water forms a definite angle with the solid. This angle is known as the contact angle θ and is given by

$$\cos\theta = \frac{\tau_{sg} - \tau_{sw}}{\tau_{wg}} \qquad (19)$$

where τ_{sg} and τ_{sw} are the interfacial tensions between solid and gas and solid and water, respectively. If $\tau_{sg} - \tau_{sw} > \tau_{wg}$ then no equilibrium is possible and the water spreads out over the surface of the solid. The high affinity of clay minerals for water suggests that clay surfaces are always naturally wet and that gas-mineral contact is impossible under normal circumstances. A film of adsorbed water will therefore always exist between the gas and the clay mineral. We note that the thickness of these residual films is of great importance.

Given that water totally wets the solid phase, the Young-Laplace equation is frequently used to evaluate the entry condition for the penetration of gas into narrow, water-filled capillary pathways in a porous medium. In clays, which have been sufficiently compacted for the double layers to interpenetrate, we run into a number of major difficulties in applying this relationship: (1) pressure p_w is not a simple pore pressure term as is apparent from our discussions; (2) p_w is not constant over the cross-section of a capillary pathway, since only $(p_w - \Pi)$ may remain constant as we approach the clay surface; (3) the gas-water meniscus is probably not hemispherical and may be very distorted in a narrow capillary; and (4) it is very uncertain whether the interfacial tension τ_{wg} remains constant across the pathway cross-section. To reinforce the third of these points, we note that Bolt and Miller (1958) make the comment "Where the influence of the double layer is felt at a curved interface, the classic condition of constancy of the mean film curvature no longer applies".

The development of a more realistic relationship between the gas and water pressures in a small capillary pathway is mathematically complex and is certainly beyond the scope of the present work. For the time-being we must recognise the deficiencies of the Young-Laplace equation when applied to compact clay systems and be aware of the implicit errors in its use to calculate pore size distributions from immiscible phase (mercury) intrusion data or to estimate gas entry pressures from pore size data.

2.11 Preliminary criterion for gas entry

Ignoring the complications discussed above, we assume that gas will enter the clay when its pressure is sufficient to overcome the sum of the capillary pressure drop at the entrance of the flow path and the midplane pore water pressure. By inserting Equation (17) into Equation (18) we obtain the following preliminary criterion for the entry of gas at pressure p_g into an initially water-saturated, compact clay:

$$p_g \geq \left[\frac{2\,\tau_{gw}}{a_p} + \Pi_m + p_{we} - \Pi_e\right] \qquad (20)$$

where a_p is the half-thickness of the newly-formed gas pathway, τ_{gw} is the interfacial tension between gas and water, $\Pi_m = R_m$ and p_{we} and Π_e are the hydrostatic pressure and osmotic pressure, respectively, of the external aqueous solution in equilibrium with the clay. Our specification of pathway half-thickness a_p rather than pore radius in Equation (20) acknowledges the possibility that the very large forces acting on the clay at the time of gas entry might actually deform the fabric so as to produce pathway dilation. If we use

Equation (16) for p_m we obtain an exactly equivalent expression

$$p_g \geq \left[\frac{2\,\tau_{gw}}{a_p} + \sigma - \sigma_i + A_m\right] \qquad (21)$$

where σ is the total (isotropic) stress, σ_i is the interparticle stress and A_m is the attractive stress due to London - van der Waals' forces. The interfacial tension τ_{gw} between gas and pure water is approximately equal to the interfacial tension between pure water and a vacuum (i.e. the surface tension of water) and is 7.275×10^{-2} N.m^{-1} at 20°C.

We note, in reference to our comments of Section 2.6, that if a full thermodynamic analysis of this problem reveals that the attraction term A_m has a direct effect on midplane pore pressure, then it would be perfectly justifiable to subtract A_m from the right hand sides of Equations (20) and (21).

2.12 Indirect measurement of parameters by vapour pressure

Many indirect measurements of appropriate soil properties are measured on de-stressed samples in the laboratory. If a saturated clay at *in situ* stress σ is sampled and exposed to atmospheric pressure $p_g = p_0 = 0$ then, provided the gas entry criterion is not exceeded and temperature is not changed from T_0, the stress components can be expressed using Equation (11) by

$$\sigma - \Delta\sigma = \sigma_i + R - A + p_{w0} - \Delta\sigma \qquad (22)$$

where $\Delta\sigma = \sigma$. Provided that the interparticle spacings of the clay are not significantly changed by sampling, the effective stress $\sigma_{eff} = \sigma_i + R - A$ will remain unaltered during the sampling process. This indicates that the pore pressure p_{wo} will decrease during sampling by an amount $\Delta\sigma$. We can reach the same conclusion formally by assuming that pore pressure parameter B is equal to 1 (Skempton, 1954). Recalling Equation (13) we can therefore write

$$p_g = 0 = \sigma_i + \Pi_m - A_m + (p_{w0} - \sigma) \qquad (23)$$

If the pore water pressure was positive in the field situation, then it will be negative in the laboratory. Using Equation (16) the pressure at the midplane in the sample p_{ms} is then given by

$$p_{ms} = \Pi_m + (p_{w0} - \sigma) \qquad (24)$$

The partial vapour pressure of the water in the midplane solution p_{vm} can be calculated in two stages; first the effect of the Π_m term given by Equation (5), and second, the effect of a decrease in pressure $\Delta p_w = p_0 - (p_{w0} - \sigma)$ which is given by a relationship (Atkins, 1986) which is analogous to Equation (5). Combining the two stages we obtain

$$p_0 - (p_{w0} - \sigma) + \Pi_m = -\frac{RT}{v_w\,\omega_w}\log_e\left(\frac{p_{vm}}{p_{vp}}\right) \qquad (25)$$

where p_{vp} is the vapour pressure of pure water at atmospheric pressure and temperature T_0. As we noted in Section 2.5, the magnitude of the osmotic term and the pore pressure term vary continuously throughout the sample. Only the difference between these two terms remains constant. If we compare this relationship with Equations (4.2) and (4.3) of Fredlund and Rahardjo (1993) we identify $p_0 - (p_{w0} - \sigma)$ as the "matric suction" and Π_m as the "osmotic suction" of unsaturated soil mechanics. The sum of the two terms is the "total suction". If we multiply $(p_{w0} - \sigma)$ and Π_m by $-v_m$ we obtain the pressure potential ψ_p and the osmotic potential ψ_o of the laboratory sample as defined by Equation (1). Based on our analysis, it would seem inadvisable to attempt to separate these two components when dealing with compact clays.

Provided that the *in situ* stress σ and pore water pressure p_{w0} (using fresh water) are known, Equation (25) indicates that a simple measurement of the equilibrium vapour pressure p_{vm} of the aqueous phase of an undisturbed clay sample (at natural water content) can provide information which is pertinent to the problem of gas migration in a clay. The repulsion stress R and the combination $(\sigma_i - A_m)$ could, in theory, both be evaluated in this way, although the likely precision of such measurements remains uncertain. A variety of techniques for measuring soil suction, and its variation with water content and gas saturation, are described in Marshall and Holmes (1979) and Fredlund and Rahardjo (1993).

Total soil suction is sometimes quoted using the pF-scale, which is the logarithm (base 10) of suction is expressed in centimetres of water (Schofield, 1935). In the laboratory, samples of clay undergoing drying remain saturated to very high values of suction. No air-water interfaces are present except at the boundaries of the sample. Air enters the sample when the volume has reduced to the point where the interparticle interference prevents shrinkage and the suction is sufficiently large to overcome the forces of water retention. This point is known as the shrinkage limit (geotechnical index property), which for heavy clays such as Boom Clay occurs at a total suction of $pF \approx 4$ (≈ 1 MPa) which provides some preliminary guidance on the magnitude of the likely gas entry pressure $(p_g - p_{w0})_e$.

2.13 Gas phase in equilibrium (very low gas saturation)

In this section we examine a special case of a gas phase in equilibrium with the soil solution under *in situ* stress conditions. Our purpose is to examine some of the factors governing the pressure of the gas in the clay at very low levels of gas saturation.

Let us suppose that, after entry, the gas follows a discrete pathway through the clay along the midplanes between innumerable pairs of near-parallel clay particles. With the supply of gas to the pathway shut-off, this pressure will equilibrate at some pressure p_{gq}.

Between each pair of clay particles, the two interfaces between the gas and the adsorbed film will be flat, near-parallel, surfaces. Now, where gas is in contact with a liquid at a flat surface, the full pressure of the gas must be transmitted to the liquid (Figure 1). If the full

gas pressure is transmitted to the adsorbed film, then it must also be transmitted to the clay particle. The net force per unit area on the reverse side of each pair of clay particles is

$$\sigma - \sigma_i = R_m - A_m + p_{w0} \qquad (26)$$

where the forces associated with the σ_i term are accommodated somewhere outside the region of interest. Balancing the forces on the two particles, we can write

$$p_{gq} = R_m - A_m + p_{w0} \qquad (27)$$

We introduce the dimensionless quantity α, defined by

$$\alpha = \frac{R_m - A_m + p_{w0}}{\sigma} \qquad (1 - \alpha) = \frac{\sigma_i}{\sigma} \qquad (28)$$

which can be interpreted as the fraction of the total stress that is transmitted across the thin film between particles (Croney and Coleman, 1953). The quantity α was originally specified as the "compressibility factor", but we prefer to regard it as a simple ratio. Equation (26) then simplifies to nothing more than

$$p_{gq} = \alpha \sigma \qquad (29)$$

We draw particular attention to our comments of Section 2.9 concerning spatial variability of the α parameter. The pertinent values for gas migration studies are the small-scale values which may be significantly lower than the "continuum average". Using Equation (15), the midplane pressure p_m is given by $\Pi_m + p_{w0}$. Inserting this into Equation (14), the equilibrium gas pressure p_{gq} is also given by

$$p_{gq} = \frac{2\tau_{gw}}{a_{pq}} + R_m + p_{w0} \qquad (30)$$

Combining Equations (27) and (30) we reach the tentative conclusion that, at very low levels of gas saturation, equilibrium is achieved when

$$\frac{2\tau_{gw}}{a_{pq}} = -A_m \qquad (31)$$

This suggests that quantity A_m may be viewed as the cohesive strength of an interparticle water film with a half-thickness of a_{pq}. If we attempt to back-substitute A_m into our basic effective stress equation for a saturated clay, then the choice of an appropriate interfacial tension parameter in not immediately obvious. A strong contender is the interfacial tension between water and its own vapour. Since a clay soil stressed in tension will fail when the adsorbed water films rupture along the midplanes, the quantity A_m would then also represent the cohesive strength of the soil. We recognise some parallels between this behaviour and the adhesion of two flat glass plates separated by a thin film of water.

Our reasons for emphasising the tentative nature of this conclusion rests in the fact that it is based on our specific treatment of the attraction term A_m. We draw attention to the

discussions of Section 2.7. Equation (30) can be rearranged in the form

$$p_c = p_{gq} - p_{w0} = \frac{2\,\tau_{gw}}{a_{pq}} + R_m \qquad (32)$$

where p_c is the "capillary pressure" or "soil suction" at very low levels of gas saturation. This result differs from classic definitions of these terms since it includes the quantity $R_m = \Pi_m$ due to osmosis or to other non-specific mechanisms affecting the chemical activity of the constituent water of the soil solution. This emerges as a direct result of using Equation (11) in place of the conventional Terzaghi theory of effective stress. The definition of "matric potential" in Bolt (1976) is inappropriate to this model.

Thin gas films in clay colloids are generally very unstable. If the injection gas pressure rises, then the film will tend to rapidly propagate. If the gas pressure falls, adsorbed water will push back on the meniscus causing the gas film to retreat. Only very minor changes in the forces acting in these systems can lead to very significant changes in both the geometry of the films and in the capacity of the pathways to conduct gas. We are confident that a full thermodynamic analysis of the problem would pay dividends.

2.14 Pathway dilation and gas fracturing

Since a plastic clay will invariably have low bulk tensile strength, it is highly improbable that the gas pressure could every significantly exceed the total stress σ. If the gas pressure does rise to total stress then there is a strong probability of gas fracturing. The pressure regime in which a clay might exhibit classic two phase flow, as opposed to induced-fracture flow, is quite tightly bounded by the simple relationship

$$\sigma < p_g \geq \alpha\,\sigma \qquad (33)$$

Parameter α is reported to vary from 0.02 for a sand, through 0.3 for a silty clay; up to a theoretical value of 1 for a "pure clay". We might anticipate that a compacted bentonite backfill would display a value approaching unity, indicating the difficulty of gas phase movements in such a material.

It seems almost certain that the high gas pressures at gas entry will cause fabric deformation along the newly formed gas pathway causing its aperture to increase substantially. If the half-thickness of the pathway at equilibrium is substantially larger than the half-thickness at initial gas entry ($a_{pq} >> a_p$) then we expect to see a substantial drop in pressure from the gas entry condition to the "shut-in" condition.

It is important to note that we treat total stress σ as being isotropic. If the *in situ* state of stress is not isotropic, then all the key relationships must be couched in terms of the stress tensor. We note that the direction of gas flow in dilatant pathways is likely to be strongly affected by the orientation, in space, of the principal stress axes. There will be a strong tendency for gas to migrate in a plane which is normal to the minor principal stress.

Further discussion of this issue is beyond the scope of the present work, but the problem does require further examination.

2.15 Desaturation

At the microscopic scale, the component potentials of total soil water potential are spatially-varying quantities, depending locally on pore size, proximity to mineral surfaces and on small-scale variability of parameter α. The amount of work which must be expended in countering the forces of water retention must also vary locally. As we attempt to increase the gas saturation and decrease the volumetric water content we must displace water from progressively thinner films which is more strongly adsorbed to the mineral surfaces. The experimentally-determined total suction of the mudrock therefore increases rapidly as the volumetric water content decreases. The relationship between suction and volumetric water content is variously known as the "water retention function" or "moisture characteristic" and is fundamental in examining the gas transport properties of clay-rich media. The water retention function is not unique and exhibits very strong hysteresis from sorption (water content increasing) to desorption, which in clays may be due to fabric changes which occur during these processes. The desorption curve is of specific interest to the gas migration problem and can be evaluated using a number of well-known techniques (Marshall and Holmes, 1979).

The rapid decrease in total suction with increasing gas saturation implies that very high gas pressures are necessary to produce significantly large gas saturations in heavy clays. However, since it is quite improbable that the gas pressure could significantly exceed the total stress σ and, as a result, high gas saturations in host rocks with a high clay content are a physical impossibility. In pure clays such as bentonite, with $\alpha \approx 1$, it would appear that gas flow can only occur at $P_g \approx \sigma$ and will always be associated with flow along preferential (gas-induced) pathways. Most of the bentonite will remain 100% water-saturated. If bentonite is subject to high levels of compaction stress ($= \sigma$), then a high gas pressure will be necessary for gas entry. This observation is borne out by the work of Pusch et al. (1985) and Pusch and Hökmark (1990).

2.16 Effects of desaturation

As the gas saturation rises, the gas phase must bear an increasing proportion of the total stress on the clay medium. Bishop (1959) suggested a tentative relationship for the effective stress in an unsaturated soil

$$\sigma_{eff} = (\sigma - p_g) + \chi (p_g - p_{w0}) \qquad (34)$$

where χ is a parameter related to the degree of saturation of the soil. With no gas phase, $\chi = 1$ and the relationship reduces to the definition of Terzaghi's conventional effective stress. With no water phase $\chi = 0$ and the effective stress is the difference between the total stress and the gas pressure. This relationship can be rearranged as

$$\sigma_{eff} = \sigma - (1 - \chi) p_g - \chi p_{w0} \qquad (35)$$

Guided by Equation (12), we propose that the effective stress for a clay very close to 100% water saturation ($\chi \approx 1$) is given by

$$\sigma_{eff} = \sigma_i + \chi (R - A) \qquad (36)$$

If the entire pore space is filled with gas ($\chi = 0$), none of the the interparticle mechanisms associated with the liquid phase can operate and the effective stress is then equal to the interparticle stress σ_i. By combining Equations (35) and (36) we find that the total stress is

$$\sigma = \sigma_i + (1 - \chi) p_g + \chi (R - A + p_{w0}) \qquad (37)$$

which reduces to Equation (11) at very low gas saturations.

This relationship is only meaningful when we examine the behaviour of a representative volume of clay. Parameter χ shows a functional dependence on the average water saturation of this representative volume. Experiments by Blight (1961) were interpreted using Equation (34) and indicate that, in compact boulder clays and clay-shales, the curve of χ against water saturation is not a straight line with a slope of unity. After some initial curvature near 100% water saturation, the curve does become sensibly linear but approaches an intercept of about 60 – 70 % water saturation at $\chi = 0$. We conclude from Equation (37) that the effective stress in these materials must be equal to σ_i at around 60 – 70% water saturation. This then places the maximum theoretical upper limit of gas saturation in the range 30 - 40%. However, it seems highly improbable that we could get anywhere near these levels of gas saturation in practice.

2.17 Unstable displacement during gas flow

There is additional evidence to question the development of a uniform saturation front during desorption. When a non-wetting fluid is injected into a medium, initially saturated with a wetting fluid, there may be a tendency for fingers of non-wetting fluid to penetrate the medium leading to highly non-uniform phase saturations. This unstable displacement is known to take two forms, viscous fingering and capillary fingering. The propensity for viscous fingering can be judged from the viscosity ratio $M = \eta_2 / \eta_1$ where η_1 refers to the displaced fluid and η_2 to the injected fluid. We examine the specifics of our experiments. For helium injected into water, $M \approx 0.02$ giving $\log_{10} M \approx -1.7$. The possibility of capillary fingering can be judged from the capillary number C which is given by

$$C = \frac{Q_i \eta_2}{A \tau \cos(\theta)} \qquad (38)$$

where Q_i is the volume flow-rate of the injected phase at pressure p_{gi}, A is the cross-sectional area of the specimen, τ is the interfacial tension between the phases, and θ is the

contact angle (Lenormand et al., 1988). Taking representative values gives $\log_{10}C = -10.9$.

The significance of these numeric values $\log_{10}M = -1.7$ and $\log_{10}C = -10.9$ for 2-phase flow in our idealised medium can be judged by comparison with the results of network simulations and laboratory experiments on resin models by Lenormand et al. (1988). The very negative value of $\log_{10}C$ is indicative of highly unstable immiscible displacement, dominated by the capillary fingering mechanism. Furthermore, given the moderately negative value of $\log_{10}M$ it would seem improbable that we could produce stable displacement in the clay even if we were to reduce our typical injection flow-rates Q_i by 5 orders of magnitude.

2.18 Analysis of steady-state gas flow

We now move on to provide some theoretical background relating to the interpretation of our experiments. In the first instance we assume continuum flow properties. During one-dimensional steady-state laminar flow in a laboratory specimen of cross-sectional area A_s, the volume flow-rate of gas Q passing any cross-section normal to the flow direction may be expressed using the generalised form of Darcy's law

$$Q = - \frac{k_{rg}\ k_i\ A_s}{\eta_g} \cdot \frac{dp_g}{dx} \qquad (39)$$

where k_{rg} is the relative permeability to gas, k_i is the intrinsic permeability of the medium and η_g is the absolute viscosity of the gas and dp_g/dx is the pressure gradient in the flow direction. If the density of an ideal gas is ρ_0 at unit pressure, then the density of the gas (at the same temperature) and at pressure p_g is $\rho_0 . p_g$.

The mass of gas passing any cross-section of the specimen in a second is therefore $\rho_0 . p_g . Q$ where Q is measured at pressure p_g. Multiplying each side of Equation (39) by $\rho_0 . p_g$ we obtain

$$(\rho_0\ p_g\ Q).dx = - \frac{\rho_0\ k_{rg}\ k_i\ A_s}{\eta_g} p_g . dp_g \qquad (40)$$

Referring to our experimental set-up, we assume that the pressure P_{gi} in the gas injection circuit is equal to the pressure of the gas just inside the specimen at the upstream end. If the gas pressure just inside the specimen at the downstream end is P_{go} and the length of the specimen is L, we may integrate Equation (36) as follows

$$(\rho_0\ p_g\ Q) \int_0^L dx = - \frac{\rho_0\ k_{rg}\ k_i\ A_s}{\eta_g} \int_{p_{gi}}^{p_{go}} p_g\ dp_g \qquad (41)$$

which gives

$$\rho_0\ p_g\ Q = \frac{\rho_0\ k_{rg}\ k_i\ A_s}{2\ \eta_g\ L} \left(p_{gi}^2 - p_{go}^2\right) \qquad (42)$$

The volume flow-rate at STP is then given by

$$Q_{STP} = \frac{\rho_0 \, p_g \, Q}{\rho_{STP}} = \frac{\rho_0 \, k_{rg} \, k_i \, A_s}{2 \, \rho_{STP} \, \eta_g \, L}\left(p_{gi}^2 - p_{go}^2\right) \qquad (43)$$

where ρ_{STP} is the density of the ideal gas at STP. Under steady-state flow conditions in our experiments, both the pressure p_{gi} and the volume flow-rate Q_i of gas delivered from the injection pump to the upstream end of the specimen must be constant with time. The pore pressure pump at the downstream end of the specimen contains water at pressure p_{wo}. Let the constant volume flow-rate of gas out of the specimen into this pump be Q_{pwo}. The relationship between Q_{STP} and the measured quantities p_{gi}, Q_i, p_{wo} and Q_{pwo} is then given by

$$Q_{STP} = \frac{\rho_0 \, p_{gi} \, Q_i}{\rho_{STP}} = \frac{\rho_0 \, p_{wo} \, Q_{pwo}}{\rho_{STP}} = \frac{\rho_0 \, k_{rg} \, k_i \, A_s}{2 \, \rho_{STP} \, \eta_g \, L}\left(p_{gi}^2 - p_{go}^2\right) \qquad (44)$$

The gas pressure P_{go}, just inside the downstream end of the specimen, cannot be directly measured in our experiments. However, the gas pressure at any point in the clay must exceed the downstream water pressure p_{wo} by an amount equal to the local value of the "soil suction".

We surmise that immediately after a "shut-in" ($Q_{STP} = 0$), the flow pathway will close at its most critical point. We suggest this point lies just inside the specimen at the downstream end. Provided that the overall gas saturation of the specimen is very low, then the large-scale value of χ will be close to one. Since the "shut-in" condition represents an equilibrium condition, the scoping calculations of Section 2.12 suggests the "soil suction" p_{co} at the downstream end of the sample is approximately

$$p_{co} \approx R_m - A_m - \Pi_e \quad \text{(for large-scale } \chi \approx 1) \qquad (45)$$

The Π_e term is included because we do not use pure water in our experiments. Parameter p_{co} may vary with with gas saturation, saturation history and, possibly, with gas flow-rate. As a first approximation for data reduction we assume that p_{co} does not vary over the time-period of a discrete part of a test history. We may then write

$$Q_{STP} = \frac{\rho_0 \, k_{rg} \, k_i \, A_s}{2 \, \rho_{STP} \, \eta_g \, L}\left(p_{gi}^2 - (p_{wo} + p_{co})^2\right) \qquad (46)$$

If the mean gas pressure $\overline{p}_g$ in the test sample is

$$\overline{p}_g = \frac{p_{gi} + p_{go}}{2} \qquad (47)$$

then we can also write Equation (43) as

$$Q_{STP} = \frac{\rho_0 k_{rg} k_i A_s \bar{p}_g}{\rho_{STP} \eta_g L}(p_{gi} - (p_{wo} + p_{co})) \quad (48)$$

This simplified theoretical framework provides the basis for our interpretation of test data. Numerical modelling of gas flow in our experiments will allow parameters to be quantified with much greater precision than is presently possible. However, our present concern is with the mechanisms of gas flow and we regard the complexities of modelling as a matter for the future.

3 EXPERIMENTS

3.1 Testing philosophy

Experiments on compact clays of low permeability are always time-consuming. Recognising that there are strict limits on the number of tests that can be performed over any reasonable time-scale, we have opted to design experiments which reveal as much about the material responses of the clay as possible. Each test comprises a complex experimental history in which the independent variables of the problem (the permeant, the flow-rate and, in some cases, the state of stress) are deliberately varied throughout the course of the test. The differential pressure between the injected phase (water or gas) and the the downstream phase (water) is regarded as the main dependent variable. Since the total testing time for each sample is not insignificant, this philosophy has been followed at the expense of obtaining statistically repeatable results. In viewing our test results on gas transport, it must always be borne in mind that gas will follow the path of least resistance through the clay. This of course raises the issues of sampling strategy and of the size effects inherent in most laboratory testing. Our samples are of the largest cross-sectional area that can be prepared from the supplied material.

3.2 Apparatus

The apparatus (Figure 2) comprises 5 main components: (a) a sample assembly, (b) a pressure vessel together with its associated pressure control equipment, (c) a fluid injection system, (d) a back pressure system and (e) a microcomputer-based data acquisition system. We have demonstrated that total stress σ is a fundamental parameter in gas migration and a key feature of the apparatus is that the sample is subjected to an isotropic total stress σ which is maintained constant during the course of a test. By applying a fixed back pressure P_w, the sample can be consolidated at the onset of testing under predetermined effective stress conditions.

Control of the injection flux is achieved using a stepper-motor driven syringe pump. The fluid injected into the sample can be either water-saturated helium or a synthetic groundwater solution with chemistry matched to the "bulk interstitial porewater" of the clay. Helium has been selected for the gas-phase as a safe replacement for hydrogen.

The apparatus is assembled in an air-conditioned laboratory at maintained temperature of 20°C. Precise temperature control is important in gas transport experiments, and the effects of occasional temperature fluctuations are observable in some of our results.

A typical test sequence for a sample comprises the following stages: (a) resaturation and consolidation at *in situ* effective stress, (b) hydraulic conductivity and intrinsic permeability determination using "synthetic pore solution" at a number of preset flow-rates, (c) re-equilibration, and (d) gas injection at a number of pre-set pumping rates (see Section 5.3).

3.3 Pressure vessel

The pressure vessel (Figure 3) comprises an Autoclave Engineers Inc., single closure reactor vessel, manufactured from 316 stainless steel and pressure rated to 40 MPa. The cylindrical vessel has an internal capacity of 1 litre, an internal diameter of 7.62 cm, a wall thickness of 1.75 cm and is 22.9 cm in length. A port is provided in the base of the vessel. The end-closure is secured to the vessel by six alloy steel cap screws and sealed by a Gasche-type metal gasket. A central port in the end-closure communicates with the vessel. The closure has been modified to have four extra ports, evenly distributed about the centre, with 1/8-inch NPT female threads at either side. These extra ports enable tubing connections to be made from the sample assembly to the external gas and water circuits.

3.4 Sample assembly

The sample assembly (Figure 3) consists of a cylindrical clay sample, two 0.50 cm thick "high air-entry" sintered-bronze porous discs, two tapered end-caps, a thin copper sheath, two locking-rings, and the tubing connections to the vessel end-closure. The clay samples are 4.90 cm in diameter and of two different lengths; 4.90 cm for samples with flow axes normal to bedding and 2.45 cm for those with axes parallel to bedding.

The 316 stainless steel end-caps have a minimum diameter of 4.85 cm and are tapered at an angle of 0.024 radians to a final diameter of 5.00 cm. A groove is machined in each end-cap to accepts a Viton "O"-ring. This provides a backup seal against the copper during the early stages of vessel pressurisation, when confining pressures are too low to deform the sheath. Each end-cap has two ducts communicating with the porous disc, enabling test fluid to be circulated to remove any unwanted phase (gas or water) from the system. The injection end-cap has a circular groove cut into its surface and linked to the outflow duct. With injection at a central duct, this arrangement allows the injected fluid to sweep radially through the porous disc during preliminary fluid circulation. The pore pressure end-cap has no circular groove and the two ducts emerge at the load-bearing surface at points equidistant from the centre.

Copper sheaths were selected to avoid the leakage of helium by diffusion during very low flow-rate experiments. Metals exhibit significantly lower gas diffusion coefficients than most polymers and rubbers. However we recognise that, since copper is less deformable

than other possible jacketing materials, the use of a copper sheath may place constraints on the volumetric responses of the clay during consolidation and swelling. The choice of a jacketing material is therefore a trade-off between the requirements for low diffusion losses and flexibility. In order to maximise flexibility we make our sheaths as thin as possible. They are precisely machined on a lathe from 10 cm lengths of copper tubing stock and have a uniform internal diameter of 4.80 cm, a wall thickness of 0.020 cm and a very smooth inside surface. Comparing drained bulk compressibility values for our specimens with reported values from triaxial testing, we detect no significant constraints on volumetric behaviour associated with the use of copper sheaths. Prior to sample installation, the sheaths are lightly lubricated internally with silicone grease and flared-out at both ends, at an angle of 0.024 radians over a distance of about 3 cm, using a specially-manufactured tool. In practice, this combination of precisely-determined sizes guarantees a slight interference fit between the clay sample and the copper as the sample is pushed into the central section of the sheath (see Section 5.2).

The bore of each of the stainless steel locking-rings is tapered at the same angle as the other components. With a minimum internal diameter of 4.95 cm, these rings must be fitted over the copper sheath before the flaring operation. By tapping each ring towards its corresponding end-cap, the copper sheath is pinched between the ring and the side surface of the end-cap, effecting a very good gas-tight seal. Friction holds each ring in place.

The complete assembly is suspended from the vessel end-closure by the four lengths of nickel tubing which link the sample end-caps to the ports on the lower surface of the closure.

3.5 Injection, pore pressure and confining pressure circuits

Volumetric flow-rate of the injected fluid and pressure control of the downstream fluid are controlled using a pair of ISCO-500, Series D, syringe pumps, operating from a single digital control unit. The piston in these very precise pumps is advanced by a linear actuator driven by a microprocessor-controlled stepper-motor. An in-built pressure transducer monitors the outgoing pressure and can provide a feedback signal to the microprocessor when the pumps are set in pressure control mode. Alternatively, the pumps can be set to constant volume flow-rate mode, whereby the piston is advanced at constant velocity. The syringe pumps are rated to 26 MPa (3750 psi) and, with cylinder capacities of 507 mL, are capable of resolving volume change to about ± 32 nL. We have found no difficulty operating these pumps at flow-rates as small as 3 μL per hour.

Given the possibility that gas might leak past the sliding seal of the injection pump, we have opted to pump water, not gas, and to develop a constant helium flow-rate by displacing the gas from a pre-charged vessel. This arrangement has a second advantage in that it ensures that the helium is water-saturated and therefore cannot produce any dessication of the clay specimens. This gas/water interface vessel is a Whitey, 35 MPa rated, 500 mL mixing cylinder equipped with an upper and lower threaded port. Using a system of concentric

tubing, we have provided the vessel with an internal "overflow tube" which terminates at approximately mid-height. Thus we can determine the starting volume of helium with reasonable precision. In order to give us flexibility in future testing, the pore pressure circuit at the downstream end of the sample is almost identical to the injection circuit.

The confining fluid in the pressure vessel is water pressurised using a third pump or, alternatively, by the injection of nitrogen gas, from a supply cylinder equipped with a Victor Model SR4G gas regulator, into a gas/water interface vessel. A complex system of needle-type shut-off valves is provided to facilitate operations such as system filling and the changeover of the injection phases. Nickel tubing (1/8-inch OD) is used for all pipework because of its strength, flexibility and resistance to corrosion. All pipe connections are very carefully made-up and a liquid sealing compound is used with all copper gasket compression-type seals to avoid leakage.

3.6 Instrumentation and data acquisition

The injection pressure of the fluid at the upstream end of the sample, the water pressure at the downstream end and the confining pressure are monitored using pressure transmitters linked to three Druck DPI-203 digital pressure indicators. The ISCO pump controller has an RS232 serial port, which allows volume, flow-rate and pressure data from the two syringe pumps to be transmitted to the equivalent port of a 32-bit personal computer. A simple logging programme written in BASIC prompts the pump controller to transmit the data to the computer at pre-set time intervals and then records the data in disc files. Typically we record data at a rate of one scan per half hour, although much higher rates (up to one scan per 3 seconds) have proved necessary to record the details of intermittent gas flow. The raw data are transferred to a spreadsheet for processing and plotting.

3.7 Gas-tightness testing and calibration

Gas-tightness testing was performed systematically. With the system filled with pressurised helium, all connections were tested using a wash-bottle containing soapy water. Leaking pipe connections were tightened and re-tested. After these preliminary checks, we conducted three long-term pressurisation tests using a sample made of vulcanised rubber in place of a clay sample. The longest test was 150 hours in duration. We then compared the the three pressure versus volume curves with the theoretical curve for helium based on the van der Waals relationship. No significant helium leakage was detected over the time-scale of these tests.

All pressure transmitters were calibrated against a Budenberg dead-weight tester, with a Druck PTX-610 transmitter, calibrated by the manufacturer to ± 6.895 kPa, as a secondary standard. Pressure readings were taken at 0.5 MPa intervals up to a maximum of 5.0 MPa, at which point the procedure was reversed to detect hysteresis. Least squares linear regression of these data provided the slopes and intercepts necessary for processing the logged data. Checks on pump volume calibration were made by pumping water into a

Volac 100 mL graduated flask which had been factory calibrated under BS 1792 (ISO 1042). As an additional check, the masses of expelled water were determined using a Sartorius E2000 electronic balance and converted to volumes assuming a density of 1 $Mg.m^{-3}$.

4 TEST MATERIAL

Tube samples of Boom Clay were taken, under the supervision of SCK/CEN, by jacking a series of stainless steel sampling tubes with sharpened cutting edges into the exposed floor of a test gallery, at a location 224 m below surface in the Hades underground laboratory. The sampling tubes had an internal diameter of 6.9 cm and a wall thickness of 0.3 cm. After removing some clay from the tube ends, the resulting space was filled with hot paraffin wax. The tubes were then capped, sealed in polythene and dispatched to BGS. Upon receipt at Keyworth, the samples were stored in an environmentally-controlled store at 4 °C and 95% relative humidity to minimise water-loss and degradation.

4.1 Sample details

Details of the three 30 cm long samples received to date are shown in Table 1. The calculations of the *in situ* pore pressure and effective stress for these samples assume no perturbation by tunnel drivage.

Tube No.	Reference Depth (m)	Mid-point Depth (m)	Total Stress σ (MPa)	Pore Pressure p_w (MPa)	Effective Stress σ_{eff} (MPa)	Comments
1	1.00-1.30	226.40	4.42	2.21	2.21	Some sand
2	3.00-3.30	228.40	4.46	2.23	2.23	
3	5.00-5.30	230.40	4.50	2.25	2.25	Some pyrite

Table 1 - Details of the tube samples, including reference depth, mid-point depth and comments. The total stress (vertical) is calculated from overlying bed thicknesses and bulk densities. Pore water pressure is calculated from depth below phreatic surface. Effective stress (vertical) is total stress less pore water pressure.

5 EXPERIMENTAL PROCEDURES

5.1 Synthetic pore fluid

The hydraulic conductivity of clay is known to be sensitive to the chemistry of the permeating solutions (Quirk and Schofield, 1955; Hardcastle and Mitchell, 1973; Frenkel et al., 1977; Shainberg et al., 1977). If the major cation present in the permeant differs from that of the clay-water-solute system, then flow will be accompanied by cation exchange and associated changes in clay fabric and transport properties. If the concentration of salts in

the permeant is substantially less from that of the interstitial pore fluid in the clay, then it is possible that osmotic pore water movement will lead to swelling. Conversely, if the external water has too high a salt content then this may lead to chemico-osmotic consolidation of the clay (Mitchell et al., 1973).

Given the broad range of possible chemical interactions between the clay and the permeant, we have chosen to use "synthetic pore solution", rather than pure water, as the aqueous phase in the injection and back pressure systems of the test apparatus. We have based the composition of this synthetic pore solution on an early reference water chemistry for Boom Clay. The aqueous solution contained 16 mol.m^{-3} $NaHCO_3$, 0.7 mol.m^{-3} Na_2CO_3, 0.34 mol.m^{-3} NaCl, 0.24 mol.m^{-3} NaF, 0.53 mol.m^{-3} KCl and 0.25 mol.m^{-3} $MgSO_4$. Calcium carbonate was added at saturation concentration. The osmotic pressure of the solution Π_e at laboratory temperature is approximately 0.04 MPa. The synthetic pore fluid is made up in batches and vacuum de-aired prior filling the apparatus. This de-airing procedure is intended to assist in the process of sample resaturation. We note that our "synthetic pore water" has a lower ionic strength than the expelled solutions from more recent clay-squeezing experiments. Given that we interpret our experiments in terms of $\Pi_m - \Pi_e$, this difference is unimportant.

5.2 Specimen preparation

The clay was removed from the sample tube using a hydraulic extruder and cut into three sticks, each 10 cm long. Orientation and identification numbers were marked directly on the clay surface of each stick. The surplus sticks of clay were immediately preserved in aluminium foil and wax and returned to the environmental store, awaiting future use. One end of the remaining stick was flattened by trimming so as to provide a sound base for the preparation procedure. The cylindrical test specimens were prepared with the aid of a 4.90 cm internal diameter stainless steel ring-former with a sharpened leading edge. Two versions of this ring have been made, the first 4.90 cm long for specimens cut normal to bedding and the second 2.45 cm long for samples cut parallel to bedding. The former was placed on the flattened surface of the clay and, using a scalpel, the clay was carefully paired away around the periphery of the former allowing it to move downward under the action of a light, manually applied pressure. This process was continued until the ring-former had almost cut through to the lower surface, leaving about 0.5 cm of surplus material projecting above and below the former. The upper and lower surfaces were trimmed virtually flush to the ring and then finished-off by a scraping action with a straight knife-blade. This leaves the specimen end-surfaces perfectly flat and parallel.

The clay samples were extruded from the ring-former into the copper sheaths by application of a gentle pressure. The porous discs were saturated in "synthetic pore solution" using the vacuum technique and placed at either end of the sample. The tapered end-caps were placed in position and the locking rings tapped in place. Tubing connections were then made between the end-caps and the end-closure of the pressure vessel.

Clay trimmings and off-cuts were collected, weighed and oven-dried at 105°C for moisture content determination. All trimmings were logged and stored for future reference.

5.3 Test history

After sample installation and vessel connection, the testing system was filled with de-aired synthetic pore fluid. The pipework and porous discs were flushed with pore fluid to remove any air bubbles. The confining, injection and pore pressure circuits were then pressurised incrementally so as to maintain, as closely as possible, a constant effective stress on the sample, equivalent to the calculated *in situ* effective stress. A confining pressure of 4.40 MPa was used in all tests, with the exception of the later stages of one particular test which was designed to examine sensitivity to effective stress. The injection and pore pressure pumps were set to hold constant pressure (≈ 2.2 MPa) and the sample left to resaturate and consolidate for period of, typically, 4 days. The equilibrium state was judged by determining the point at which all net flow in or out of the sample had ceased. In view of the compliance of the upstream and downstream pressure measuring systems, it did not prove possible to evaluate pore pressure parameter B as a measure of water saturation (Skempton, 1957). Given the high back pressure and the use of de-aired "synthetic pore fluid" as a saturation medium, we are confident that the samples were 100% saturated at the commencement of testing. Measured values of specific storage during transient hydraulic flow support this assertion.

After achieving equilibrium, the hydraulic conductivity testing sequence was initiated. The injection pump was set to constant flow mode with typical synthetic pore fluid injection rates in the range 5 to 50 μL/hr (1.39×10^{-12} to 1.39×10^{-11} $m^3.s^{-1}$). Back pressure at the downstream end of the sample p_{w0} was held constant at approximately 2.2 MPa, the exact value varying slightly between tests. Constant flow-rate was maintained until the differential pressure across the sample became sensibly constant with time, within the limits of resolution of the testing system. In some test stages, particularly at low flow-rates, experimental noise was of sufficient magnitude to make judgments about steady-state slightly problematic.

After hydraulic testing, samples were allowed to re-equilibrate at a constant pore pressure of about 2.2 MPa, applied at both ends. Once again, net flows were monitored to establish the point of equilibration. Helium gas was then admitted into the upper part of the gas-water interface cylinder and the tubing to the vessel, the porous disc and drainage tubing were gas flushed. The initial helium pressure in the injection system was set using the gas regulator. After closing the valve to the regulator, the injection pump was then set to constant flow-rate mode. An initial pumping rate of 375 μL/hr (1.042×10^{-10} $m^3.s^{-1}$) was used in all test to raise the injection gas pressure to the point of breakthrough. Depending on the specific objectives of each test, the pumping rates were then changed in step-wise manner in order to examine the sensitivity of differential pressure to flow-rate.

At the end of testing, the samples were photographed, weighed and oven-dried to obtain moisture content. All samples were then sealed in plastic bags and stored for future reference.

6 BASIC PROPERTIES OF SAMPLES

Table 2 shows the basic properties of the samples. Water contents are typical of saturated Boom Clay from this depth. Fractional porosities are based on the water extracted from initially saturated clay by drying at 105°C. The values are therefore indicative of the total macroporosity of the clay plus that part of the microporosity containing adsorbed water extractable by oven drying. We emphasize that all porosity definitions for compact clays are somewhat arbitrary.

Test No.	Natural Water Content w_b	Fractional Porosity n	Bulk Density ρ_b (Mg.m^{-3})
T1S1	0.25	0.40	2.00
T2S1	0.23	0.38	2.03
T2S2	0.24	0.39	2.01
T2S3	0.23	0.37	1.99
T3S1	0.23	0.39	2.05
Average	0.24	0.39	2.02

Table 2 - Basic properties of samples including natural water content, porosity and saturated bulk density.

The average dry density was determined to be 1.63 Mg.m^{-3} and the average grain density to be 2.66 Mg.m^{-3}. The average void ratio for all material tested is 0.63.

7 CONSTANT FLOW-RATE HYDRAULIC TESTS

The governing differential equation for the one-dimensional transient flow of water through a saturated homogeneous, compressible medium is

$$\frac{\partial^2 h}{\partial x^2} = - \frac{S_s}{K} \frac{\partial h}{\partial t} \qquad (49)$$

where h is the hydraulic head (m), x is coordinate in the flow direction, S_s is the specific storage (m^{-1}) and K is the hydraulic conductivity (m.s^{-1}) of the medium.

We examine the case of a laboratory specimen of length L and cross-sectional area A_s subject to a constant flux q_i (m.s^{-1}) at the upstream end and a fixed head $h_o = 0$ at the downstream end. It is assumed that pumping commences as time $t = 0$. We define a dimensionless time parameter τ by

$$\tau = \frac{4\,K\,t}{S_s\,L^2} \tag{50}$$

The upstream head h_i and the downstream flux vary with elapsed time, $h_i = h_i(t)$ and $q_o = q_o(t)$. Analytical solutions for the upstream head are

$$h_i(t) = \frac{q_i\,L}{K}\left\{1 - \frac{8}{\pi^2}\sum_{n=0}^{\infty}\left(\frac{1}{(2n+1)^2}\right)\exp\left[-(2n+1)^2\pi^2\frac{\tau}{16}\right]\right\} \tag{51}$$

and

$$h_i(t) = \frac{q_i\,L}{K}\sqrt{\tau}\sum_{n=0}^{\infty}\left\{-1^n\left[\text{ierfc}\left(\frac{2n}{\pi}\right) - \text{ierfc}\left(\frac{2(n+1)}{\sqrt{\tau}}\right)\right]\right\} \tag{52}$$

where

$$\text{ierfc}\,(z) = \frac{e^{(-z)^2}}{\sqrt{\pi}} - z\ \text{erfc}\,(z) \tag{53}$$

Solutions for the downstream flux are

$$q_o(t) = q_i\left\{1 - \frac{4}{\pi}\sum_{n=0}^{\infty}\left(\frac{(-1)^n}{(2n+1)}\right)\exp\left[-(2n+1)^2\pi^2\frac{\tau}{16}\right]\right\} \tag{54}$$

and

$$q_o(t) = 2\,q_i\sum_{n=0}^{\infty}\left\{(-1)^n\,\text{erfc}\left[\frac{2n+1}{\sqrt{\tau}}\right]\right\} \tag{55}$$

The exponential solutions are better for long time periods, while the error-function solutions are more suitable for small time periods. In order to fit the transient data from the hydraulic tests, a numerical approach was adopted in which a type curve was obtained by numerical inversion of the Laplace transforms. The data curves were then fitted using a nonlinear least-squares regression routine.

It became apparent during processing of the data that there were significant nonlinearities in the flow response over a stepped history of applied flow-rate. This is, of course, indicative of a departure from Darcy's law. Since this nonlinearity generates a cumulative error in curve fitting, we have opted to report fitted results for the first stage of each history only. We have yet to attempt any analyse of the transient flow behaviour using a nonlinear flow law.

Differential pressures across the specimens during transient flow are plotted against the logarithm of time in Figure 4. Although some "experimental noise" is evident, many of the curves exhibit the classic sigmoidal shape.

7.1 Specific storage

The specific storage S_s of a porous medium is the volume of water that the medium releases or takes into storage, per unit volume, per unit change in hydraulic head. Specific storage values based on the analysis of the first stage flow transients are presented in Table 3. The best estimate for this parameter for the Boom Clay can be seen to be about 1.0×10^{-4} m^{-1}. Specific storage of a water-saturated medium is the sum of the contributions from the elasticity of the water and the elasticity of the porous skeleton of the medium, expressed in terms of their bulk moduli K_w and K_{sk}. The appropriate modulus for the medium is the "drained bulk modulus", which in clays is known to be very sensitive to effective stress. For a sample of overconsolidated clay under an isotropic state of stress, the modulus K_{sk} may be expressed in terms of the effective stress σ_{eff}, the void ratio $e = n/(1 - n)$, and the critical state soil mechanics parameter κ (Schofield and Wroth, 1968). The specific storage (m^{-1}) is then given by

$$S_s = \rho_w g \left[\frac{n}{K_w} + \frac{1}{K_{sk}}\right] = \frac{\rho_w g}{(1+e)}\left[\frac{e}{K_w} + \frac{\kappa}{\sigma_{eff}}\right] \qquad (56)$$

where ρ_w is the density water and g is the acceleration due to gravity. Parameter κ is dimensionless and can be obtained from consolidation test data by using the approximate relationship $\kappa = 0.0434\ c_s$, where c_s is the swelling index. The bulk modulus of water may be taken as 2.2×10^3 MPa. Taking $e = 0.63$ and typical effective stress values for the test stages gives a κ value of around 0.033. Horseman et al. (1993) estimated κ to be 0.03, based on isotropically consolidated, undrained triaxial experiments on the same material.

Specific storage falls by 20%, or so, for a 0.5 MPa increase in effective stress. This is one of the sources of nonlinearity in transient flow. It is easily accommodated in numerical codes by making S_s vary with σ_{eff} according to Equation (56).

Test and Stage No.	Upstream Water Flux q_i 10^{-9} ($m.s^{-1}$)	Hydraulic Conductivity K 10^{-12} (m.s-1)	Specific Storage S_s 10^{-4} (m^{-1})	Duration of Transient t_{95} 10^4 (s)
T1S1-H10	1.47	0.9	1.03	32
T2S1-H5	0.74	0.4	1.14	79
T2S2-H10	1.47	1.7	0.4	6
T2S3-H10*	1.47	3.0	1.00	2

Table 3 - Results of transient flow analysis of the first stage of the hydraulic tests showing the upstream water flux, best-fit hydraulic conductivity, specific storage and the predicted duration of the flow transients (at t_{95}).

7.2 Hydraulic conductivity

Given the difficulties in processing the later-stage flow transients of our multi-step tests we have chosen to pick steady-state differential pressures (p_{wi} - p_{wo}) and calculate hydraulic conductivity from these values. Data are presented in Table 4.

Based on this relatively small number of tests, we confirm that the hydraulic conductivity of Boom Clay is greater parallel to bedding than it is perpendicular to bedding. Well-compacted natural clays often display this form of hydraulic anisotropy. Comparing values for a fixed magnitude of flux of 1.47 x 10^{-6} $m.s^{-1}$, we find the ratio K_H/K_V to be in the range 3 and 5, although we draw attention to the observations of Section 7.3 on the role of effective stress in determining K, since these are pertinent to the accurate determination of this ratio. The preferred orientation of clay minerals is probably the most significant factor in determining this anisotropy, although we cannot exclude the possibility that flow may also be occurring in very small microfissures, aligned parallel to the bedding plane, leading to enhanced horizontal hydraulic conductivity. A supplementary study (Appendix 1) of the fabric of the Boom Clay using ordinary scanning electron microscopy (SEM) and environmental scanning electron microscopy (ESEM) has revealed the presence of bedding plane orientated, pyrite-lined microfissures, several millimetres in length, with apertures exceeding 20 μm. Since these features are very sensitive to dessication and de-stressing, it remains unclear whether or not they are closed under *in situ* conditions

The data of Table 4 show a fairly systematic variation in hydraulic conductivity with flow-rate and steady-state hydraulic gradient, with K increasing with both flow-rate and gradient. Departures from Darcy's law in clays, including nonlinearities and thresholds, have frequently been observed and have been variously ascribed to the high viscosity of pore water, the presence of the adsorbed water layers, electrokinetic effects, swelling, coupled flow, clogging by clay minerals and other causes (Swartzendruber, 1962; Olsen, 1965; Mitchell, 1967; Bolt and Groenevelt, 1969; Kutelek, 1969). If a clay displays a nonlinear flow law or a threshold in the laboratory, then extrapolation to the field situation may be problematic. We have examined our data in some detail and believe that at least some of the variation in hydraulic conductivity can be ascribed to a pronounced sensitivity of this parameter to effective stress. However, we cannot totally preclude the existence of a finite threshold gradient for the movement of water by advection.

7.3 Sensitivity to effective stress

The average effective stress σ_{eff} at the steady-state condition in our constant flow-rate experiments is given by

$$\sigma_{eff} = \sigma - \frac{(p_{wi} - p_{wo})}{2} \qquad (57)$$

Appropriate values are given in Table 4. Figure 5 shows a composite plot of $\log_{10}(K)$ against σ_{eff} at apparent steady-state for tests with flow normal to bedding (lower group)

and parallel to bedding (upper group). Data for tests normal to the bedding include points which were established with fluxes increasing and decreasing and there would appear to be a degree of hysteresis in the response. This hysteresis may be analogous to the voids ratio e versus $\log(\sigma_{eff})$ hysteresis seen in consolidation testing. Data points for flow parallel to bedding are for increasing fluxes only.

In Figure 6 we show the least-squares fits to the two data sets. Curvefitting was undertaken using linear regression of the transformed data and gives the following relationships

$$\log_{10}(K_V) = -1.877\,\sigma_{eff} - 8.442 \qquad (58)$$

$$\log_{10}(K_H) = -0.553\,\sigma_{eff} - 10.304 \qquad (59)$$

where K_V and K_H are the hydraulic conductivities ($m.s^{-1}$) normal and parallel to bedding, respectively, and σ_{eff} is the effective stress (MPa).

These expressions are probably only valid for overconsolidated Boom Clay samples lying on a common swelling-reconsolidation line. At high effective stresses (> 6 MPa, or so) we might anticipate that irreversible plastic volumetric deformation would commence leading to an increased sensitivity between K and effective stress. Extrapolation to these higher pressures suggests that advection probably gives way to diffusion as the dominant transport mechanism of water in the clay under such circumstances.

The implications of these relationship are quite profound. In the hydraulic testing of mudrocks, whether in the field or the laboratory, the imposed hydraulic gradient must be high enough to obtain measurable flow over a sensible time-scale. Because of the very low hydraulic conductivity, the gradients imposed during testing are generally 4 - 5 orders of magnitude greater than naturally-occurring gradients. These high gradients are achieved by raising the water pressure at some point in the system. This increase in water pressure leads to a reduction in the local effective stress, and through Equations (58) and (59), this leads to a significant increase in the hydraulic conductivity. Thus the act of testing a mudrock may so alter the state of stress that the hydraulic conductivity obtained may not be representative of natural *in situ* conditions unless, of course, corrections are made for this effect. If, during testing, the average effective stress in the clay falls by only 10%, then the measured hydraulic conductivity will increase by a factor of about 5.

The "true" hydraulic conductivities can be obtained by extrapolating Equations (58) and (59) to the *in situ* effective stress. If we assume a value of 2.2 MPa at the sampling depth, then K_V is close to 2.7×10^{-13} $m.s^{-1}$ and K_H close to 3.0×10^{-12} $m.s^{-1}$ for the material used in our tests. These values are significantly smaller than the commonly reported values for the Boom Clay. The ratio K_H / K_V of around 11 is higher than the value obtained above by comparing results for equal flow-rates and is certainly higher than commonly quoted values.

Test and Stage No.	Water Flux q_i 10^{-9} (m.s^{-1})	Head Gradient at Steady-State dH/dx	Hydraulic Conductivity K 10^{-12} (m.s-1)	Ave. Eff. Stress at Steady-State σ_{eff} (MPa)
T1S1-H10	1.47	1462	1.0	1.86
T1S1-H20	2.95	1794	1.6	1.79
T1S1-H30	4.42	1960	2.3	1.75
T1S1-H20D	1.47	1586	1.9	1.84
T1S1-H10D	2.95	1337	1.1	1.90
T1S1-H5D	0.74	922	0.8	2.00
T1S1-H2D	0.29	652	0.5	2.06
T1S1-H5A	0.74	735	1.0	2.04
T1S1-H10A	1.47	776	1.9	2.03
T1S1-H20A	2.95	880	3.3	2.00
T2S1-H5	0.74	1254	0.6	1.92
T2S1-H10	1.47	1566	0.9	1.84
T2S1-H20	2.95	1836	1.6	1.78
T2S1-H10D	1.47	1566	0.9	1.84
T2S1-H5D	0.74	880	0.8	2.01
T2S2-H10	1.47	838	1.7	2.02
T2S3-H10*	1.47	159	4.6	2.15
T2S3-H30*	4.42	602	3.7	2.04
T2S3-H50*	5.74	954	3.9	1.96
T3S1-H10*	1.47	229	3.2	2.13
T3S1-H30*	4.42	577	3.8	2.05
T3S1-H50*	5.74	873	4.2	1.98

Table 4 - Results of constant flow-rate hydraulic conductivity tests showing the head gradient, hydraulic conductivity and average effective stress at the apparent steady-state. Tests marked (*) were performed with the direction of flow parallel to bedding.

It is apparent that, using the well-known soil mechanics relationships between the void ratio and the effective stress acting on an overconsolidated clay, the above relationship between K and σ_{eff} could be rewritten as a dependency of K on void ratio. In exploring the interrelationship between parameters we have observed that K is a very highly sensitive function of void ratio (and hence porosity). The order of magnitude changes in K with effective stress are difficult to reconcile with the relatively small voids ratio changes occasioned by these stress changes. In our view the fundamental relationship is between K and σ_{eff}, and not between K and void ratio or porosity. We recall Equation (12)

$$\sigma_{eff} = \sigma - p_{w0} = \sigma_i + R - A \qquad (60)$$

and note that any change in effective stress will also produce a change in the osmotic potential of the water molecules at the midplane between clay particles and some alteration

in the fundamental force of attraction of the water in the thin film. We reason that hydraulic flow is in some way impeded by the net physico-chemical forces acting on water molecules within the pore space. The higher the magnitude of these net forces, the lower will be the hydraulic conductivity of the clay, leading to the pronounced sensitivity between K and σ_{eff}.

7.4 Intrinsic permeability

The intrinsic or specific permeability k_i (m^2) can be calculated from the hydraulic conductivity K ($m^2.s^{-1}$) using the relationship

$$k_i = \frac{K \eta_w}{\rho_w g} \qquad (61)$$

where η_w and ρ_w are the absolute viscosity and density of water, respectively, and g is the acceleration due to gravity. At 20°C the absolute viscosity of water is 1.002×10^{-3} Pa.s and the density is 998.2 $kg.m^{-3}$ (de Marsily, 1986). Under these conditions

$$k_i = 1.01 \times 10^{-7} K \qquad (62)$$

Based on an extrapolation of Equations (58) and (59) the intrinsic permeability of the Boom Clay at an effective stress of 2.2 MPa is 2.7×10^{-20} m^2 perpendicular to bedding and 3.0×10^{-19} m^2 parallel to bedding. We use these values in our preliminary examination of 2–phase flow behaviour.

Provided that flow is non-reactive with the porous medium, the intrinsic permeability should be a property of the medium alone. Since most permeants interact in some way or another with the exchange complex at the surface of clay minerals, it is optimistic to believe that k_i derived from hydraulic tests would quantify the flow of a permeant with a chemistry which is quite different from that of water. In examining gas flow in clay, we regard k_i as a simple reference value which provides a base-line in the interpretation of gas fluxes. Since gas probably flows in a relatively small number of dilated pathways in a compact clay, it is doubtful whether there should be any direct physical relationship between permeability to water and permeability to gas.

8 GAS INJECTION TESTS

Assuming isothermal conditions, the governing differential equation of the testing system can be written in a convenient form as

$$\frac{dp_{gi}}{dt} = \frac{p_0 \rho_{STP}}{\rho_0 V_{sys}} (Q_p - Q_i) \qquad (63)$$

where p_{gi} and V_{sys} are the instantaneous pressure and volume, respectively, of the helium in the upstream injection system, ρ_{STP} is the density of helium at STP, ρ_0 is the density at

20°C and unit pressure p_0 = 1 MPa, Q_p is the volumetric rate of pumping and Q_i is the volumetric rate of flow into the specimen. Both rates are corrected to STP conditions. We assume ideal gas behaviour. For a constant rate of volume displacement of the injection pump C, we may write

$$V_{sys} = V_{sys}(t) = V_{start} - C\,t \qquad (64)$$

where V_{start} is the initial volume of helium in the injection system and t is the elapsed time after starting the pump. If there is no gas flow through the specimen (Q_i = 0) and pressure rises with time according to the simple relationship

$$p_{gi} = p_{gi}(t) = \frac{p_{start}\ V_{start}}{(V_{start} - C\,t)} \qquad (65)$$

We can see from Equation (63) that P_{gi} becomes constant when the STP volumetric rate of pumping Q_p is exactly equal to the STP volumetric flow-rate of gas Q_i into the sample. If we are also able to demonstrate that the STP flow-rate into the specimen Q_i is equal to the STP flow-rate emerging from the downstream face Q_o, then gas flow must be occurring under steady-state conditions. The theoretical framework of Section 2.16 can then be applied, provided that the flow is laminar. This has been the basis of our data interpretation up to the present time.

It is also apparent from Equations (63) and (64), that the parameters, other than the volume flow-rate Q_i into the specimen, are either known or can be quantified in our experiments. This means that Q_i can be evaluated over an entire test history. The data processing is somewhat more complex and relies on accurate values of V_{start}. To date, we have undertaken this type of processing on calibration data and on the results from one of the experimental histories.

8.1 Description of results

Five multi-stage gas injection experiments have been performed to date, three with flow normal to bedding (T1S1-G, T2S1-G and T2S2-G) and two with flow parallel to bedding (T2S3-G and T3S1-G). In Figures 7 - 12 we plot the differential pressure (p_{gi} - p_{wo}) between the gas at the upstream face and the water at the downstream face of each specimen against the elapsed time in seconds from the start of injection. Also shown are the STP volumetric flow-rate into the testing system Q_p and the volumetric flow-rate out of the specimen Q_o. Values for the parameters identified in the following description are given in Table 5.

The early stages of experimental histories T2S2-G (Figure 10) and T2S3-G (Figure 11) exhibit common characteristics and we will examine these tests in some detail before proceeding. Early in each test we see a gradual build-up of upstream gas pressure with time. No measurable quantities of gas emerge from the downstream end of the samples during this pressure build-up. The response can be interpreted as a rise in injection gas

pressure caused by slowly and isothermally decreasing the volume of the fixed mass of gas contained in the upstream system. This behaviour is described by Equation (65).

The pressure build-up curves in these tests terminate at a very well-defined peak which exactly coincides with the start of flow from the downstream end of the sample. The initial flow-rates of fluid from the sample are very large; between 5 and 15 times the pumping rate. Although our system cannot distinguish between a flow of water and a flow of gas at the downstream end of the sample, simple calculations based on clay permeability to water demonstrate that this emergent flux must be be largely gas. We will define the "excess gas pressure at breakthrough" $p_b = (P_{gi} - p_{wo})_b$ as that minimum value of excess gas pressure which causes the gas to penetrate the full length of the sample and emerge at the downstream face and note that p_b corresponds exactly with the peak pressure in these two tests ($p_b = p_p$).

We surmise that, just before the initial peak in each experimental history, there is a point on the curve at a pressure somewhat less than the breakthrough pressure, which marks the first entry of gas into the upstream face of the sample. We shall refer to the gas pressure at this point as the "excess gas pressure at entry" $p_e = (P_{gi} - p_{wo})_e$. Based on Equation (20), this can be visualised as the differential gas pressure necessary to overcome the forces due to capillarity and osmosis at the mouth of the largest gas pathway communicating with the upstream surface

$$p_e = (p_{gi} - p_{w0})_e = \left[\frac{2\,\tau_{gw}}{a_p} + \Pi_m - \Pi_e\right] \qquad (66)$$

where Π_e is the osmotic pressure of synthetic pore water solution at the downstream end of the sample and a_p is the radius of the pathway. In practice, it is difficult to resolve the very small flow of gas associated with gas entry, and the magnitude of p_e remains largely indeterminate.

Beyond the peak there is a rapid decline in differential pressure with time. The slope of the curve gradually decreases as differential pressure decreases. In the absence of extraneous factors, such as "experimental noise", we note that the curves for constant pumping rate decline to a finite value of differential pressure. This is a smooth decline in T2S2-G, but is somewhat more abrupt at lower pressure levels in T2S3-G. These negative transients are of very similar form to the transients in the flow-rate curves. When differential pressure remains sensibly constant with time, the volume flow-rate into the sample must be equal to the flow-rate out of the sample provided that both flow-rates are expressed at STP. This is therefore a steady-state condition and the pressure acting over this time-period may be referred to as the steady-state excess gas pressure $p_s = (P_{gi} - p_{wo})_s$. The later stages of T2S3-G (Figure 11) provide the most convincing visual evidence of steady-state.

In experimental history T2S3-G, after the initial pressure decline, there are almost sinusoidal-shaped fluctuations in both the differential pressure and flow-rate curves, with flow actually shutting-off completely for a period of time. No alterations were made to the

testing conditions which might have been responsible for triggering this response. During testing we have often observed unexplained anomalies in gas flow behaviour, of which T2S3-G provides the best example. Some of these may be due to gas pressure sensitivity to minor temperature variations in the laboratory. These fluctuations in the response of T2S3-G are actually fortuitous since they enable us to determine the differential pressure at zero flow-rate. T2S3–G also displays a second peak, with p_p somewhat less than the original peak.

Beyond the fluctuation, T2S3-G settles into more or less steady-state behaviour. Close inspection of the later stages of T2S2-G (Figure 10), and of other tests, reveals that the flow-rate out of the specimen is not smooth with time. The flow-rate actually varies quite considerably about the mean value. There is strong evidence that, at lower differential pressures, the gas moves through the clay in "bursts" and, during steady-state, it is the product of the average burst frequency and the average STP volume of a burst which remains constant over time. This is an important finding and we will address it in more detail later. For the time being, when we discuss the flow-rate through the sample we will understand this to mean the time-averaged flow-rate.

In experimental history T2S2-G (Figure 10), we have attempted to determine the functional form between Q_0 at steady-state and the pressure gradient of the gas within the specimen. The basic theory of steady-state gas flow was described in Section 2.16. After achieving breakthrough and post-peak steady-state, the flow-rates were decreased in steps, then increased in steps, and finally decreased in the same manner. Values of the steady-state gas pressure were picked at points where the volumetric flow-rate into the system Q_p (STP) was sensibly equal to the time-averaged, flow-rate Q_o (STP) out of the specimen. Figure 13 illustrates this approach. Values are given in Table 5.

We find that for a single specimen, steady-state gas pressures obtained from a history of decreasing flow-rates do not coincide with those from an ascending history. This is indicative of hysteresis. If we think in terms of gas moving out of storage in the clay during a descending history and into storage during an ascending history, then this behaviour is reminiscent of the suction / saturation hysteresis seen between imbibition (sorption) and drainage (desorption).

We move on to examine the later stages of T2S2-G. At the lowest part of the differential pressure history, the STP flow-rate was 3.3×10^{-12} m^3.s^{-1}. If we examine this part of the curve we find that the gas moves in bursts separated by "quiescent periods" in which no gas flows through the clay. On increasing the flow-rate, the pressure builds rapidly. This stage of the test was of insufficient duration to determine the steady-state excess gas pressure. The flow-rate was again increased and the rate of pressure build-up responded accordingly. At an excess pressure of 1.75 MPa, we observe another peak. This is similar to the first peak in T2S2, but is at a slightly lower pressure and has a more rounded appearance. The peak is coincident with a massive increase in flow-rate from the sample. Beyond the peak, we observe a well-defined negative transient as the differential pressure

declines to its steady-state value, followed by two more negative transients which follow step-decreases in pumping rate.

Test and Stage No.	Gas Pumping Rate C 10^{-12} ($m^3.s^{-1}$)	Excess Gas Pressure at Breakthrough $P_b=(p_{gi} - p_{wo})_b$ (MPa)	Peak Excess Gas Pressure $P_p=(p_{gi} - p_{wo})_p$ (MPa)	Steady-State Excess Gas Pressure $P_s=(p_{gi} - p_{wo})_s$ (MPa)	Downstream Water Pressure p_{wo} (MPa)
T1S1-G375	104.2	1.21	1.27	1.22	2.18
T1S1-G90	25.0	-	-	1.12	2.18
T2S1-G45	12.5	-	-	1.17	2.18
T2S1-G375a	104.2	1.89	1.89	1.73	2.18
T2S1-G375b	104.2	-	1.86	-	2.18
T2S1-G375c	104.2	1.84	1.87	-	2.58 (4.80)
T2S1-G375d	104.2	1.75	1.89	-	2.98 (5.20)
T2S1-G375e	104.2	-	1.89	-	3.57 (5.80)
T2S1-G375f	104.2	-	2.13	-	3.57 (6.20)
T2S2-G375	104.2	1.93	1.93	1.46	2.18
T2S2-G180	50.0	-	-	1.38	2.18
T2S2-G90	25.0	-	-	1.27	2.18
T2S2-G45	12.5	-	-	1.25	2.18
T2S2-G22	6.1	-	-	1.18	2.18
T2S2-G12	3.3	-	-	1.13	2.18
T2S2-G375	104.2	1.60	1.75	1.64	2.18
T2S2-G180	50.0	-	-	1.42	2.18
T2S2-G90	25.0	-	-	1.30	2.18
T2S3-G375*	104.2	0.47	0.47	0.38	2.21
T3S1-G375*	104.2	1.01	1.02	0.83	2.21
T3S1-G0*	0.00	-	-	0.64	2.21
T3S1-G375*	104.2	0.83	0.95	0.90	2.21
T3S1-G0*	0.0	-	-	0.63	2.21

Table 5 - Results of gas injection tests showing the volumetric displacement rate of the injection pump C, excess pressure at breakthrough , peak excess gas pressure and steady-state excess gas pressure. Tests with gas flow parallel to bedding are marked (*). Confining pressure is 4.40 MPa, except in the later stages of T2S1 where it is shown in parentheses after the downstream water pressure.

We now examine experimental history T1S1-G (Figure 7) which differs, in detail, from T2S2–G. In this test there is clear evidence of gas breakthrough before the peak differential pressure, indicating that $p_b < p_p$. Furthermore, the breakthrough flow-rate is considerably less than it was in T2S2-G and the post-peak negative transient is less pronounced. Two more negative transients are discernable and are the result of step-decreases in pumping

rate. We suggest that some initial desaturation of this specimen occurs prior to the development of well-defined gas pathways.

T2S1-G (Figures 8 and 9) represents the most complex experimental history that has been attempted. In this experiment the gas pressure was increased in the usual way. However, in the absence of a conspicuous gas breakthrough, the gas pressure was reduced to just above water pressure, held constant for a while and then increased to 1.80 MPa. At this point in the history the pump was set in constant pressure mode and the gas pressure held at 1.80 MPa for about 3 days. No significant gas flow through the sample was observed. The pump was then set for constant volume displacement rate C of 1.042×10^{-10} $m^3.s^{-1}$. The differential gas pressure rose to a small peak (Figure 9) at 1.89 MPa which is very nearly coincident with the emergence of a gas at the downstream end of the specimen ($p_b \approx p_p$). Although the plot of flow-rate out of the specimen shows some minor pulses prior to the peak, since these are fairly balanced either side of the zero datum line they do not represent a true flow of gas into the specimen and are probably temperature-related. After the first peak, there is a small negative transient and a period of near steady-state flow. This is characterised by very pronounced "bursts" and short quiescent periods and it is only when we time-average the data that the flow emerges as being sensibly constant. Beyond this point, the gas pressure spontaneously rises to a second peak, followed by another negative transient.

The occurrence of spontaneous increases in gas pressure is indicative of highly unstable flow pathways, which collapse due to very minor changes in gas pressure or effective stress. It would seem that our observations of Section 2.21 on the likely instability of thin gas films are confirmed by the experiments.

The remainder of T2S1-G (Figure 9) represents a preliminary examination of the roles of effective and total stress in determining breakthrough and peak excess gas pressures. A constant pumping rate was maintained throughout. The first sharp drop in differential pressure coincides with the application of 0.40 MPa positive increment to both water pressure and confining pressure. The drop in differential pressure ($p_{gi} - p_{wo}$) is solely a response to the rise in water pressure p_{wo}. The application of the additional confining pressure completely shuts off the gas flow in the specimen. As differential pressure builds-up there would appear to be some intermittent gas flow, but the main breakthrough appears to the left of the peak ($p_{gb} < p_{gp}$). Shortly after the peak, the water and confining pressure were again raised by 0.40 MPa. Differential pressure and gas flow respond in the usual manner and we observe another peak, followed by a negative transient. This procedure was then repeated, this time with positive increments of 0.60 MPa. Due to inadvertent failure to switch on the data logger, the pressure ramp is missing from the record. However, the logger was re-started early enough to capture the response close to the peak. In the final part of this experimental history the total stress was raised by 0.40 MPa while the water was held at its previous value. There is no significant drop in differential pressure and the curve climbs away to a new peak which is significantly higher than all previous values of p_{gp} for this specimen.

Inspection of the peak excess gas pressures of Table 5 for the stages of T2S1-G identified by the letters c, d and e reveals that p_b is a more or less a fixed fraction of the effective stress. For this particular test we can write

$$p_p = (p_{gi} - p_{w0})_p \approx 0.85\,(\sigma - p_{w0}) \qquad (67)$$

where σ is the total stress on the specimen. For the last stage of this test (marked f), the numeric factor on the right of Equation (67) falls to about 0.81. This suggests that p_p is functionally dependent on the effective stress acting on the material.

The final experimental history of the series, T3S1-G (Figure 12), with flow parallel to bedding, provides a very good illustration of the overall behaviour of the Boom Clay. This history exhibits a very pronounced peak, followed by the usual spontaneous negative transient. There is some evidence of a slow upward drift in differential pressure in the latter part of the transient. Inspection of the plot of flow-rate into the system versus time reveals that we then stopped pumping (i.e. set C = 0) and monitored p_g against time. Using the terminology of Section 2.12, the equilibrium or "shut-in" excess gas pressure ($p_{gq} - p_{w0}$) is 0.64 MPa in this particular test.

Gas flow was then re-instated at the same rate as before and pressure climbed to a broad peak followed by another spontaneous negative transient. It should be noted that flow out of the specimen continued through the re-pressurization period. The new post-peak steady-state excess gas pressure is considerably higher than the original. The test was then completed with a final stage of "shut-in" (C = 0) in which the pressure declined towards an equilibrium pressure close to the original value.

8.2 Processing of data for gas flux into the specimen

Figure 14 shows the results for history T3S1-G of the more complex data processing procedure which yields the volumetric flow of gas (STP) directly into the specimen Q_i and the emergent flow of gas Q_o (STP) from the downstream end. It is very clear from this plot that the flow into the specimen is approximately equal to the flow out at all points along the history. Our assertion that the monitored downstream flow was predominantly gas is borne out by the new processing.

A very important conclusion from these results is that Q_o can be directly related to $(p_{gi} - p_{wo})$ for all points of the history after breakthrough. Expressed in another way, it means that the entire history can be processed to find the relationship between gas flow and gas pressure gradient. This would not be true if duration of true gas flow transients associated with changes in flow-rate through the specimen were long in comparison with the time-scale of our experiments. The duration of the negative transients seen in our experiments is primarily determined by V_{sys}, the instantaneous volume of helium in the injection system, and not by the volume of gas stored in the specimen.

8.3 Magnitude of excess gas pressures at breakthrough and peak

Table 6 shows the ratio of the excess gas pressure at breakthrough p_b and at the peak p_p to the effective stress acting in the specimens before gas injection. Values for flow parallel to bedding are noticably higher than those for flow normal to bedding.

Test No.	Effective stress σ_{eff} (MPa)	Ratio of p_b to σ_{eff}	Ratio of p_p to σ_{eff}
T1S1-G	2.22	0.55	0.57
T2S1-G	2.22	0.85	0.85
T2S2-G	2.22	0.87	0.87
T2S3-G*	2.19	0.21	0.21
T3S1-G*	2.19	0.46	0.47

Table 6 - Ratios of excess pressure at breakthrough and peak to the effective stress acting in the specimens before gas injection. Tests with gas flow parallel to bedding are marked (*).

Ratios for T2S1-G and T2S2-G are very high and indicate that gas entry normal to bedding into this material would require very high near-field gas pressures ($p_g > 0.92\ \sigma$). Given that the gas will always follow the weakest path, then it is seems certain that gas would tend to follow the bedding planes rather than move in a direction normal to bedding.

Spatial variability of the gas flow parameters is an exceedingly important issue. If T2S3-G is representative of the lower limits of the distribution of p_b and p_p, then it is clear that the gas would tend to migrate horizontally along the horizon represented by this specimen. However, given the relatively small number of (very time-consuming) experiments, we have no evidence that this particular test does lie at the lower limit of the distribution. It would appear that this problem can only be resolved with any confidence by performing *in situ* injection tests in the same depth interval as a possible future repository.

8.4 Empirical relationship with intrinsic permeability

Given that intrinsic permeability and excess gas pressure at breakthrough both show strong anisotropy in the Boom Clay, it seems worthwhile to examine whether the two parameters can be correlated. In Figure 15 we superimpose our data on a plot of $\log(p_b)$ versus $\log(k_i)$ which was presented by Thomas et al. (1968). The original data shown on this plot are from experiments on a variety of "tight" consolidated rocks, including limestones and sandstones. The intrinsic permeabilities for Boom Clay are corrected to *in situ* stress conditions using Equations (58) and (59). The data points for the clay lie consistently below those for the consolidated rocks and can be reasonably represented by

$$p_b = (p_{gi} - p_{wo})_b = 1.694 \times 10^{-7} \left(\frac{1}{k_i}\right)^{0.357} \quad (68)$$

where p_b is expressed in MPa and k_i in m^2. This relationship is valid for both directions of flow provided that appropriate values of intrinsic permeability are used. It is important to correct the permeability to the appropriate effective stress conditions. The exponent for the consolidated rocks was determined to be 0.43.

There are several reasons for the disparity between the data for clay and those for consolidated rocks. Inspection of Equation (20) shows that the entry pressure should be raised by an amount $\Pi_m - \Pi_e$ due to the osmotic pressure at the midplane between clay particles. However, we have already emphasised that, if this pressure is too high and the local stresses exerted by the gas exceed the tensile strength of the clay, the newly-formed gas pathway will dilate. The pathway half-thickness a_p in the capillary term of Equation (20) will then be substantially greater than the undeformed radii of the clay pores. The capillary term will therefore be substantially lower than it would be in a rock with high tensile strength. It would appear that pathway dilation has an overriding effect on entry and breakthrough pressures in a clay. This suggests that the gas entry criterion should be expressed in terms of stress state rather than pore size distribution.

8.5 Post-test saturations

Post-test water saturations S_{wa} were determined from post-test moisture contents w_a using the relationship

$$S_{wa} = \frac{(1 - n)\, w_a \rho_g}{n\, \rho_w} \quad (69)$$

where n is the fractional porosity, ρ_g is the grain density of the mineral solids and ρ_w is the density of water. Parameters n and ρ_g were established by testing fresh clay samples. Values are given in Table 7. In viewing these figures, it is important to note that (a) the post-test samples were destressed at the time of removal from the pressure vessel and may have lost some of their gas content, and (b) saturation estimates from routine water content measurements are generally imprecise and second decimal place accuracies are optimistic. Sample T2S3-G and T3S1-G actually showed slight increases in water content from the pre-test to the post-test condition and we enter values of approximately 1.0 as their post-test water saturations.

Nevertheless, the results clearly demonstrate that large volumes of gas can be pumped through the Boom Clay without any major decrease in water saturation. This strongly contradicts the suggestion by Lineham (1989) that nearly all the water in a clay specimen is displaced during gas injection.

Test No.	Fractional Porosity n	Post-test Water Saturation S_{wa}	Total STP Gas Volume Injected 10^{-3} (m^3)	Excess Gas Pressure at Breakthrough P_b (MPa)
T1S1-G	0.40	0.96	1.94	1.27
T2S1-G	0.38	0.99	1.33	1.87
T2S2-G	0.39	0.99	4.99	1.93
T2S3-G*	0.37	≈ 1.0	2.70	0.47
T3S1-G*	0.39	≈ 1.0	3.54	1.02

Table 7 - Results of saturation tests on post-test gas injection specimens, showing total gas volume injected through each sample at STP and excess gas pressure at breakthrough for comparison. Tests with gas flow parallel to bedding are marked (*).

If we examine results for flow normal to bedding, we note that T1S1–G has the lowest breakthrough pressure of the set and displays the highest gas saturation. In contrast, T2S1–G and T2S3–G show high breakthrough pressures and exhibit exceedingly low gas saturations. As we noted above, T1S1–G showed evidence of gas flow in advance of the excess gas pressure peak. We will explore the reason for this behaviour later.

8.6 Gas flow

Figure 16 shows a plot of the STP volumetric flow-rate Q_o out of T2S2–G against the differential pressure (p_{gi} - p_{wo}) for the entire post-breakthrough experimental history of this test. The time-averaging procedure has been applied to the later stages of the history to distinguish the underlying trend in a data set which exhibits intermittent ("burst-type") flow behaviour.

One important observation is that the steady-state excess gas pressures p_s of Table 5 can be perfectly superimposed on this plot. The continuity of the curves between individual steady-state data points, together with the findings of Section 8.2, leads us to conclude that these curves describe the functional relationship between Q_o and differential pressure ($p_{gi} - p_{wo}$) over a succession of steady-states.

The very short duration of gas flow transients is indicative of low levels of gas saturation, minimum storage of gas in the specimen and very little displacement of water during gas flow. We regard this as additional evidence that gas moves along a number of fairly direct pathways linking the upstream and downstream ends of each sample.

For a history of decreasing applied flow-rate, the plot of Q_o against differential pressure $(p_{gi} - p_{wo})_s$ drops away from the point of breakthrough p_b to approach zero flow-rate at some finite value of differential pressure. This curve does not approach the zero flow-rate

condition in an asymptotic manner. Rather, it would appear to asymptotically approach some small, finite value of flow-rate. Cessation of flow would appear to be very abrupt at the critical value of $(p_{gi} - p_{wo})$ which is identified as the "capillary threshold" in Figure 16.

For the subsequent history of increasing pumping rate, the plot of Q_o against differential pressure follows a very different path which gradually rises, with minimal curvature, towards the secondary pressure peak at a differential pressure of 1.75 MPa. At this peak, the resistance to flow spontaneously decreases. The curve loops back on itself and differential pressure $(p_{gi} - p_{wo})$ then falls away again as flow-rate is progressively reduced. The curve eventually rejoins the post-breakthrough curve.

We may conclude that some form of irreversible change occurs to the gas pathway during the first history of decreasing flow-rate. After breakthrough, it is not possible to re-establish a differential pressure equivalent to the breakthrough pressure, even if the maximum flow-rate is applied. Subsequent cycles of increasing and decreasing flow-rate are characterised by hysteresis of the Q_o against differential pressure relationship. Although the results are not yet totally conclusive, it would appear that repeated cycles would follow a unique hysteresis loop.

Figure 17 shows the equivalent plot for history T3S1-G with flow parallel to bedding. The initial descent from breakthrough to the "capillary threshold" in this test is far more linear than it was in Figure 16. As we noted previously, the threshold is exceptionally well-defined at a differential pressure of 0.64 MPa. When pumping is restarted, there is little or no flow until differential pressure exceeds 0.83 MPa. The curve then climbs almost parallel to the post-breakthrough curve and reaches the secondary peak at 0.95 MPa. During the second "shut-in" period, flow drops away to zero at a differential pressure very close to the original threshold value of 0.64 MPa. Other than the fact that the secondary peak is lower than the initial peak, there is less evidence in this test for post-breakthrough irreversible changes in the flow-path. This variability in behaviour from specimen to specimen presents significant difficulties when we attempt to quantify the overall response of the clay.

8.7 Zero flow-rate or "shut-in" condition

Analysis of the zero flow-rate or "shut-in" condition provides a convenient starting point for the quantitative analysis of the data. Equation (39) shows that a test sample will exhibit zero gas flow-rate when

$$k_{rg} = 0 \qquad \text{and} \qquad \frac{dp_g}{dx} = 0 \tag{70}$$

Cessation of flow is caused by the collapse of the flow pathways when the gas pressure falls below some minimum value. As we already noted, the most critical point for collapse of a pathway is probably the point of emergence of the gas at the downstream end of the specimen. Based on Equation (48) we can therefore write

$$Q_0 = 0 \quad \text{when} \quad (p_{gi} - (p_{w0} + p_{co})) = 0 \tag{71}$$

where p_{co} is the "soil suction" at the downstream end. Assuming very low gas saturations, Equation (42) gives

$$p_{co} \approx R_m - A_m - \Pi_e \tag{72}$$

which is equivalent to

$$p_{co} \approx \frac{2\,\tau_{gw}}{a_{pq}} + R_m - \Pi_e \tag{73}$$

Since the the osmotic pressure Π_e of our synthetic pore solution is about 0.04 MPa, we can estimate $R_m - A_m$ either directly from shut-in data or by extrapolating cross-plots of Q_o against $(p_{gi} - p_{wo})$ to zero flow-rate. Values are presented in Table 8. As a first approximation, we can estimate $R_m - A_m$ from the swelling pressure determined in a one-dimensional swelling test, conducted under zero volume change conditions with pure water as the reservoir fluid. Horseman et al. (1993) performed two tests of this type on Boom Clay and determined values of 0.82 and 0.92 MPa. Acknowledging the obvious directional variability of $R_m - A_m$, the values presented in Table 8 are reasonably consistent with swelling data. This table also shows calculated values for the α parameter of Equations (28) and (29).

Test No.	Downstream "Soil Suction" at Shut-in p_{co} (MPa)	Net Physico-chemical Repulsive Stress $R_m - A_m$ (MPa)	Parameter α Equations (28) & (29) $(R_m - A_m + p_{w0}) / \sigma$
T1S1-G	1.00	1.04	0.71
T2S1-G	1.11	1.15	0.75
T2S2-G	1.11	1.15	0.75
T2S3-G*	0.34	0.38	0.56
T3S1-G*	0.64	0.68	0.65

Table 8 - Best estimates of "soil suction" at the zero flow-rate condition, the net physico-chemical repulsive stress $R_m - A_m$ (reference to pure water) and parameter α. Tests with gas flow parallel to bedding are marked (*).

8.8 Steady-state flow parameters

Based on the assumption that p_{co} is constant over the test history of each specimen , we are in a position to calculate the steady-state flow parameters using Equation (46). Our methodology for calculating intrinsic permeability k_i was described in Section 7.4. The results of these calculations are presented in Table 9.

The product $k_{rg}.k_i$ is the gas permeability (m^2) of the clay and is the more important experimentally-determined quantity. Like permeability to water, permeability to gas is significantly larger parallel to bedding than it is normal to the bedding plane. This emphasises our comments on the probable direction of gas migration.

Relative permeability k_{rg} is generally greater than 1 for all the pumping rates used in our experiments. Given the very low gas saturations, this provides positive proof that gas does not move in the same pore channels as water. If this were the case, then $k_{rg} = 1$ would only be achieved when water saturation $S_{wa} = 0$.

Inspection of Table 9 reveals a fairly systematic change in gas permeability from one steady-state flow-rate to another. This could be explained exclusively in terms of pathway aperture sensitivity to local gas pressure, leading to dilatancy as pressures increase and closure as pressures fall. However, we must not rule out the possibility that the lateral extent of each pathway changes with pressure or that the number of pathways conducting gas depends on pressure. It is quite possible that aperture, width and number of pathways are all variables in this problem.

Guided by the behaviour of the clay during hydraulic testing, it seems reasonable to expect the gas permeability to show a functional dependency on effective stress. However, the appropriate measure of local effective stress during gas flow would seem to be $(\sigma - p_g)$. In unsaturated soil mechanics this is referred to as "net mean stress" and, for the lack a more self-explanatory name, we will adopt this terminology. Net mean stress can be calculated at the mean gas pressure $\bar{p}_g$ in the specimen as follows

$$(\sigma - \bar{p}_g) = \sigma - \left(\frac{p_{gi} + p_{go}}{2}\right) \qquad (74)$$

This quantity should be indicative of the tendency of the gas pathways to dilate or close with changes in gas pressure. Values are given in the last column of Table 9. Comparison between gas permeabilities and net mean stress values does suggest some degree of dependence of the former on the latter.

In Figure 18 we plot $k_{rg}.k_i$ against net mean stress $(\sigma - \bar{p}_g)$ at mean gas pressure for experimental history T2S2. This plot is generated by cross-plotting the entire data set and contains many thousands of data points. Although there is a substantial amount of experimental noise in the data, the underlying trend can be clearly distinguished. In order to emphasise this trend we have sketched in the trend-lines and marked important points in the plot with the letters A through F. We surmise that the aperture of gas pathways increased considerably between gas entry and breakthrough. This region cannot be resolved in our experiments. Excess gas pressures at breakthrough and at the primary peak were the same in this test and the point of breakthrough is identified by the letter A. The specimen exhibits the highest gas permeability immediately after breakthrough. Permeability then decreases with increase in $(\sigma - p_g)$ along the line A–B. A number of our steady-state "picks" of Table 5 lie on, or close to, this line.

Test and Stage No.	Volumetric Flow-Rate at STP Q_i 10^{-10} ($m^3.s^{-1}$)	Upstream Gas Pressure p_{gi} (MPa)	Downstream Gas Pressure p_{go} (MPa)	Gas Permeability $k_{rg}.k_i$ 10^{-20} (m^2)	Relative Permeability k_{rg}	Net Mean Stress $\sigma - \bar{p}_g$ (MPa)
T1S1-G375	32.6	3.41	3.18	24.5	8.9	1.11
T1S1-G90	7.6	3.31	3.18	10.5	3.8	1.16
T1S1-G45	3.9	3.36	3.18	3.8	1.4	1.13
T2S1-G375	37.5	3.92	3.30	9.2	3.4	0.79
T2S2-G375	34.9	3.65	3.30	15.8	5.8	0.93
T2S2-G180	16.4	3.57	3.30	9.7	3.6	0.97
T2S2-G90	7.9	3.46	3.30	8.1	3.0	1.02
T2S2-G45	3.9	3.44	3.30	4.6	1.7	1.03
T2S2-G22	1.9	3.37	3.30	4.5	1.6	1.07
T2S2-G12	1.0	3.32	3.30	8.4	3.1	1.09
T2S2-G375	3.7	3.83	3.30	10.7	3.9	0.84
T2S2-G180	1.7	3.61	3.30	8.5	3.1	0.95
T2S2-G90	8.01	3.49	3.30	6.8	2.5	1.01
T2S3-G375*	24.9	2.60	2.56	66.7	2.2	1.82
T3S1-G375*	29.0	3.03	2.85	15.1	0.5	1.46

Table 9 - Analysis of steady-state gas flow, showing volumetric flow-rate Q_i at STP, upstream gas pressure p_{gi}, downstream gas pressure p_{g0} based on constant downstream capillary pressures, gas permeability $k_{rg}.k_i$, relative permeability k_{rg} and net mean stress (σ - p_g). Tests with gas flow parallel to bedding are marked (*).

We might infer from this trend that the aperture of the flow pathways is actually decreasing as we approach B. At point B, we encounter the "capillary threshold" which is marked as a dashed vertical line: Gas flow ceases instantaneously as the flow pathways collapse. When we attempt to re-establish gas flow by pumping, we move along path B-C. Interestingly, the gas permeability is sensibly constant for a while, suggesting that pathway aperture does not increase with decreasing (σ - p_g) in this region. At point C there is clear evidence of a rapid increase in permeability and pathway aperture. The curve passes through the secondary peak at D. Beyond point E, gas flow occurs at more or less constant permeability until we reach F. Section F-B appears to be coincident with the original path A–B.

The functional relationship between $k_{rg}.k_i$ and net mean stress for the post-breakthrough curve A–B has a similar form to the hydraulic conductivity relationships of Figure 5. A visual fit gives

$$\log_{10}(k_{rg}.k_i) = -3.807\,(\sigma - \bar{p}_g) - 15.381 \qquad (75)$$

where k_i is expressed in m^2 and stresses and pressures are in MPa.

This relationship applies to flow normal to bedding. For comparison, the sensitivity of k_i to effective stress (σ - p_{wo}) during hydraulic testing is obtained by combining Equations (58) and (62) and leads to

$$\log_{10}(k_i) = -1.877\,(\sigma - p_{w0}) - 15.438 \qquad (76)$$

for flow normal to bedding. The similarity between these two independently quantified relationships is quite remarkable. It suggests that there is a very fundamental control mechanism for gas permeability. We have yet to explore this complex matter in any detail.

8.9 Intermittent gas flow

Intermittent flow is, perhaps, the most complex aspect of gas movement in Boom Clay. If we examine history T2S2-G (Figure 10), then it apparent that gas flow immediately after breakthrough is continuous but that all subsequent stages of the experiment exhibit intermittent "burst-type" flow. Other test histories reveal a broadly similar picture.

One of the difficulties in analysing "burst-type" flow is that we must be able to distinguish "system effects" from true "material effects". Our testing apparatus incorporates a number of servo-controllers which continually adjust flow-rates and pressures to their pre-set values. We know that the response times of these electro-mechanical units are very short; typically less than 2 seconds for minor perturbations. We are confident that control system dynamics cannot account for the behaviour seen in the experiments.

The logging rate of the data acquisition system in most experiments was set at 1 scan per 30 minutes and, not surprisingly, many of the bursts seen in processed downstream flow data have an apparent duration of 30 minutes. In one stage of a T2S2-G, with at a time-average flow-rate of 3.9×10^{-10} m^3.s^{-1} (STP), we logged at the fastest possible rate of 1 scan per 3 seconds. We found that the shortest bursts were typically from 6 to 9 seconds in duration and were separated by "quiescent periods" in which there was no emergent gas flow. These quiescent periods varied from 6 seconds to around 400 seconds. A typical burst at this stage of the experiment contained about 6×10^{-8} m^3 (STP) of gas. The mean gas pressure inside the specimen was about 3.4 MPa, so the actual volume of a typical burst at this stage was around 2×10^{-9} m^3. This is the volume of a slot-shaped gas pathway extending the full length of the specimen (4.9×10^{-2} m), with an aperture of 2×10^{-5} m and and a width of 2×10^{-3} m. We note that a pathway with these dimensions would offer minimal capillary resistance to gas flow and, according to Equation (73), the downstream "soil suction" p_{co} would be largely determined by the R_m (osmotic repulsion) term.

As we have already noted, because of the intermittent nature of gas flow over most of our experimental histories, the "steady-state condition" is achieved when the mass of gas crossing any cross-section per second, averaged over a sufficient time span, remains constant with the passage of time. If the average mass of gas released in a burst is m_{ave} and there are an average N_{ave} bursts per unit time, the steady-state mass flux becomes

m_{ave}. N_{ave}. An initial assessment of data suggests that both of these terms change when pumping rate is altered (see, for example, Figure 13).

We believe, in the absence of any real proof at this stage, that the frequency of the bursts N_{ave} will depend, in part, on specific details of the experimental set-up. Three important parameters are the volume of compressed gas in the injection system, the rate of pumping and the length of the sample. The dynamics of gas flow are probably determined by a complex interaction between these experimental variables and the intrinsic gas flow behaviour of the clay medium. Intuitively, very long flow paths and very small applied flow-rates would lead to very low values of N_{ave}.

It is possible to explain intermittent flow in terms of gas pathway propagation and collapse. When a discrete gas pathway reaches the downstream end of the specimen, its internal pressure must drop sharply as it releases gas. Since thin films of gas are inherently unstable, this drop in pressure will cause parts of the pathway to collapse. After some period of time, which is a function of the system variables, the pressure at the upstream end of the specimen will rise sufficiently for the pathway to reform and propagate to the downstream end, leading to cyclical behaviour. The authors have compared this behaviour with a pan of simmering porridge. Steam bubbles form at the base of the pan and move upwards, deforming the gelatinous medium as they go. When they reach the surface they lose pressure and collapse completely. A new bubble then forms, possibly at another location, and the cycle repeats. We believe that this analogy is very close to the true behaviour of gas in the clay, although we emphasise the difference in scales. Porridge and clay are both colloidal suspensions in water and there is little doubt that the rheological properties of these media influence the movement of the gaseous phases.

Our scoping calculations indicate that further processing of intermittent flow data is worthwhile. It may be possible to systematically quantify the volume and number of flow paths within the clay under any particular flow conditions. We have already made the first step by applying Fourier waveform analysis to a small subset of the data. Further interpretational effort is necessary before these additional results can be reported.

8.10 Number of gas pathways

One basic requirement in modelling gas migration is an estimate of the number of active gas pathways penetrating the host-medium. Scale is, of course, a very important consideration and the problem cannot be fully resolved by laboratory experiments.

Given the generally low levels of gas saturation at the end of our tests, the obvious propensity for capillary fingering, the occurrence of intermittent flow at almost all applied flow-rates and the very sharp cessation of flow at the "capillary threshold", we are fairly confident that gas moves along a relatively small number of discrete pathways. However, one specimen out of the five tested did show measurable desaturation, and it is possible that gas flow is slightly more disperse in this specimen. We might expect to see a gradual

transition in behaviour from pathway-type flow to this more disperse form of flow as silt and sand content increases and clay content decreases.

9 CONCLUSIONS

9.1 Gas migration

Our study has aimed to provide a conceptual model of gas phase transport in clay. We start from the fundamental soil science concept of the total potential of the soil water. This quantity represents the amount of work per unit mass of pure water that must be expended to transfer water, isothermally and reversibly, from a defined reference state to the pore space of the clay-medium. In clay soils, the total potential of the soil water has three main components, the first gravitational, the second osmotic (due to the presence of solutes) and the third associated with the pressure difference between the reference state and the pore water. Our reasoning in following this approach is straightforward. If we attempt to displace unit mass of pore water by an equivalent volume of gas, then the amount of work performed in this operation must be *at least* equal to the sum of the work expended in (a) raising the pressure of the gas relative to an appropriate reference pressure, (b) moving the water from its initial location to its new location and (c) creating an interface between the two phases. Contribution (b) is calculated as the difference between the total potentials of the soil water at the two locations.

Although the concepts are clear, the quantitative treatment of this problem is far from trivial. The complications arise when we examine the way in which a compact clay carries the load of the overlying sediments. There is broad agreement that the total stress in a clay is borne partly by mineral-mineral contacts, partly by water pressure and partly by physico-chemical forces acting between the clay particles. We have chosen to represent the balance of forces by an equation first proposed by Lambe (1960). The physico-chemical forces have at least two components, the first a repulsion between particles and the second an attraction. Despite very intensive research over the years on the forces between clay minerals, there is still no totally satisfactory explanation of their origin. One popular model for the repulsion is based on the interpenetration, at small interparticle separations, of the Gouy-Chapman adsorbed double layers. The repulsive stress is calculated as the difference between the osmotic pressure of the cation-dominated midplane solution and the osmotic pressure of an external solution which is in equilibrium with the medium. We point out that there are alternative theories. The attraction between clay minerals is often attributed to London - van der Waals forces, with possible contributions from hydrogen bonding. These are the fundamental forces of cohesion between water molecules. Work on colloids suggests that, at small interparticle separations, water molecules can act "in concert" to produce an attraction between the particles.

An important point which emerges from studies of clay-water-solute systems is that the aqueous phase between clay minerals actually transmits a very significant part of the total stress acting on the clay medium. The actual proportion of the stress carried by interparticle

water is given by parameter α (Croney and Coleman, 1953), which we have shown experimentally to be as high as 75% for Boom Clay.

Returning to our original problem of displacing the water in thin films between clay particles by an equivalent volume of gas. Since the gas phase can neither develop nor transmit the physico-chemical forces of repulsion and attraction acting across water-filled interparticle spaces, then it is unable to occupy these spaces until its pressure is at least equal to $\alpha\sigma$ where σ is the total stress. Our calculations suggests that the quantity $\alpha\sigma$ is actually the equilibrium pressure of a gas phase in a clay-medium at low levels of gas saturation.

If the gas pressure exceeds $\alpha\sigma$ at any point in the clay-medium, then there must be a local imbalance of forces. We suggest that there is a tendency for the volume of gas to increase by pushing back the clay particles and displacing water from adjacent interparticle spaces. With no additional gas flow, the system will re-equilibrate with the gas pressure once again equal to the product $\alpha\sigma$. This observation provides the basis of our explanation of gas entry. In order for gas to enter the clay its pressure must exceed the "local pore pressure" by an amount equal to the maximum pressure drop across the gas-water meniscus at the mouth of the largest pathway. Although there are some reservations about the validity of the Young-Laplace equation when applied to very narrow interparticle spaces, we assume that gas entry would normally occur when the radius of curvature of the meniscus is equal to the half-thickness of the critical flow pathway. If the pore size distribution of the medium is such that excessively high gas pressures are necessary to overcome capillarity, then the gas pressure will simply force the clay minerals apart. We call this process "pathway dilation" but note that there are close similarities with the processes of microcrack initiation and propagation. Gas will enter a dilated pathway at a pressure which is lower than we might anticipate from the pore sizes and "local pore water pressures".

Provided that the gas pressure continues to rise then it is possible for additional dilated pathways to form. These will propagate through the medium following routes which lead to a continuous lowering of the pressure (or free energy) of gas near the tip of the pathway. There are a number of possible controls on the direction of propagation: (a) anisotropy of the clay fabric, (b) anisotropy of the stress field, (c) pore water pressure gradients, (d) stress gradients, (e) lithological variability, and (d) fissuring. It is premature to say which of these will have the dominant effect.

When the stress field in the clay is both uniform and isotropic, as it is in our experiments, then the gas will probably move along the bedding planes. Test results indicate that the excess gas pressure for gas entry $(p_g - p_w)_e$ is lower parallel to bedding than it is normal to bedding and that the effective gas permeability of the clay is significantly higher for flow along the bedding planes. Ease of pathway dilation provides a probable explanation.

If the stress field is not isotropic but the clay is sensibly homogeneous, then gas pathways will tend to propagate in a plane which is normal to the minor principal stress.

Furthermore, there will be a strong tendency for pathways to follow a direction which coincides with the maximum stress gradient, with the gas moving down gradient. In simple terms, the pathway attempts to lower the combined-stress (3-D) equivalent of the $\alpha\sigma$ term. Since we have not investigated the effect of anisotropic stress and stress gradients, it is difficult to assess whether fabric anisotropy or stress would exercise the dominant control on the direction of gas migration in a homogeneous bed of clay.

The tendency for gas to move down the maximum gradient of pore water pressure ($p_w + \Pi$) is probably overridden by the other factors. It seems entirely possible that water may move in one direction in a clay host-medium and that gas may move in an entirely different direction.

Lithological variability, is difficult to assess in the laboratory unless very careful attention is paid to sampling strategy. We have detected variability from sample to sample of Boom Clay but, given the relatively small number of experiments, we are unable to comment on the true extent of this variability. We would argue that in most bedded clay sequences there are likely to be horizons with lower than average clay content. Since entry pressure will decrease and effective gas permeability will increase with decreasing clay content, it seems likely that gas migration would be focused along these horizons. We have no specific information on Boom Clay with which to judge this issue.

We have made only brief reference to fissuring in overconsolidated clays. This is an issue that cannot be properly addressed in laboratory testing. Fissures, if present at typical repository depths, are likely to be "incipient features" with little or no aperture. Even then, we can see no real reason why they should not form preferential routes for the propagation of dilatant gas pathways. It is debatable whether these features would exercise any real control on the direction of gas migration at the larger scale (< 1 m, or so).

The propagation of a gas pathway ceases when it encounters a medium with large pores that can accommodate normal-2-phase flow. In our laboratory experiments, this medium is represented by the porous bronze disc at the downstream end of the specimen. An important experimental finding is that the gas pathways are inherently unstable. If they lose pressure they collapse and gas flow ceases. In the laboratory this leads to intermittent "burst-type" flow. The periodicity of the "bursts" depends on system variables and the properties of the clay.

It is possible that gas migration around a repository will show very similar characteristics. The rate of propagation of gas pathways in the clay host-medium would then depend on the gas production rate. As in the laboratory, these pathways would be highly unstable. If they were to move upwards, then they would dilate as total stress gradually decreases. Any drop in pressure would temporarily arrest their progress. On reaching a medium with large pores (e.g. a sand or sandstone) there would be a tendency for the gas to exhibit intermittent flow. A key factor governing the overall dynamics of the system is the amount of gas stored in void space in the repository near-field. With efficient backfilling, this void

space would be minimal and the energy necessary to support pathway propagation would be very limited. Under these circumstances propagation would probably be very slow and the "time-constants" determining the periodicity of the process would be lengthy.

Our tentative scoping calculations suggest the a dilated gas pathway in Boom Clay under typical *in situ* stress might have an aperture of around 20 μm. We are confident that we can refine this initial estimate. Figure 19 is a sketch of a typical pathway moving sub-parallel to bedding. These thin gas films are so unstable that that they collapse when subject to only minor reductions in gas pressure, flow-rate or temperature. Over a sufficient time period, the gas in residual films left after pathway collapse would tend to diffuse away. Some time after the the gas migration phase, the only evidence of the passage of gas in a plastic clay would be imperceptibly small regions of clay fabric deformation. These are very unlikely to affect groundwater or solute transport in the host-medium. We emphasise that the long-term impact of gas transport is likely to vary with the state of induration of the formation. This is likely to be minimal in a plastic clay, but could be more important in a clay-shale.

Figure 20 is intended to summarise our main findings on gas migration in Boom Clay. We define three zones of behaviour on the basis of the principal mechanism of gas transport in each zone. We relate these zones to the curve of total soil suction against water saturation for the clay. This is the "water retention curve" for a desorption or drainage history. Our choice of total suction, as the appropriate parameter for this plot was justified in Section 2.12. To the right we show a scale of the typical half-spacing between clay particles (before gas entry). We could have equally well identified this scale as "water film half-thickness".

In the lower part of the diagram we plot the relative permeability curves for gas k_{rg} and water k_{rw} against water saturation. Our choice of these "continuum parameters" is not intended to imply any advocation of the 2-phase flow modelling approach. We use relative permeabilities simply to provide an illustration of the overall behaviour.

In **Zone 1** the gas pressure is less than the sum of the excess gas entry pressure and the external equilibrium water pressure ($P_g < p_e + p_{w0}$) so the only gas transport mechanisms that can operate in the clay are associated with movement of gas molecules in solution. Fickian diffusion will be the dominant gas transport mechanism in this zone.

Zone 2 is only present in material with lower than average clay content. Gas flow commences when the threshold for gas entry into pores is exceeded. Only then is gas migration by 2–phase flow physically possible and may be accompanied by a small degree of desaturation. Based on our calculations of capillary number, stable displacement of water seems highly improbable. Depending on clay content, flow probably ranges from being fairly dispersed to being concentrated in a relatively small number of pathways. The overall flow pattern may display the "dendritic" arrangement typical of capillary fingering. The relative permeability to water k_{rw} will be little affected by the gas phase and will be close to unity. The relative permeability to gas k_{rg} will be very small. Gas pressure will

rise rapidly with small increases in gas saturation. Pathway dilation at high gas pressures may cause a sudden increase in gas permeability and the flow behaviour will then assume the main characteristics of Zone 3. This sudden change may correspond with a drop in pressure.

Zone 3 commences when the gas pressure exceeds the pressure necessary to cause pathway dilation. In material with high clay content, Zone 2 is absent and pathway dilatancy is a necessary pre-requisite for gas entry. Flow in this zone will occur predominantly along a small number of discrete pathways. Instability of these pathways will lead to the intermittent behaviour seen in our experiments. Relative permeability to gas will rise dramatically ($k_{rg} > 1$) with increasing gas pressure, as the aperture of the flow paths increase. We propose a relationship between gas permeability and net mean stress ($\sigma - \overline{p}_g$). It is physically impossible for the gas pressure to exceed the total stress σ. If gas pressures ever did approach this level, then the effective gas permeability of the medium would be enormous and flow would probably be focused in gas-induced macroscopic fractures. Since significantly large flows can be accommodated at much lower pressures, it is highly unlikely that this situation could ever arise.

9.2 Hydraulic flow

Our brief examination of the component potentials of the constituent water in a clay-medium leads us to suppose that water will move under both hydraulic and chemical potential gradients. Although we have not focused our attention on this phenomenon, coupled flow is well-known in clays and has been demonstrated in the laboratory on numerous occasions.

The key to a full understanding of water flow in clays lies in the complex interactions between the clay particles, water and solutes. If we consider the equilibrium state in a compact clay then we consider not only the equilibrium of the aqueous phase and its dissolved solutes but also the equilibrium of forces associated with the stress field. Based our simple treatment of this problem, we conclude that the pore water pressure at any fixed height varies continuously from point to point within the clay medium and is the sum of a "hydrostatic term" p_w and an "osmotic term" Π. It is not actually necessary to invoke osmosis as the cause of this phenomenon. A more general explanation would be that the additional pressure Π arises because water molecules are drawn into interparticle spaces because of a lowering of the chemical potential of water in these regions. Close to the clay particle surfaces the pressures are probably very large and there are local minima at the midplanes between particles.

In common with a number of other researchers, we believe that it is not possible to separate the p_w and Π terms when we consider the local water pressure in a compact clay. Furthermore, we must be very careful how we measure local water pressure. There is an accumulating volume of evidence to suggest that hydraulic measurements in compact clays are sensitive to the chemistry of the test fluid.

Our experiments on hydraulic flow in Boom Clay were intended to provide intrinsic permeability data for the interpretation of gas flow. The data exhibit a significant degree of nonlinearity between flow-rate and hydraulic gradient. Departures from Darcy's law, in the form of nonlinearities and thresholds, have commonly been reported and have been attributed to a wide variety of possible causes. The nonlinearities seen in our tests can be largely explained in terms of the very pronounced sensitivity of hydraulic conductivity to effective stress. We are confident that this sensitivity is due, not to the minor changes in void ratio or porosity which are occasioned by changes in effective stress, but to the changes in the fundamental forces acting on water molecules in the interparticle spaces. Since up to 75% of the total stress acting on the Boom Clay is borne by the aqueous phase, any change in stress state is likely to have an effect on the mobility of the water molecules which support these forces.

We have quantified the relationships between hydraulic conductivity and effective stress for flow normal and parallel to bedding. We confirm that, for comparable stress states, hydraulic conductivities parallel to bedding are significantly larger than those normal to bedding. If the results are extrapolated to *in situ* stress conditions, we find that these "small-scale" hydraulic conductivities are, in both cases, substantially lower than the commonly reported values for Boom Clay.

By the analysis of transient flow data we have obtained reasonable values for the specific storage of Boom Clay. This parameter also varies with effective stress and we have also quantified this relationship.

The stress-dependency of the hydraulic parameters has important consequences in field testing. If the testing procedure results in large excess water pressures being applied to a test section, then the effective stress in the clay will locally decrease and the measured hydraulic conductivity will be significantly larger than the true *in situ* value. In this context, we also draw attention to our comments regarding the chemistry of the test fluid since these are also pertinent to the specification of testing procedures. These considerations are likely to be most important when testing highly compacted clays (e.g. clay-shales) and may be far less of a problem when testing superficial deposits.

In mathematical modelling, it is a relatively simple matter to represent the functional dependency of hydraulic conductivity K, intrinsic permeability k_i and specific storage S_s on effective stress σ_{eff}, if the need arises.

REFERENCES

Agg, P.J., Moreton, A.D., Rees. J.H., Rodwell, W.R. and P.J. Sumner (1992). "NSARP reference document: gas generation and migration." NIREX Safety Studies Report NSS/G120, Harwell, Oxfordshire.

Aitchison, G. D. (1973). "The quantitative description of the stress-deformation behaviour of expansive soils." Proc. 3rd Int. Conf. Expansive Soils, Haifa, Israel, 1: 75-77.

Alonso, E. E., Gens, A. and A. Josa (1990). "A constitutive model for partially-saturated soils." Geotechnique, 40(3): 405-430.

Atkins, P.W. (1986). Physical Chemistry. W. H. Freeman and Company, New York.

Aziz, K. and A. Settari (1979). Petroleum Reservoir Simulation. Applied Science, London, 476 pp.

Bear, J. (1972). Dynamics of Fluids in Porous Media. Elsevier, New York.

de Beer, E. (1967) "Shear strength characteristics of the Boom Clay." Proc. Geotech. Conf. Shear Strength Properties of Natural Soils and Rocks, Oslo, 1: 83-88.

Bishop, A. W. (1959). "The principle of effective stress". Lecture delivered in Oslo, Norway in 1955, published in Teknisk Ukeblad, 106 (39):859-863.

Blight, G. E. (1961). "Strength and consolidation characteristics of compacted soils". Ph. D. Thesis, University of London, 217 pp.

Bolt, G. H. (1976). "Soil physics terminology." Int. Soc. Soil Sci. Bull., 49: 16-22.

Bolt, G. H. and R. D. Miller (1958). "Calculation of total and component potentials for water in soil." Trans. Am. Geophys. Union, 39(5).

Bolt, G.H. and P.H. Groenevelt (1969). "Coupling phenomena as a possible cause for non-Darcian behaviour of water in soil." Bull. Int. Assoc. Scientific Hydrology (IASH), 14(2): 17-26.

Bonne, A., Beckers, H., Beaufays, R., Buyens, M., Coursier, J., de Bruyn, D., Fonteyne, A., Genicot, J., Lamey, D., Meynendonckx, P., Monsecour, M., Neerdael, B., Noynaert, L., Voet, M. and G. Volckaert (1992) "The Hades demonstration and pilot project on radioactive waste disposal in a clay formation." CEC, Nuclear Science and Technology Series, Rept, EUR 13851 EN, Luxembourge.

Buckingham, E. (1907). "Studies in the movement of soil moisture." U.S. Dept. Agr. Soils Bull., 38: 29-61.

Chenevert, M. E. (1969). "Adsorptive pore pressure of argillaceous rocks." Proc. 11th Symp. Rock Mech., Berkeley, California,

Childs, E. C. and N. Collis-George (1950). "The permeability of porous materials." Proc. Roy. Soc. Am., 201: 392-405.

Corey, A. T. (1957). "Measurement of water and air permeability in unsaturated soils." Proc.Soil Sci.Soc. Am., 21: 7-10.

Corey, A. T., Rathgens, C. H., Henderson, J.H., and M.R.J. Wyllie (1956). "Three-phase relative permeability." Trans. SPE of AIME, 207: 349-351.

Cornell, D. and D. L. Katz (1953). "Pressure gradients in natural gas reservoirs." Trans. SPE of AIME, 198: 61-71.

Croney, D. and J. D. Coleman (1953). "Soil moisture suction properties and their bearing on moisture distribution in soils." Proc. 3rd Int. Conf. Soil Mech. Found. Eng., 13-18.

Dullien, F.A.L. (1979) Porous Media: Fluid Transport and Pore Structure. Academic Press, New York.

Edlefsen, N.E. and A.B.C. Anderson (1943). "Thermodynamics of soil water." Hilgardia, 15: 31-298.

Fredlund, D. G. and N. R. Morgenstern (1977). "Stress rate variables for unsaturated soils." ASCE J. Geotech. Eng. Div., 103(GT5): 261-276.

Fredlund, D. G. and H. Rahardjo (1993). Soil Mechanics for Unsaturated Soils. John Wiley, 517 pp.

Frenkel, H., J. O. Goertzen and J. D. Rhoades (1978). "Effects of clay type and content, exchangeable sodium percentage and electrolyte concentration on clay dispersion and soil hydraulic conductivity." J. Soil Sci. Soc. Am., 42: 32-39.

Fritz, S. J. (1986). "Ideality of clay membranes in osmotic processes : a review." Clays & Clay Minerals, 34(2): 214-223.

Gens, A. and E. E. Alonso (1992). "A framework for the behaviour of unsaturated expansive clays." Can. Geotech. J., 29: 1013-1032.

Graham, J. (1964). "Adsorbed water in clays." Rev. Pure and Appl. Chem., 14: 81-90.

Hale, A.H, Moody, F.K. and D.P. Salisbury (1993). "The influence of chemical potential on wellbore stability." SPE Drilling and Completion, September, 207-216.

Hardcastle, J. H. and J. K. Mitchell (1974). "Electrolyte concentration-permeability relationships in sodium illite-silt mixtures." Clays & Clay Minerals, 22(2): 143-154.

Homsy, G.M. (1987) "Viscous fingering in porous media". Ann. Rev. Fluid Mech., 19: 271-311.

Horseman, S. T., J. Alexander, and D.C. Holmes (1991). "Implications of long-term transient flow, coupled flow and borehole effects on hydrogeological testing in the Opalinus Clay - a preliminary study with scoping calculations." NAGRA Technical Rept. NTB 91–11, Baden, Switzerland.

Horseman, S. T., Winter, M. G. and D. C. Entwisle (1993). "Triaxial experiments on Boom Clay." In: The Engineering Geology of Weak Rock, 26th Annual Conf. Eng. Group Geol. Soc. of London, Leeds University. Balkema, Rotterdam, 35-43.

Hubbert, M.K. (1956). "Darcy's law and the field equations of the flow of underground fluids." Trans. SPE of AIME, 207: 222-239.

Hunter, R.J. (1991). Foundations of Colloid Science. Oxford Science Publications, Clarendon Press, Oxford (2 vols).

Jones. M.A. (1990). "Gas generation in deep radioactive waste repositories; a review of processes, controls and models." Rept. to UK Dept. Environment, DoE/HMIP/RR/90/086, W.S. Atkins Engineering Sciences Ltd., Epsom, Surrey.

Kallmann, H. and Willstätter (1932). Naturwissenschaften, 20: 952.

Kutelek, M. (1969) "Non-Darcian flow of water in soils (laminar region)." 1st IAHR Symp. on Fundamentals of Transport Phenomena in Porous Media, Haifa, Israel.

Lambe, T. W. (1960). "A mechanistic picture of shear strength in clay." Proc. ASCE Res. Conf. Shear Strength of Cohesive Soils, 555-580.

Langmuir, I. (1938). "The role of attractive and repulsive forces in the formation of tactoids, thixiotropic gels, protein crystals and coacervatives." J. Chem. Phys., 6: 873–896.

Lenormand, R., Touboul, E. and C. Zarcone (1988). "Numerical models and experiments on immiscible displacements in porous media." J. Fluid Mech., 189: 165-187.

Lever, D. A. and J. W. Rees (1987). "Gas generation and migration in waste repositories." Proc. OECD/NEA Workshop on Near-field Assessment of Repositories, Baden, Switzerland.

Lineham, T. R. (1989). "A laboratory study of gas transport through intact clay samples." NIREX Safety Studies Report NSS/R155, Harwell, Oxfordshire.

Low, P. F. (1961). "The physical chemistry of clay-water interactions." Adv. in Agron., 13: 269-327.

Low, P. F. (1979). "The nature and properties of water in montmorillonite-water systems." J. Am. Soil Sci. Soc., 43: 651-658.

Low, P. F. (1987). "The clay-water interface." Proc. Int. Conf., Denver, Clay Minerals Soc., 247-256.

de Marsily, G. (1986). "Quantitative Hydrogeology for Engineers." San Diego, Academic Press Inc.

Marshall, T. J. and J. W. Holmes (1979). Soil Physics. Cambridge University Press, Cambridge, 345 pp.

Martin, R.T. (1962). "Adsorbed water on clay: a review. " Proc. 9th Conf. Clays and Clay Min. Pergammon Press, New York, 28-70.

Matyas, E.L. and H.S. Radhakrishna (1968) "Volume change characteristics of partially saturated soils." Geotechnique, 18(4): 432-448.

Miller, R.H. and P.F. Low (1963). "Threshold gradient for water flow in clay systems." Proc. Soil Sci. Soc. Am., 27(6): 605-606.

Mitchell, J. K. (1976). Fundamentals of Soil Behavior. New York, John Wiley.

Mitchell, J.K. and J.S. Younger (1967). "Abnormalities in hydraulic flow in fine-grained soils." In: Permeability and Capillarity of Soils, ASTM Spec. Tech. Pub. 417, 106-141.

Mitchell, J. K., J. A. Greenberg and P.A. Witherspoon (1973). "Chemico-osmotic effects in fine-grained soils." J. Soil Mech. Found. Div. ASCE, 99: 307-322.

Neerdael, B. and P. Manfroy (1985). "Geotechnical characterization of clay at great depth and its connection to tunnel construction." Radioactive Waste Management and the Nuclear Fuel Cycle, 6(3-4): 293-312.

Olphen, van H. (1977). An Introduction to Clay Colloid Chemistry. New York, John Wiley.

Olphen, van H. (1975). "Water in soils." In: Soil Components 2 - Inorganic Components, Ed: J.E. Gieseking, Springer-Verlag, Berlin.

Ouvry, J.F. (1986). "Etudes physique et rhéologique des argiles congelées: application à l'argile profonde de Boom (Belgique)." Ph.D. Thesis, INPL (also produced as a report by BRGM, Orleans, France).

Pusch, R., Ranhagen, L. and K. Nilden (1985). "Gas migration through MX-80 bentonite." NAGRA Technical Report NTB 85-36, Baden, Switzerland.

Pusch, R., Hökmark, H. and L. Börgesson (1987). "Outline of models of water and gas flow through smectite clay buffers." SKB Technical Report 87-10, Stockholm, Sweden.

Pusch, R.. and Hökmark, H. (1990). "Basic model of water- and gas-flow through smectite buffers." Eng. Geol., 28: 379-389.

Quirk, J. P. and R. K. Schofield (1955). "The effect of electrolyte concentration on soil permeability." J. Soil Sci., 6: 163-178.

Ravina, I. and D. Zaslavsky (1972). "The water pressure in the electrical double layer." Israel J. Chem., 10: 707-714.

Rees, J.H. (1989). "Gas evolution and migration in repositories: current status." NIREX Safety Studies Rept. NSS/R262, Harwell, Oxfordshire.

Richards, L. A. (1928). "The usefulness of capillary potential to soil moisture and plant investigators." J. Agric. Res., 37: 719-742.

Richards, L.A. (1949). "Methods of measuring soil moisture tension." Soil Sci., 68: 95–112.

Richards, B.G. (1966). "The significance of moisture flow and equilibria in unsaturated soils in relation to the design of engineering structures built on shallow foundations in Australia." presented at the Symp. on Permeability and Capillarity of Soils, ASTM, Atlantic City, New Jersey.

Rodwell, W.R. and P.J. Nash (1991). "Mechanisms and modelling of gas migration from deep radioactive waste repositories." NIREX Safety Studies Rept. NSS/R250, Harwell, Oxfordshire.

Rosenqvist, I. T. (1959). "Soil-water systems." J. Soil Mech., ASCE, 85.

Scheidegger, A.E. (1960). The Physics of Flow through Porous Media. University of Toronto Press, Toronto.

Schofield, R. K. (1935). "The pF of the water in soil." Trans. Third Int. Congr. Soil Sci., 2: 37-48.

Schofield, A. and P.W. Wroth (1968). "Critical State Soil Mechanics." McGraw-Hill, London.

Schrauf, T.W. and D.D. Evans (1986). "Laboratory studies of gas flow through a single natural fracture." Water Resources Research, 22(7): 1038-1050.

Shainberg, I., R. Keren, Alperovitch, N. and D. Goldstein (1987). "Effect of exchangeable potassium on the hydraulic conductivity of smectite-sand mixtures." Clay and Clay Minerals, 35(4): 305-310.

Skempton, A.W. (1954). "The pore-pressure coefficients A and B." Geotechnique, 4(1) 143-147.

Skipper, N.T., Refson, K. and J.D.C. McConnell (1991). "Computer simulation of interlayer water in 2:1 clays." J. Chem. Phys., 94(11): 7434-7445.

Stallman, R. W. (1964). "Multiphase fluids in porous media - a review of theories pertinent to hydrological studies". U.S. Geol. Surv. Professional Paper No 411-e.

Stenhouse, M.J. and H. Grogan (1992) "Review of reactions of hydrogen and methane in the geosphere and biosphere." NIREX Safety Studies Rept. NSS/R262, Harwell, Oxfordshire.

Swartzendruber, D. (1962). "Modification of Darcy's law for the flow of water in soils." Soil Sci., 93: 27-29.

Terzaghi, K. (1943). Theoretical Soil Mechanics. John Wiley, New York.

Terzaghi, K. and R. B. Peck (1967). Soil Mechanics in Engineering Practice. John Wiley, New York.

Thomas, L. K., D. L. Katz and M.R. Tek (1968). "Threshold pressure phenomena in porous media." SPE J. (June): 174-184.

Thomlinson, M.J. (1988). "Migration of gases through argillaceous rocks - a literature review." NIREX Safety Studies Rept. NSS/R146, Harwell, Oxfordshire.

Vanderberghe, N. (1975). "A sedimentological study of the septaria clay of Boom (Rupelian age) in Belgium." Proc. Int. Congr. Sedimentology, Nice, France.

Vanderberghe, N. and E. van Echelpoel (1987) "Field guide to the Rupelian stratotype", Bull. Belgian Society for Geology, 96(4) 325-337.

Verwey, E. J. W. and J. T. G. Overbeek (1948). The Theory of Stability of Lyophobic Colloids. Elsevier, Amsterdam.

Voinis, S., J. Gago and W. Muller (1992). Modelling of gas generation (Pegasus Project). In: Haijtink, B. and T. McMenamin (Eds.) Proc. Progr. Meeting of Pegasus Project, CEC, pre-print volume, Brussels, June 11-12.

Worgan, K.J., Pearson, J. and T. Nunez-Menally (1989). "A review of modelling of gas migration in porous and fractured rock." Rept. to UK Dept. Environment, DoE/RW/89/101, Intera Sciences, Henley-on-Thames, Oxfordshire.

Wroth, C.P. (1971). "Some aspects of the elastic behaviour of overconsolidated clay." Proc. Roscoe Memorial Symp. on Stress-Strain Behaviour of Soils, Henley-on-Thames, published by Fowliss.

APPENDIX 1

Supplementary studies of clay fabric and mineralogy

As a component of the work on gas migration, the fabric of clay samples was examined, with particular emphasis on porosity, the preferred orientation of clay particles and the occurrence of microfissuring. This work was undertaken by Miss Cécile Javelle (formerly of the Ecoles des Mines de Paris) under the direction of Dr Paul Hooker. This appendix provides a brief summary of some of the more important findings.

A1.1 Scanning electron microscopy (SEM)

Forty one clay samples were prepared for the SEM study, including four Boom Clay samples that had been previously squeezed for pore-water extraction. Surfaces were chosen to be either parallel or perpendicular to the bedding. Samples were either air-dried or freeze-dried. Stub-mounts were prepared by breaking off small (c. 1 cm) fragments of material using a hammer or scalpel. These were mounted on aluminium pin-type stubs using conducting carbon cement and then coated with carbon using an Edwards High Vacuum 306A evaporation coater. A nominal 25 nm thickness of carbon was coated onto the specimen.

The samples were observed using a Cambridge Instruments Stereoscan S250 scanning electron microscope, fitted with a K. E. Developments four-element solid-state (diode) back scattered electron detector and Link Systems energy dispersive X-ray micro analysis (EDXA) 860A attachment. A beam voltage of 20 kV was maintained during analysis. Images were observed on a TV monitor and photographed and recorded using a Polaroid camera.

A1.2 Environmental scanning electron microscopy (ESEM)

Three more samples of undisturbed material were examined using an Electro Scan Corporation Environmental SEM at Manchester University. This required no drying or carbon coating preparation prior to analysis. Observations were made in a controlled atmosphere at pressures varying from 1 to 100 torr (133 to 13300 Pa). The ESEM is fitted with a secondary electron detector and a Link System X-ray detector. The gas used in the chamber was water vapour. Pressure and temperature could be controlled separately. A standard accelerating voltage of 20 kV was maintained during analysis.

For observation, the specimen was placed on a stub that fitted onto a cooling stage. The specimen chamber was closed and pumped down to 8 torr, while the electron gun was isolated from the specimen chamber and independently maintained at a high vacuum. While pumping, the specimen was cooled to the desired temperature so that the system was at equilibrium on the vapour/liquid curve.

Wetting-drying cycles were performed by increasing and decreasing the pressure. Images were photographed from the TV screen using a 35 mm camera.

A1.3 Comparison of SEM and ESEM

SEM and ESEM are operated under different vacuum conditions, thus different detectors must be used for imaging. One of the shortcomings with the ESEM is its limitation at low magnification. "Ripples" were observed on the image at high magnification, which is assumed to be caused by some form of electronic interference.

Parameters such as working distance and chamber pressure could be adjusted as required during ESEM observation but because of the complexity of the cooling stage, sample manoeuvrability is severely limited, compared to conventional SEM. Contrast and brightness are very sensitive on the ESEM, and variation in one parameter has a significant influence on the other.

The controls on the ESEM for the contrast and brightness are not precise because of their sensitivity. Photographs taken during wetting/drying cycles were often blurred because of the dynamic conditions in the chamber.

All the samples of Boom Clay examined appeared to be petrographically similar. This similarity suggests a degree of homogeneity, though sedimentology studies indicate the presence of interbedded clays and silts (Vanderberghe and van Echelpoel, 1987). The matrix of the Boom Clay comprises an assemblage of smectite, illite and kaolinite in which smectite appears to be dominant. Within the clay matrix there is clastic material, mainly quartz, mica and feldspar. Iron oxides are also present, as well as very rare calcite particles (fossil debris). Compaction of the sediment has caused distortion and draping of clay around larger more competent particles (Plate 1).

In undisturbed Boom Clay, the clay particles show a strong planar fabric developed parallel to bedding. However, in material which had been squeezed as well as material from off-cuts, disturbance of this fabric was apparent with clay particles being orientated parallel to the plane of shear deformation.

A1.4 Detrital mineralogy

Clays are the most common minerals and occur as packed flakes which form continuous horizontal layers. As a result of compaction, all other minerals are surrounded and wrapped in clay particles. This preferred orientation is responsible for the differences in appearance when viewed in the two directions as shown in Plates 2 and 3. Surfaces cut parallel to the bedding are very flat, controlled by the orientation of the basal faces of clay particles. Surfaces cut perpendicular to the bedding show a compact "deck of cards" texture.

The packing of clay minerals exhibits a high degree of orientation. The clay particles are generally ragged flakes about 2 μm or less in size. Micaceous particles are usually present as larger 20 - 100 μm flat plates with rough edges and are generally less than 10 μm thick.

Detrital quartz is the most common clastic component. The quartz content of the Boom Clay varies between 20 - 25 % (Ouvry, 1986). It occurs as sub-angular fine sand to silt grains typically of the order of 50 μm size, though grains can range from 20 to greater than 100 μm. Feldspar occurs as smaller 20 - 40 μm size angular grains.

Calcite represents about 1% of the mineralogy of the samples. The few micro-fossils found were mainly benthonic foraminifera, proving the marine origin of the sediment.

A1.5 Authigenic material

The authigenic mineralogy is dominated by the growth of pyrite and siderite. Pyrite seems to be the third most abundant mineral (after clays and quartz). It is widespread in every sample, forming either single crystals or spherical aggregates called framboids. Crystals of varying dimensions can be found in the same area. Framboids vary in diameter from 10 up to 80 μm. Though single crystals are scattered in the samples, high concentrations of pyrite form seams or burrow fills. These structures indicate an anaerobic diagenesis process, where pyrite crystals developed in relation to bacterial breakdown of organic matter. Surfaces of most of the biggest microfissures are lined with pyrite. There is no evidence that these minerals were affected by the drying process. Siderite occurs less frequently than pyrite, forming crystals scattered in the matrix. Previous studies report the presence of glauconite as well as kyanite (Vanderberghe, 1975). The latter is usually found in metamorphic rocks, so is likely to be of detrital origin, as is the mineral glauconite.

A1.6 Intergranular porosity

Intergranular porosity dominates the pore space. It is controlled by the packing and orientation of the clay mineral flakes in the matrix. Stacked flakes parallel to bedding form a fabric which appears to have little vertically-connected porosity due to the overlapping of the stacked clay particles.

Parallel to the bedding, porosity is higher and the pores exhibit lamina shapes. The pore walls are the surfaces of original detrital components, principally illite-smectite and other clay particles. The interparticle distance between clay flakes is not much greater than 100 nm.

A1.7 Microfissuring

All of the fissures observed are on a microscopic scale, from a few microns to 50 μm aperture. Two kinds can be distinguished. Firstly, linear fissures whch are parallel to the bedding. The biggest of these are lined with authigenic pyrite and continue through the

The packing of clay minerals exhibits a high degree of orientation. The clay particles are generally ragged flakes about 2 μm or less in size. Micaceous particles are usually present as larger 20 - 100 μm flat plates with rough edges and are generally less than 10 μm thick.

Detrital quartz is the most common clastic component. The quartz content of the Boom Clay varies between 20 - 25 % (Ouvry, 1986). It occurs as sub-angular fine sand to silt grains typically of the order of 50 μm size, though grains can range from 20 to greater than 100 μm. Feldspar occurs as smaller 20 - 40 μm size angular grains.

Calcite represents about 1% of the mineralogy of the samples. The few micro-fossils found were mainly benthonic foraminifera, proving the marine origin of the sediment.

A1.5 Authigenic material

The authigenic mineralogy is dominated by the growth of pyrite and siderite. Pyrite seems to be the third most abundant mineral (after clays and quartz). It is widespread in every sample, forming either single crystals or spherical aggregates called framboids. Crystals of varying dimensions can be found in the same area. Framboids vary in diameter from 10 up to 80 μm. Though single crystals are scattered in the samples, high concentrations of pyrite form seams or burrow fills. These structures indicate an anaerobic diagenesis process, where pyrite crystals developed in relation to bacterial breakdown of organic matter. Surfaces of most of the biggest microfissures are lined with pyrite. There is no evidence that these minerals were affected by the drying process. Siderite occurs less frequently than pyrite, forming crystals scattered in the matrix. Previous studies report the presence of glauconite as well as kyanite (Vanderberghe, 1975). The latter is usually found in metamorphic rocks, so is likely to be of detrital origin, as is the mineral glauconite.

A1.6 Intergranular porosity

Intergranular porosity dominates the pore space. It is controlled by the packing and orientation of the clay mineral flakes in the matrix. Stacked flakes parallel to bedding form a fabric which appears to have little vertically-connected porosity due to the overlapping of the stacked clay particles.

Parallel to the bedding, porosity is higher and the pores exhibit lamina shapes. The pore walls are the surfaces of original detrital components, principally illite-smectite and other clay particles. The interparticle distance between clay flakes is not much greater than 100 nm.

A1.7 Microfissuring

All of the fissures observed are on a microscopic scale, from a few microns to 50 μm aperture. Two kinds can be distinguished. Firstly, linear fissures whch are parallel to the bedding. The biggest of these are lined with authigenic pyrite and continue through the

rock for several millimetres. The aperture can exceed 20 μm. Smaller aperture fissures occur more frequently and are lined with detrital clay components. A few irregular fissures disrupt the uniformity of the clayey plateaus. With a maximum 10 μm aperture, they are lined with bigger detrital components coated with clays, quartz, etc.

From the comparison of SEM and ESEM observations of surfaces parallel to the bedding wet specimens appear to have lower porosity and appear gelatinous. This suggests that the clays are in an expanded state due to hydration. Fracture density also seems to be lower in wet specimens, which tends to confirm that many fractures are actually drying artifacts.

Wetting-drying cycles with the ESEM reveal that the effect of loss/gain of water is locally enhanced in the fissures. Drying leads to widening of the biggest fissures, as shown in Plates 4, 5 and 6. No other effects could be detected in the range of pressure 1 – 100 torr. On the screen, the image became blurred while wetting and the elements of the image moved. A higher resolution would have been useful to study the modifications at the scale of the clay particles.

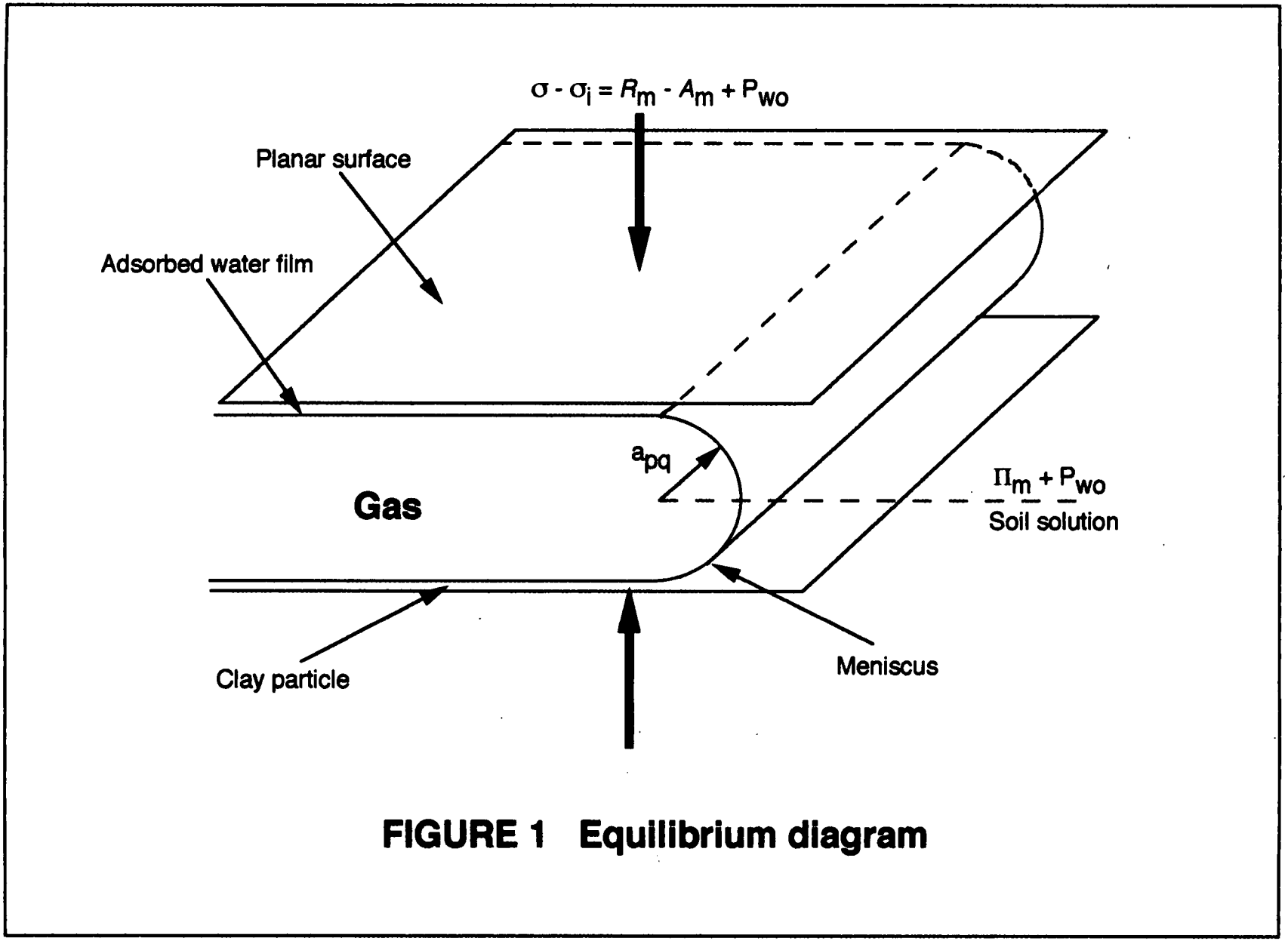

FIGURE 1 Equilibrium diagram

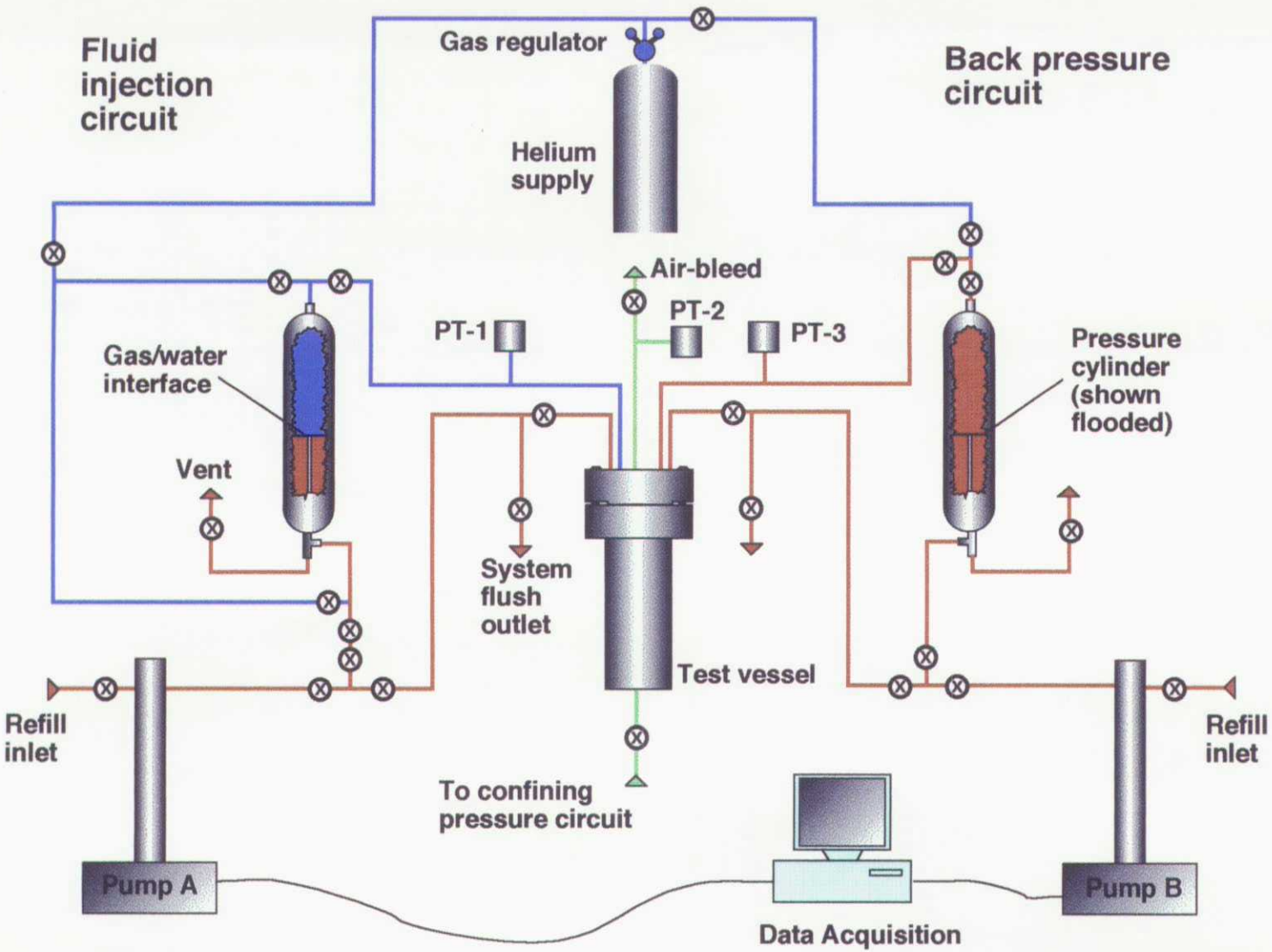

FIGURE 2 Schematic of the testing system

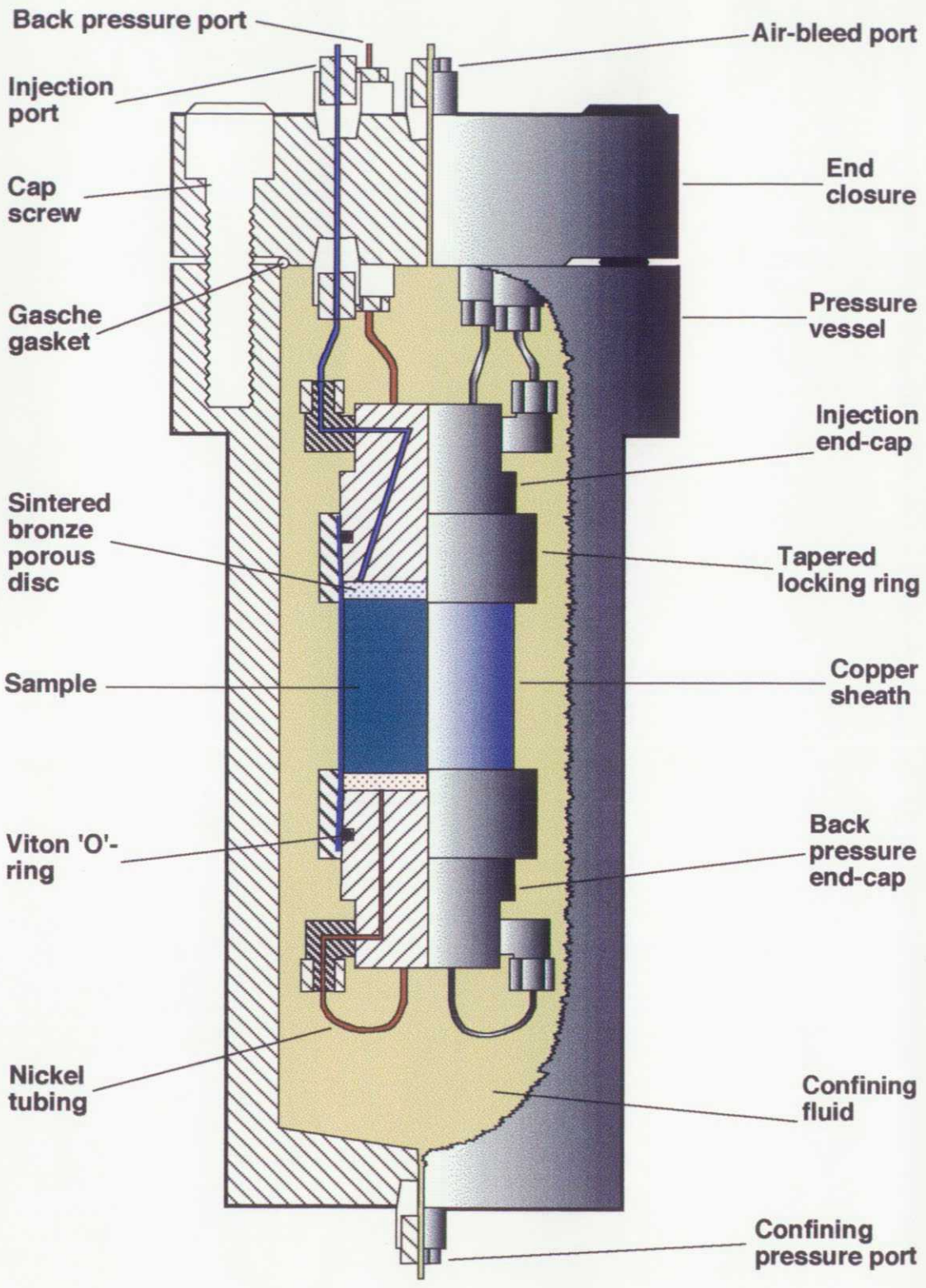

FIGURE 3 Schematic of pressure vessel and sample assembly

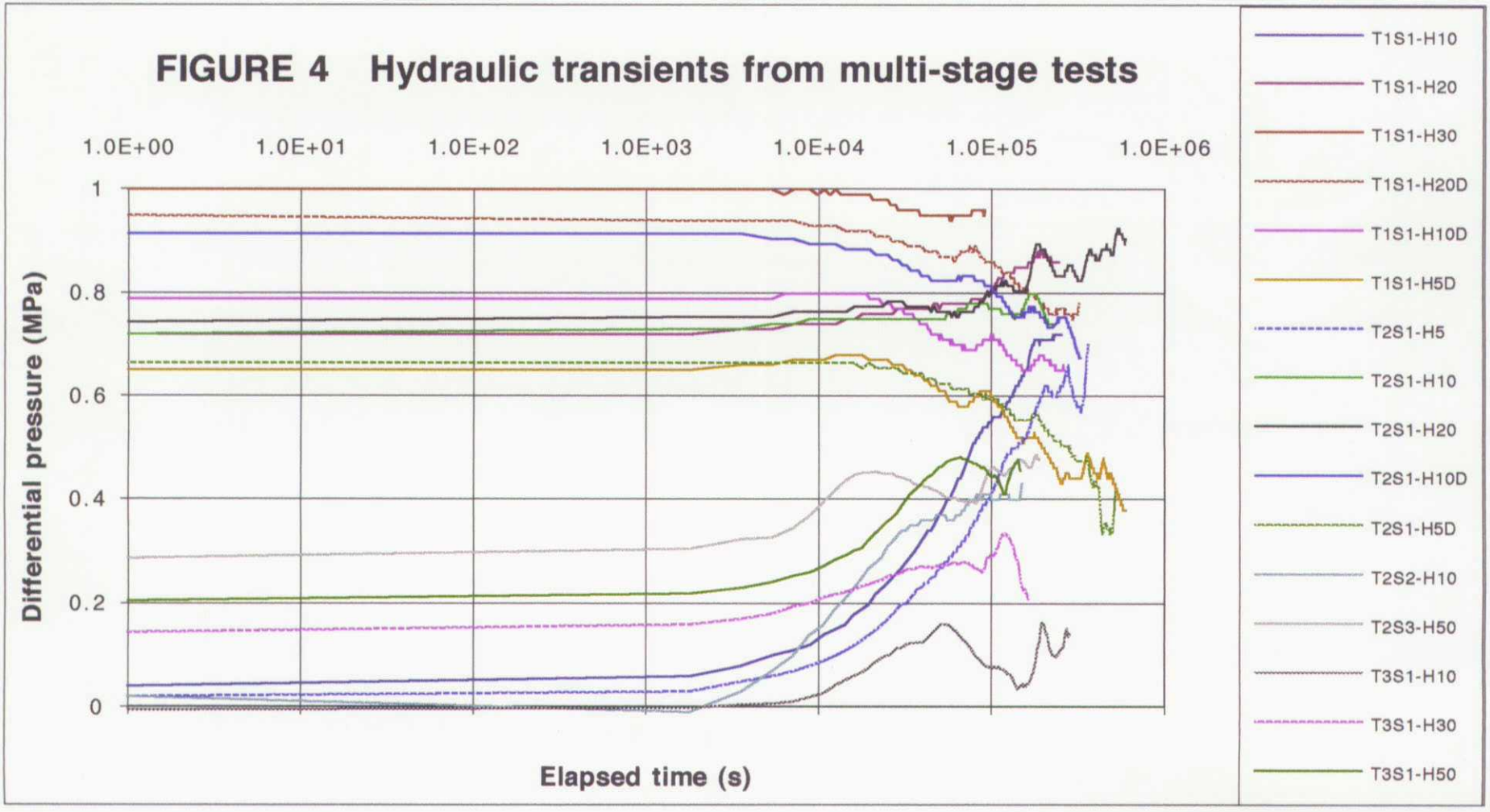
FIGURE 4 Hydraulic transients from multi-stage tests
1.0E+00
1.0E+01
1.0E+02
1.0E+03
1.0E+04
1.0E+05
1.0E+06
1
0.8
0.6
0.4
0.2
0
Differential pressure (MPa)
Elapsed time (s)
T1S1-H10
T1S1-H20
T1S1-H30
T1S1-H20D
T1S1-H10D
T1S1-H5D
T2S1-H5
T2S1-H10
T2S1-H20
T2S1-H10D
T2S1-H5D
T2S2-H10
T2S3-H50
T3S1-H10
T3S1-H30
T3S1-H50

FIGURE 5 Relationship between hydraulic conductivity and effective stress showing individual regression lines for all the data

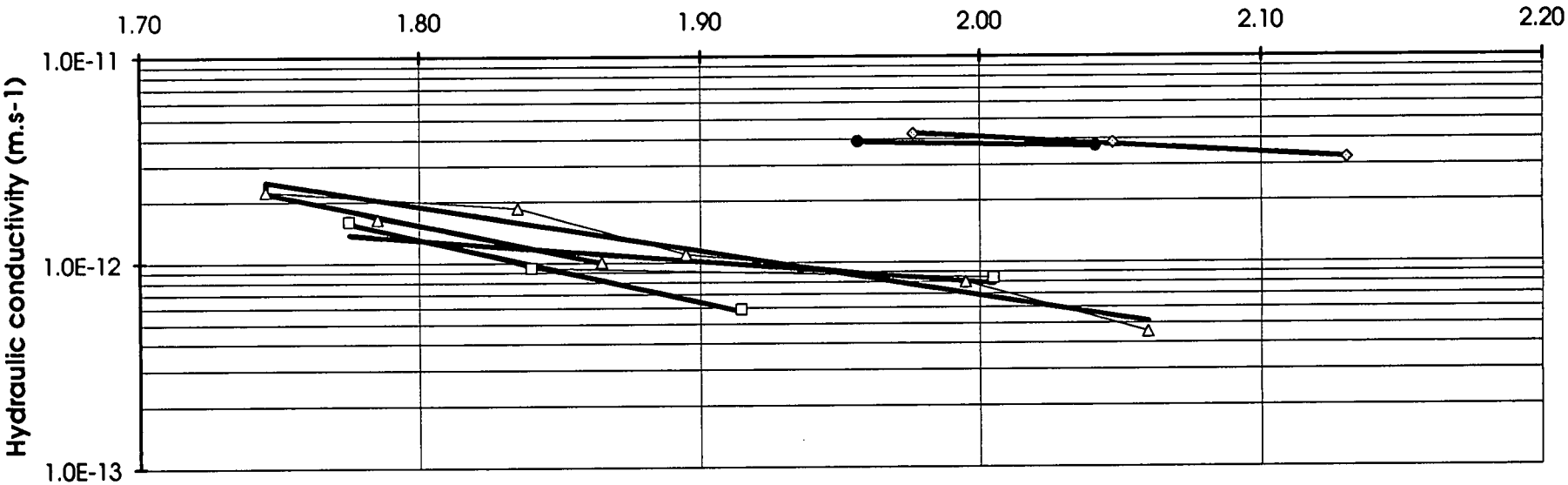

FIGURE 6 Relationship between hydraulic conductivity and effective stress showing regression lines for the two data sets

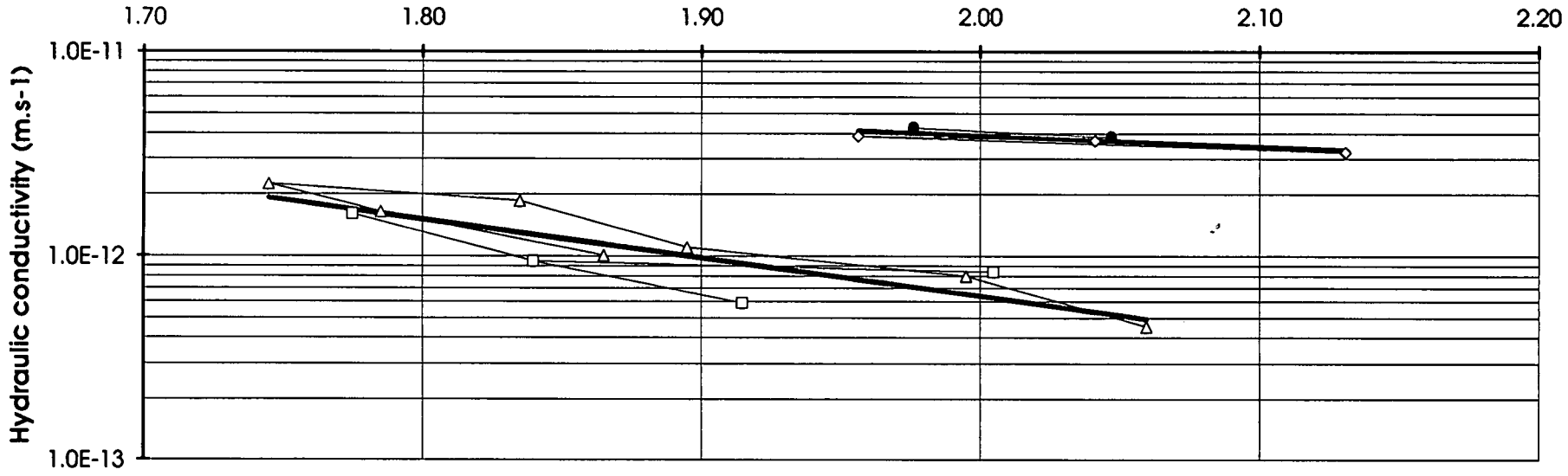

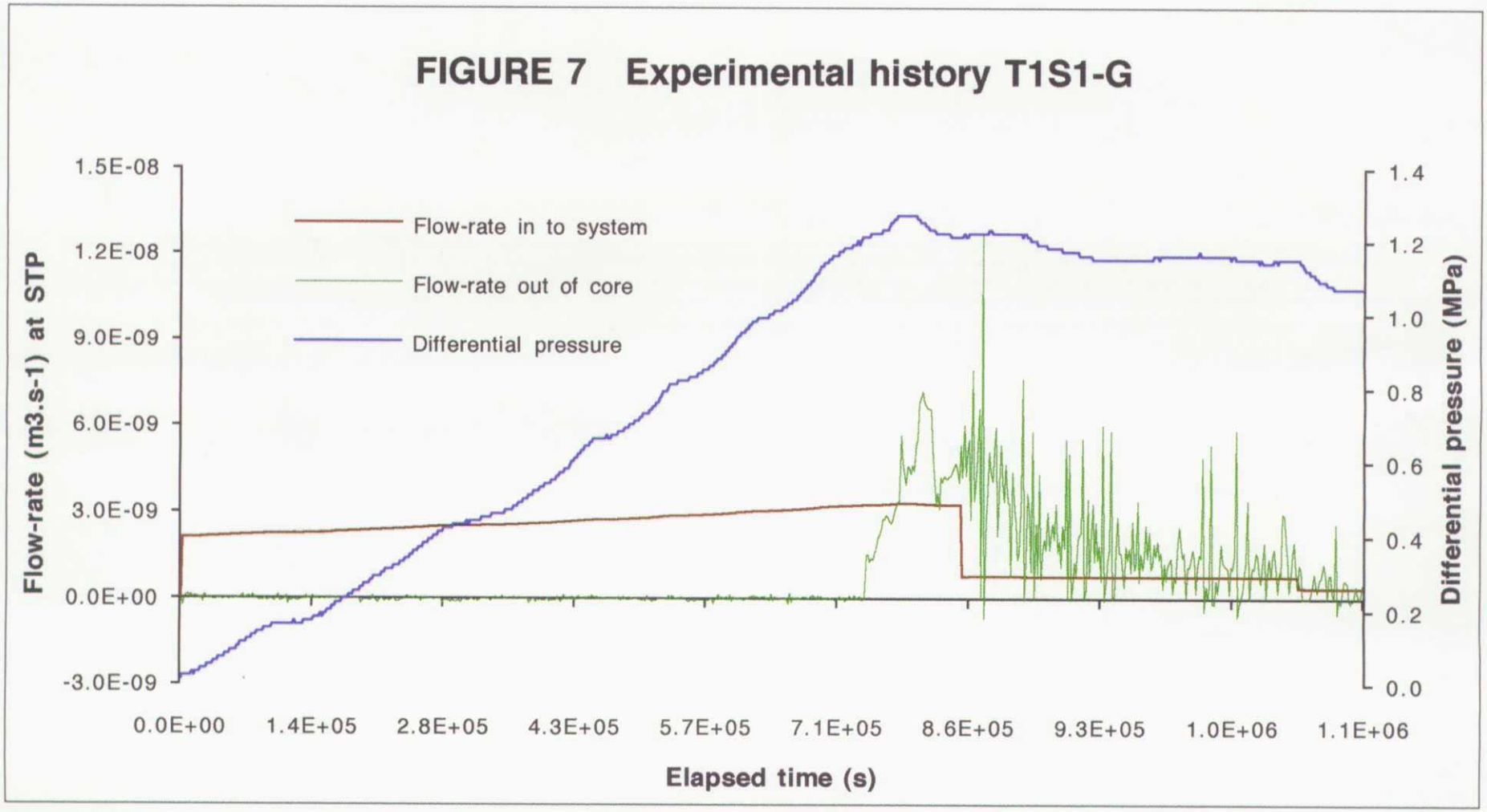
FIGURE 7 Experimental history T1S1-G
Flow-rate in to system
Flow-rate out of core
Differential pressure
Flow-rate (m3.s-1) at STP
Differential pressure (MPa)
Elapsed time (s)
1.5E-08
1.2E-08
9.0E-09
6.0E-09
3.0E-09
0.0E+00
-3.0E-09
1.4
1.2
1.0
0.8
0.6
0.4
0.2
0.0
0.0E+00
1.4E+05
2.8E+05
4.3E+05
5.7E+05
7.1E+05
8.6E+05
9.3E+05
1.0E+06
1.1E+06

FIGURE 8 Experimental history T2S1-G (part 1)

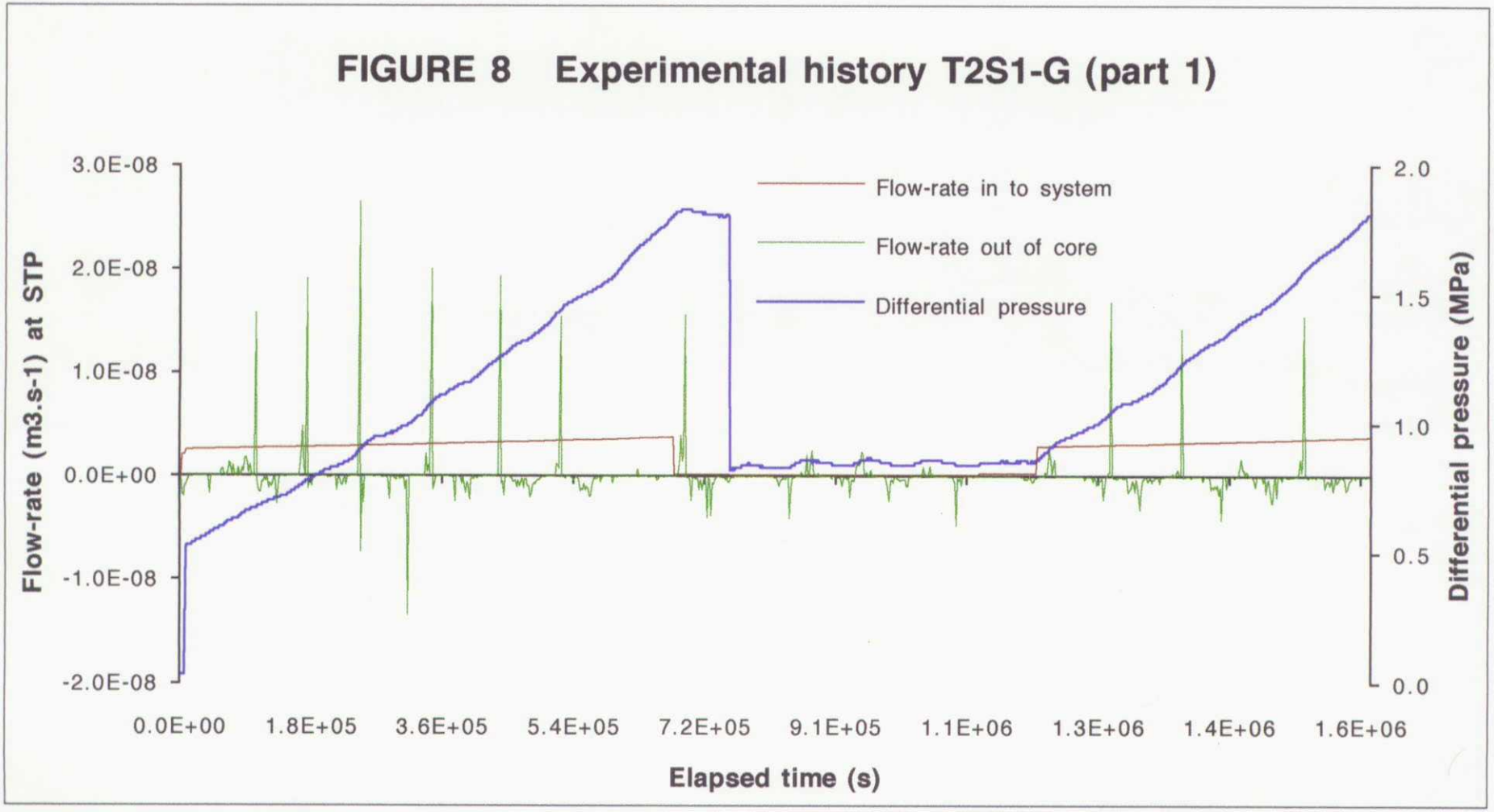

FIGURE 9 Experimental history T2S1-G (part 2)

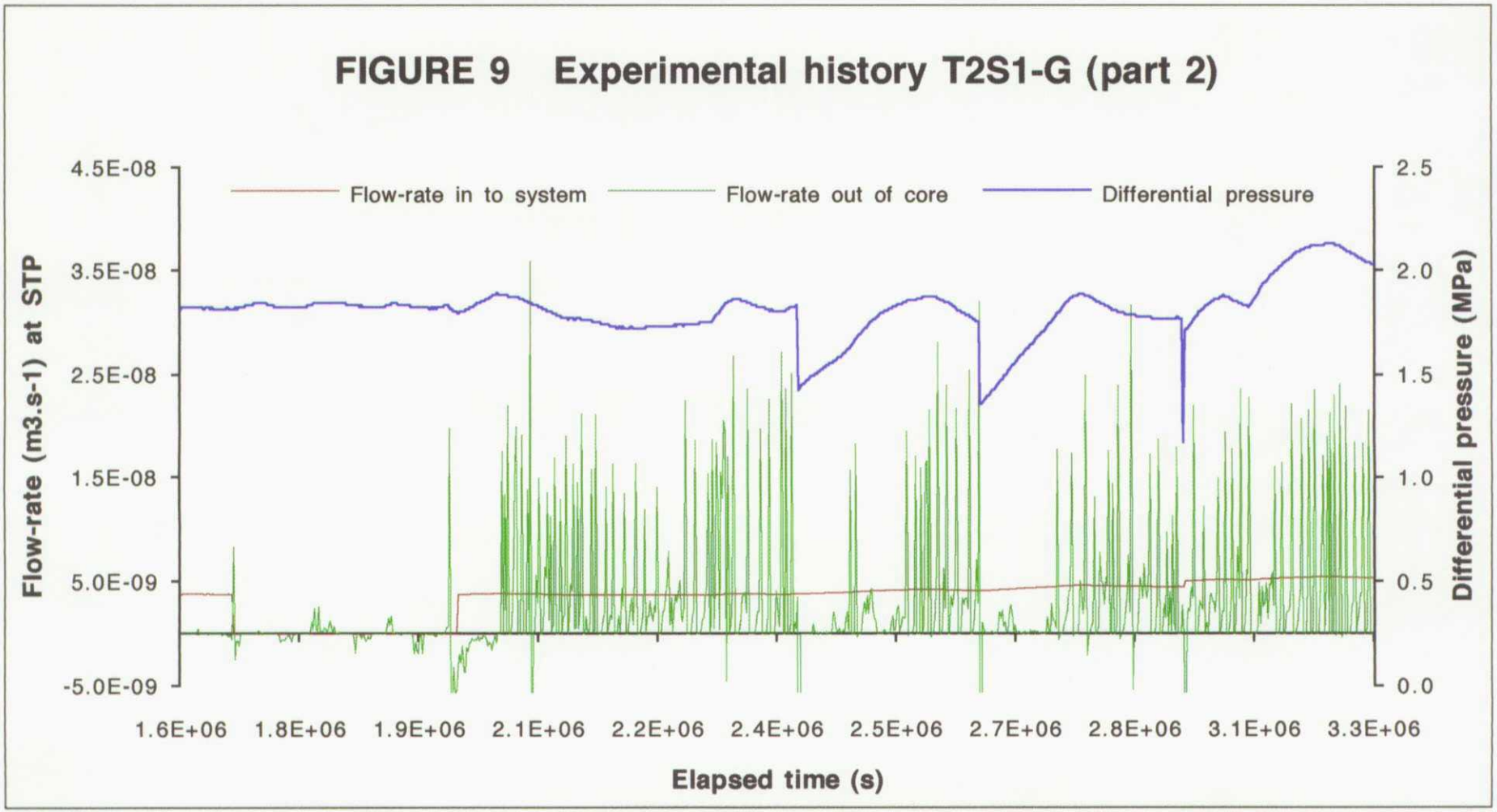

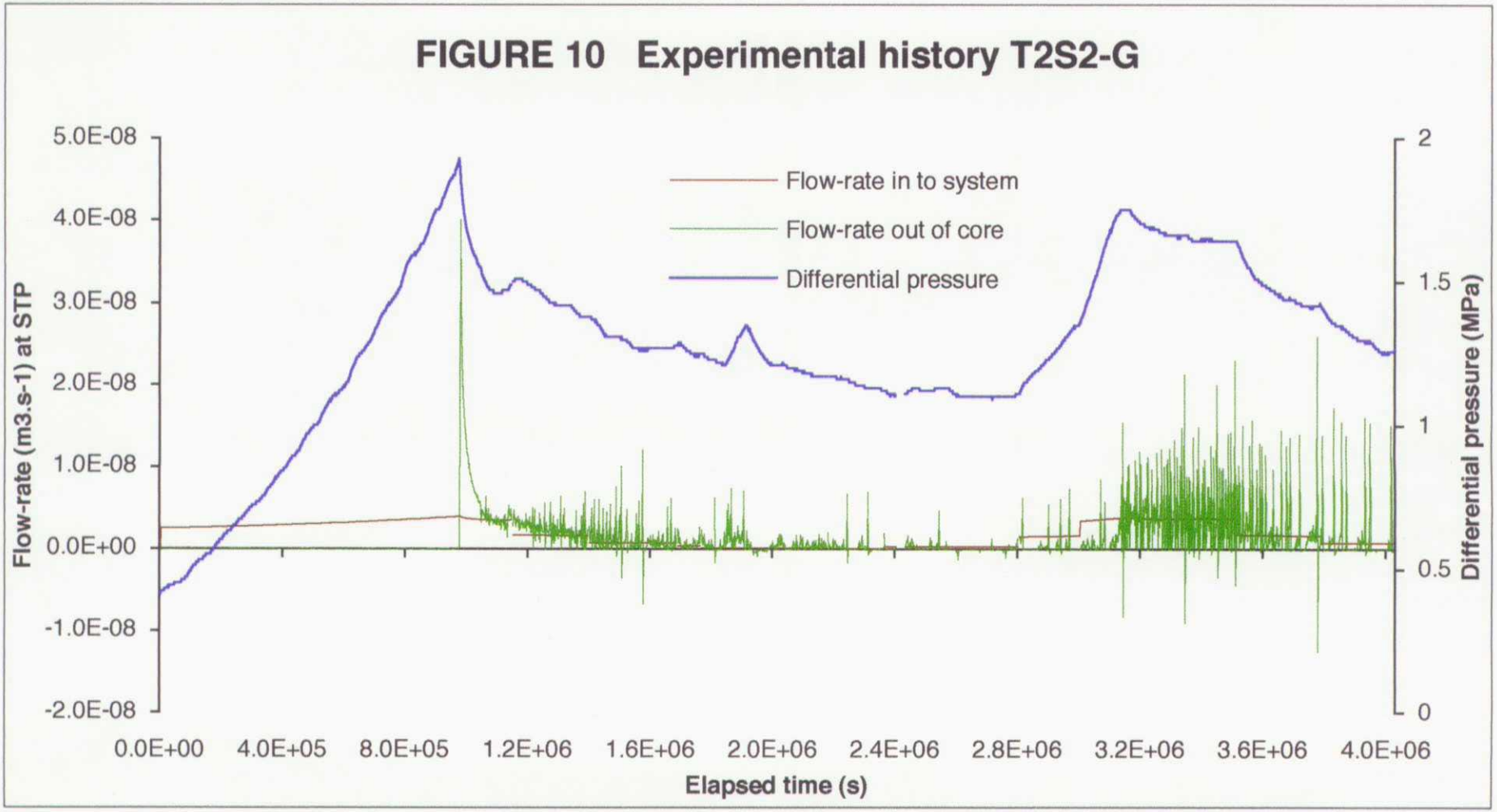
FIGURE 10 Experimental history T2S2-G
Flow-rate in to system
Flow-rate out of core
Differential pressure
Flow-rate (m3.s-1) at STP
Differential pressure (MPa)
Elapsed time (s)
5.0E-08
4.0E-08
3.0E-08
2.0E-08
1.0E-08
0.0E+00
-1.0E-08
-2.0E-08
2
1.5
1
0.5
0
0.0E+00
4.0E+05
8.0E+05
1.2E+06
1.6E+06
2.0E+06
2.4E+06
2.8E+06
3.2E+06
3.6E+06
4.0E+06

FIGURE 11 Experimental history T2S3-G

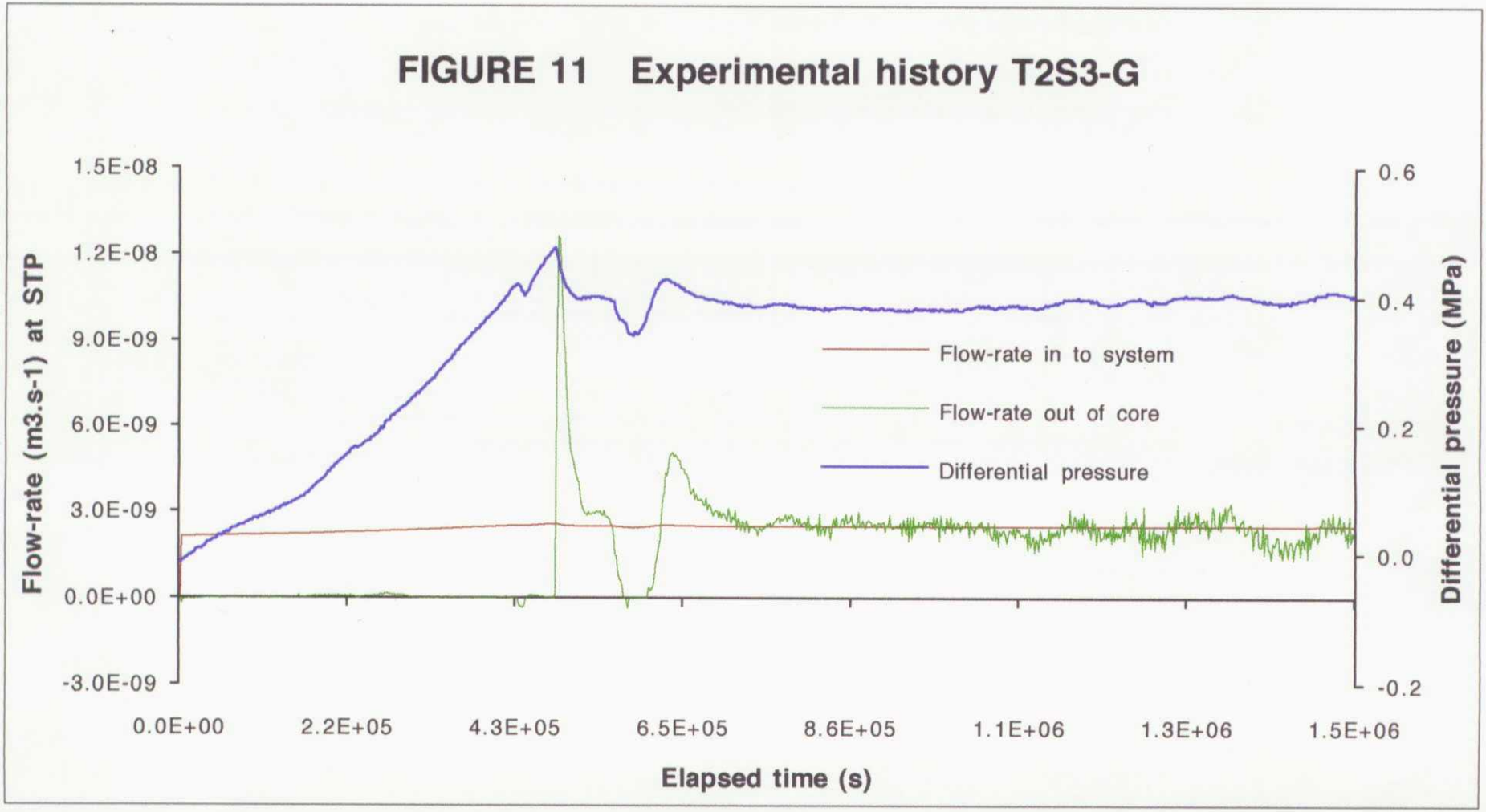

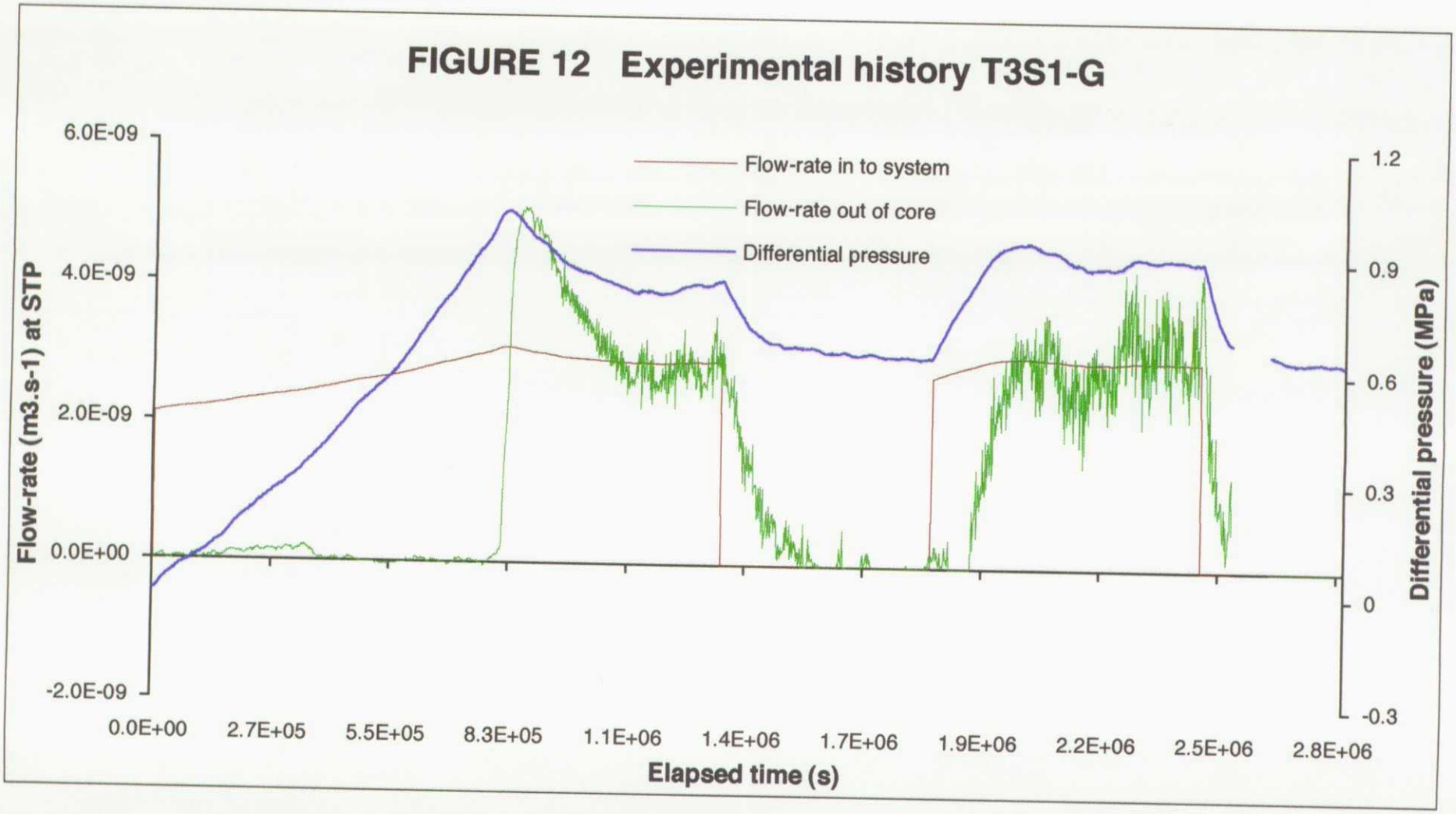
FIGURE 12 Experimental history T3S1-G
6.0E-09
4.0E-09
2.0E-09
0.0E+00
-2.0E-09
Flow-rate (m3.s-1) at STP
Flow-rate in to system
Flow-rate out of core
Differential pressure
1.2
0.9
0.6
0.3
0
-0.3
Differential pressure (MPa)
0.0E+00
2.7E+05
5.5E+05
8.3E+05
1.1E+06
1.4E+06
1.7E+06
1.9E+06
2.2E+06
2.5E+06
2.8E+06
Elapsed time (s)

FIGURE 13 Steady-state picks using time-averaging (T2S2-G)

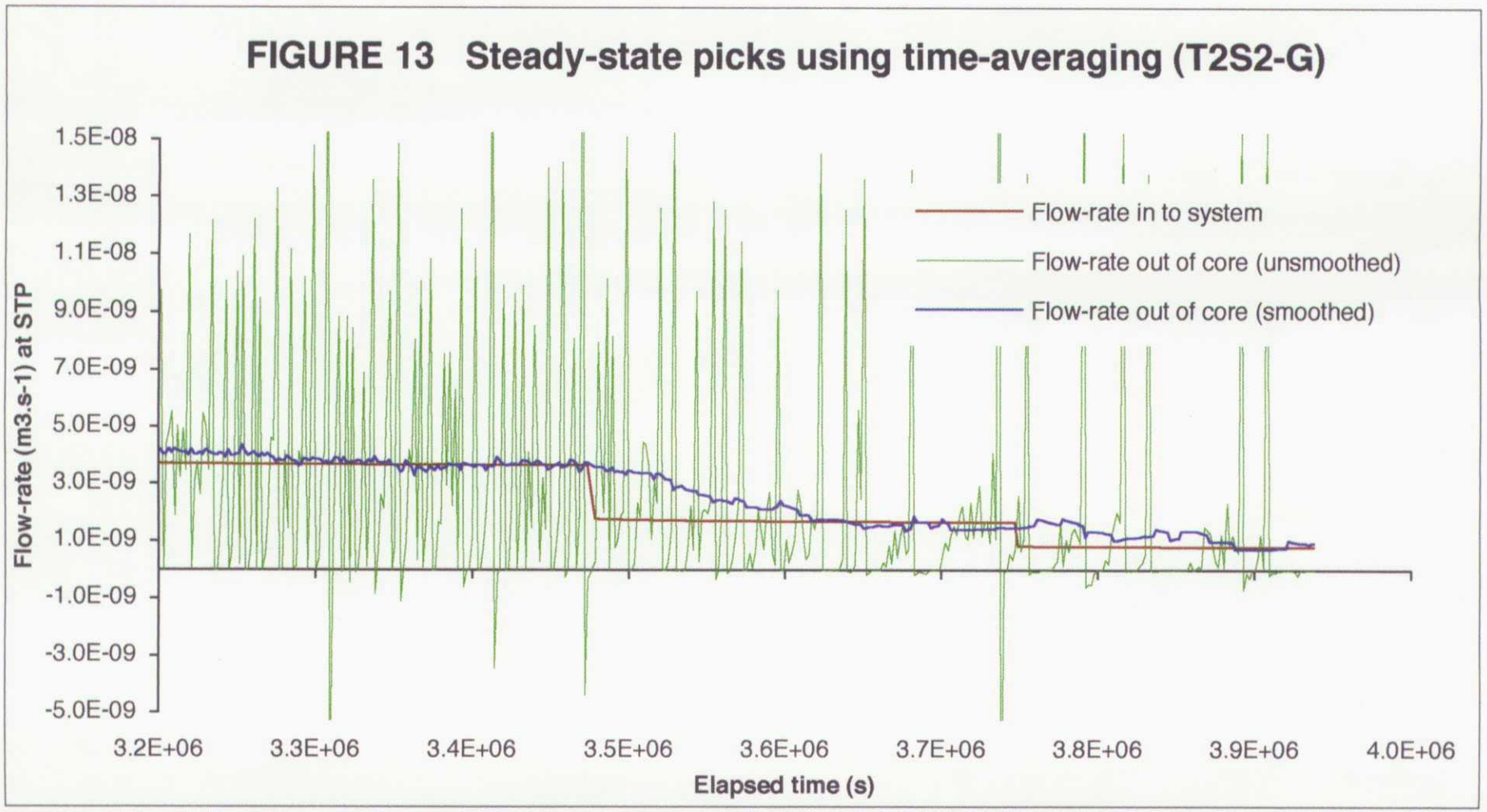

FIGURE 14 Volumetric flow-rate (STP) into and out of specimen (T3S1-G)

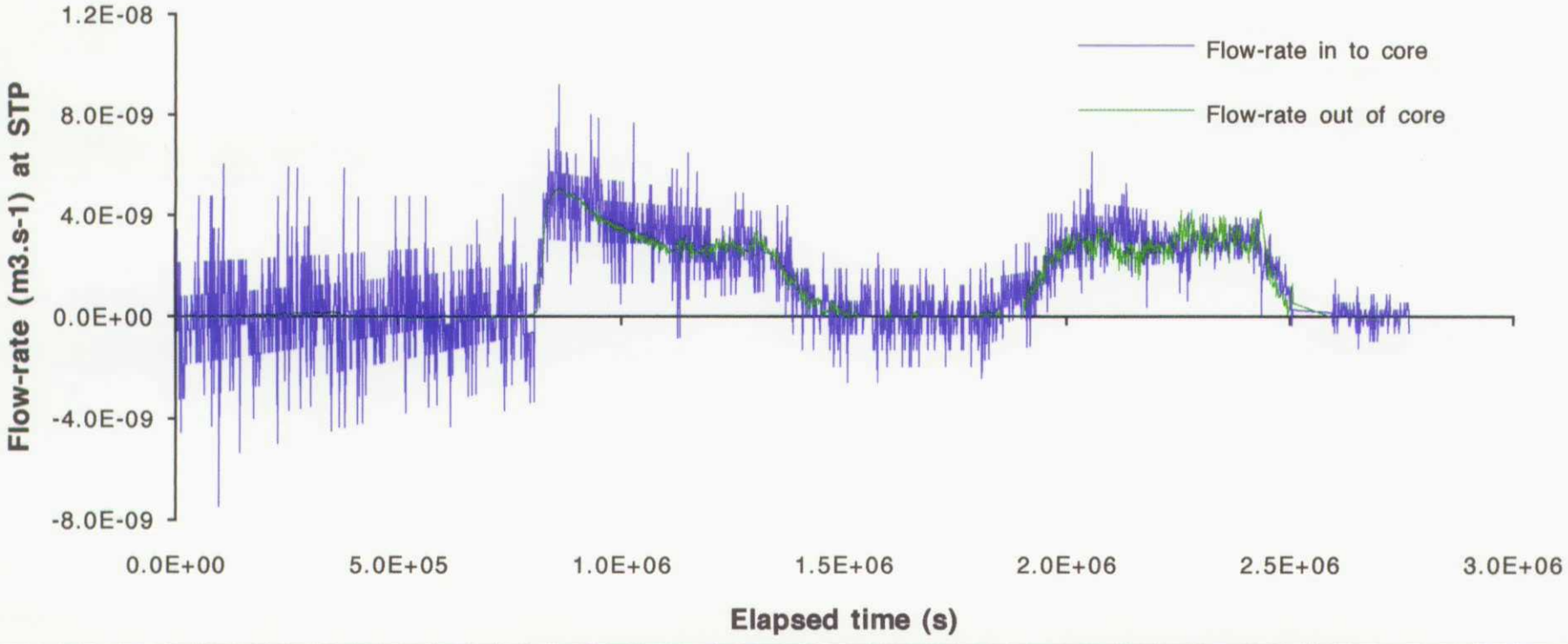

FIGURE 15 The relationship between excess gas pressure at breakthrough and intrinsic permeability

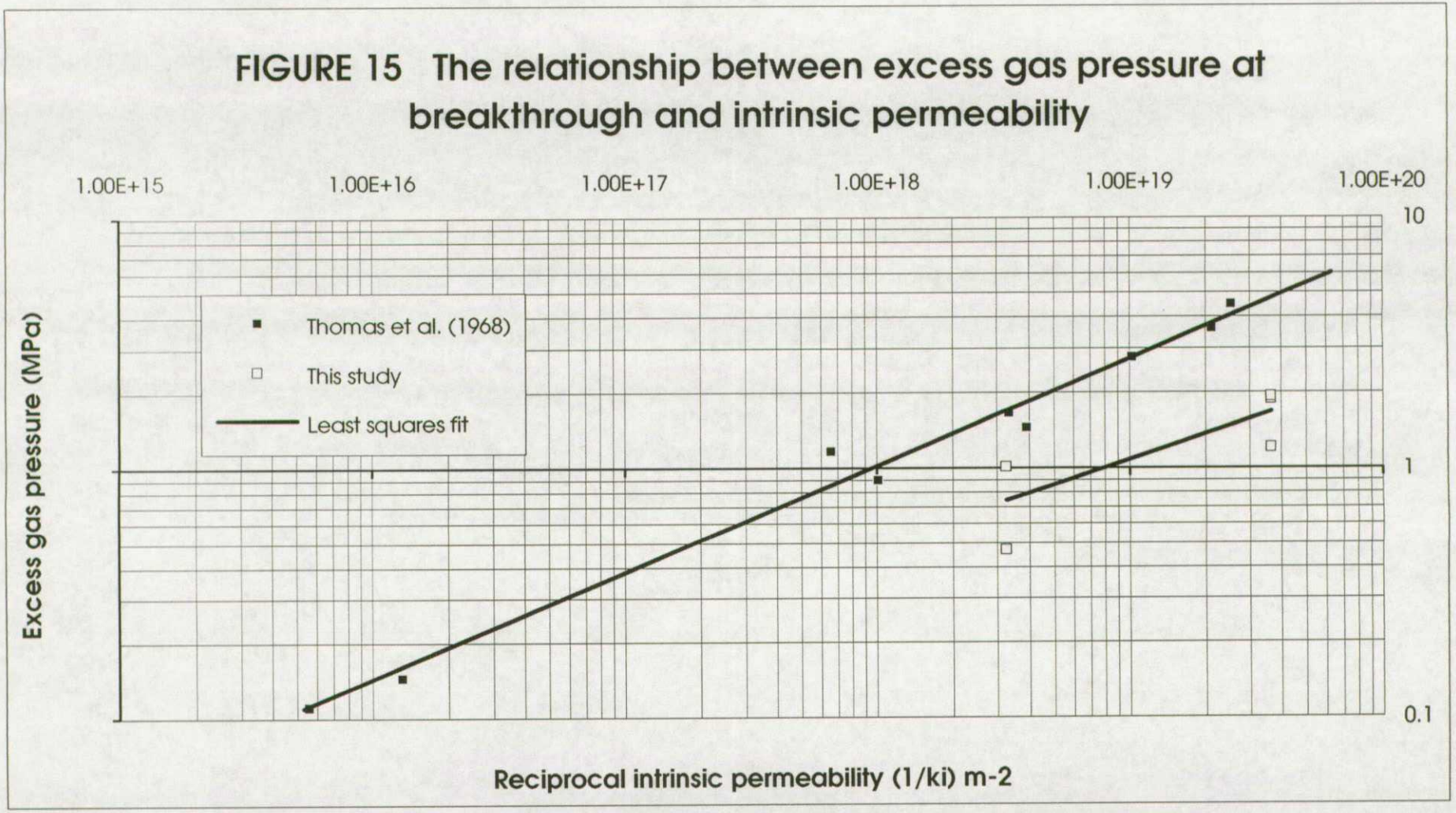

FIGURE 16 Gas flow-rate (STP) against differential pressure for history T2S2-G

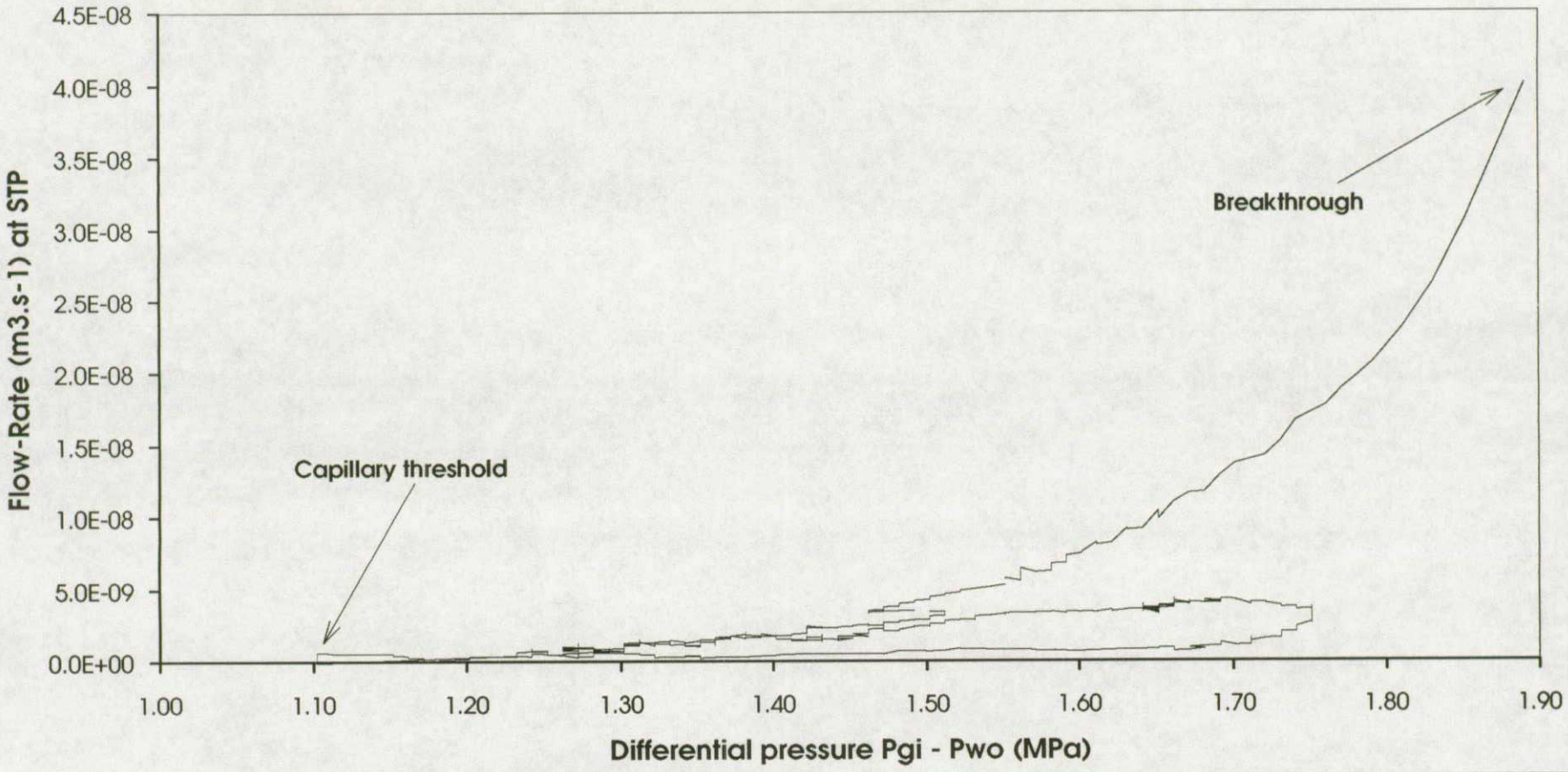

FIGURE 17 Gas flow-rate (STP) against differential pressure for history T3S1-G

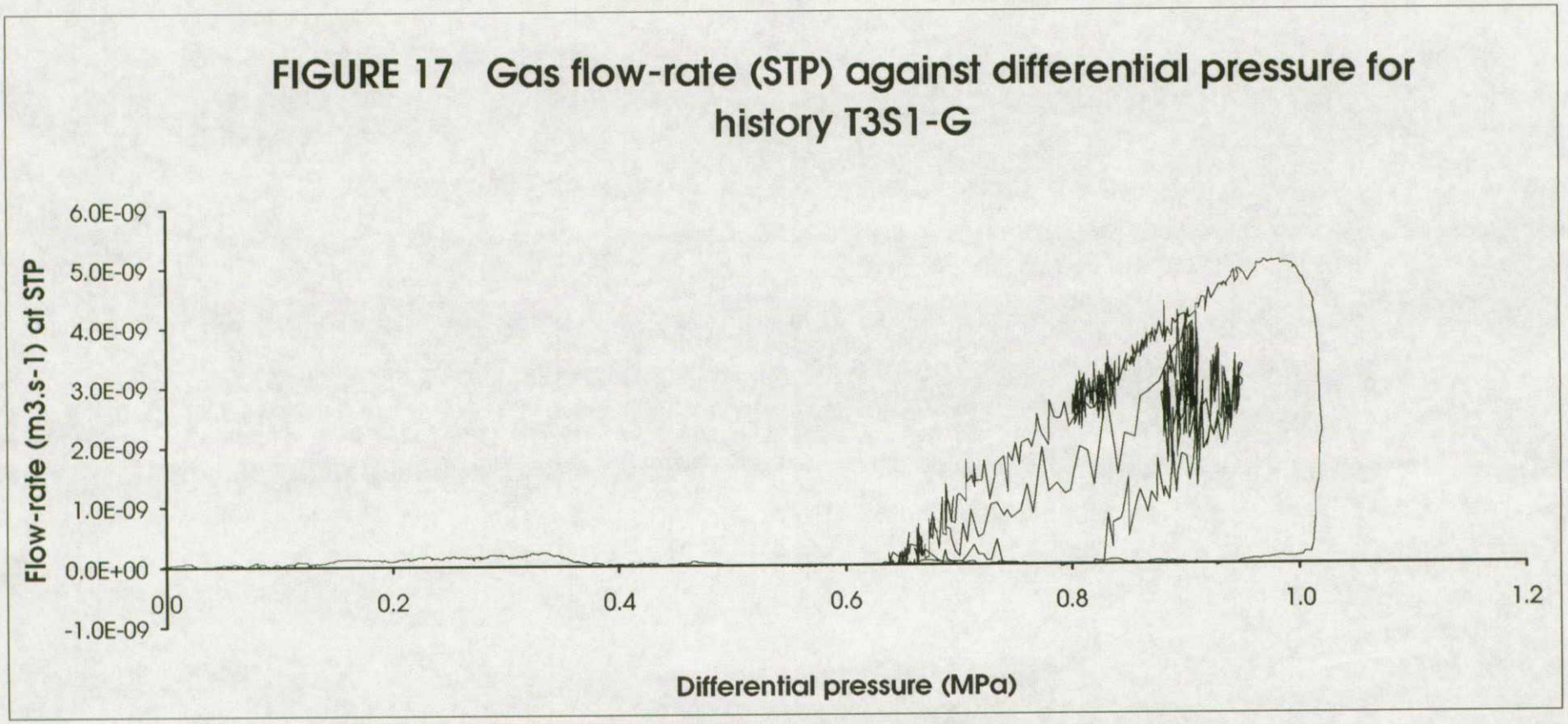

FIGURE 18 Gas permeability against net mean effective stress for history T2S2-G

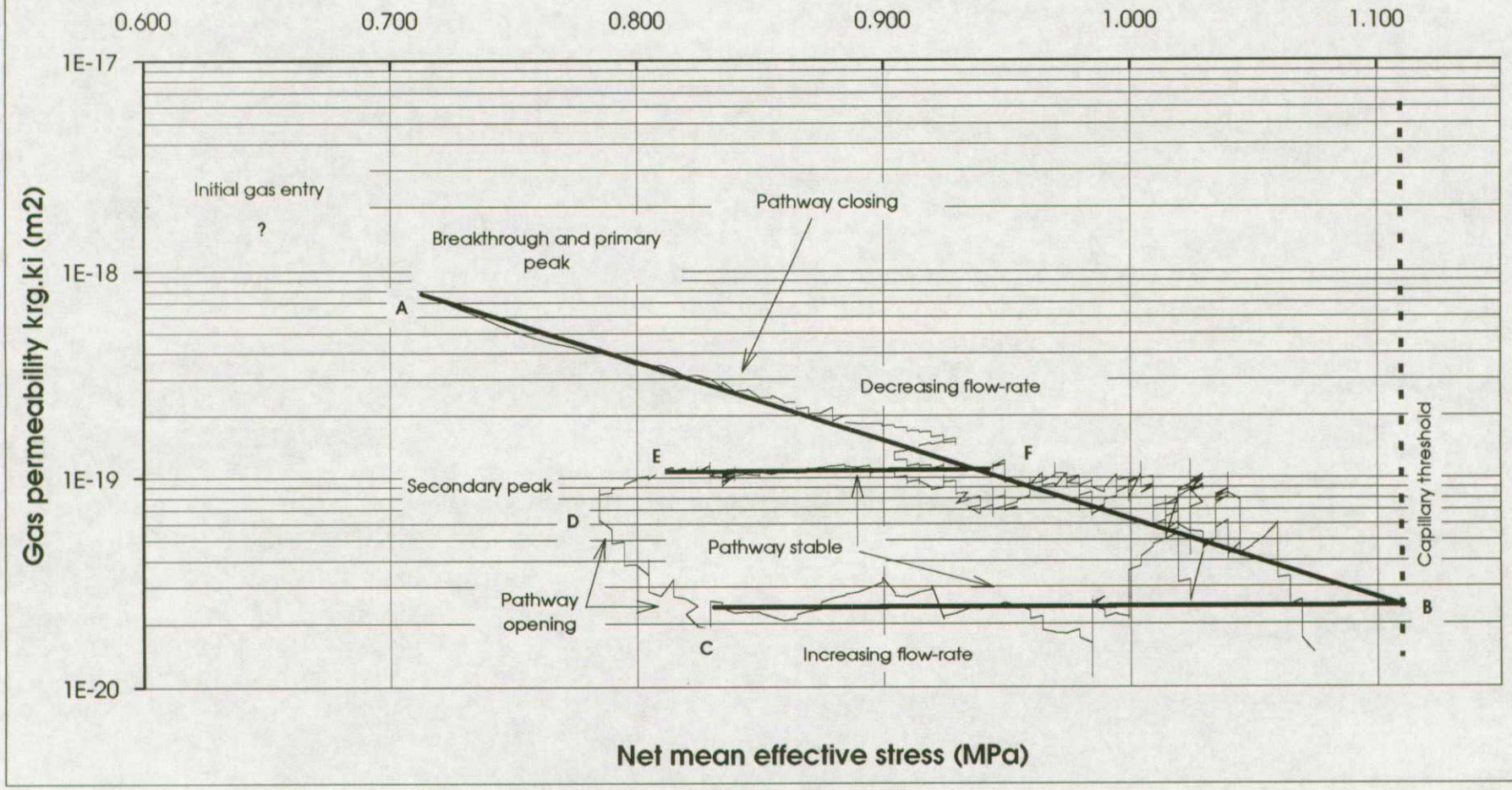

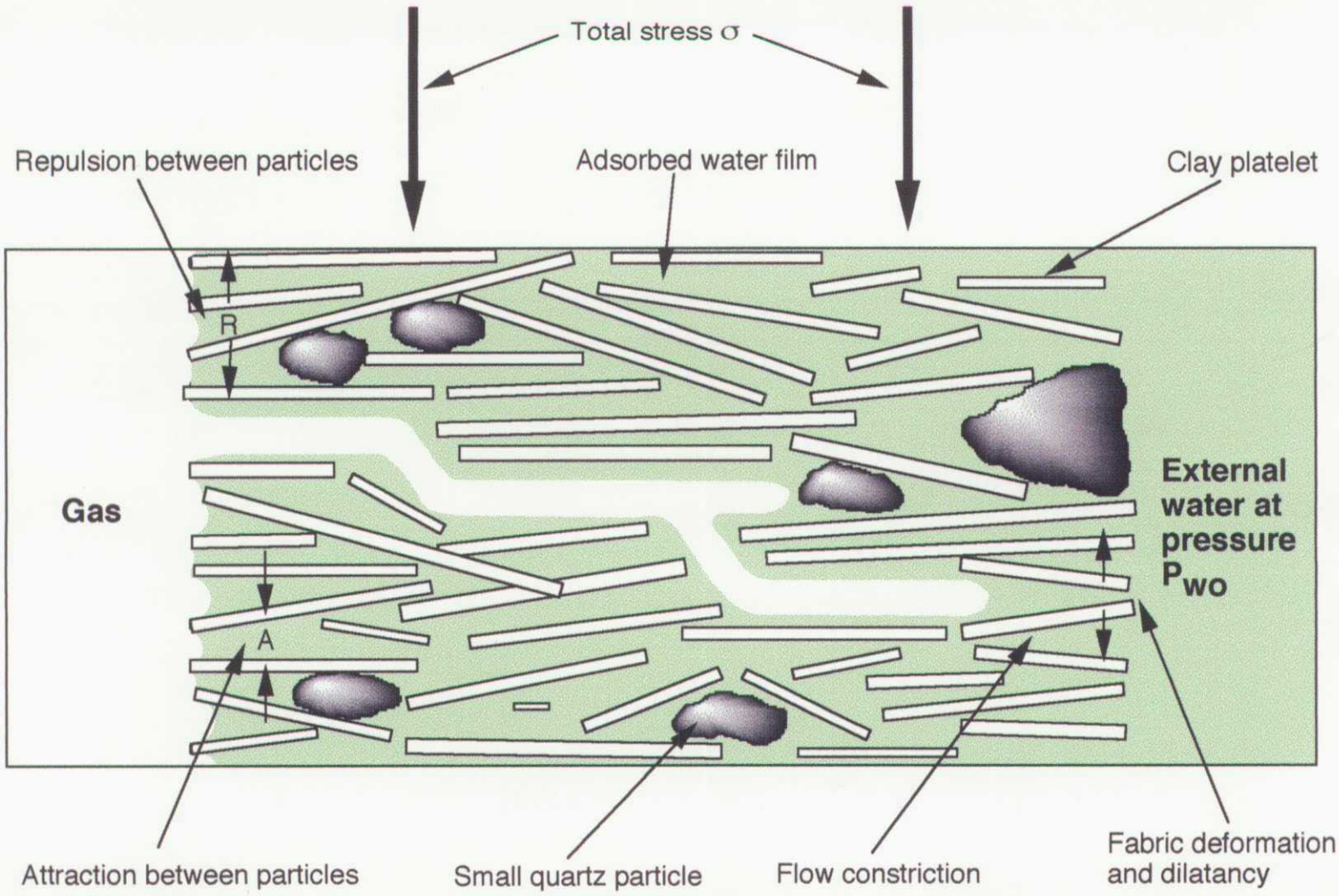

FIGURE 19 Gas migration pathway in clay

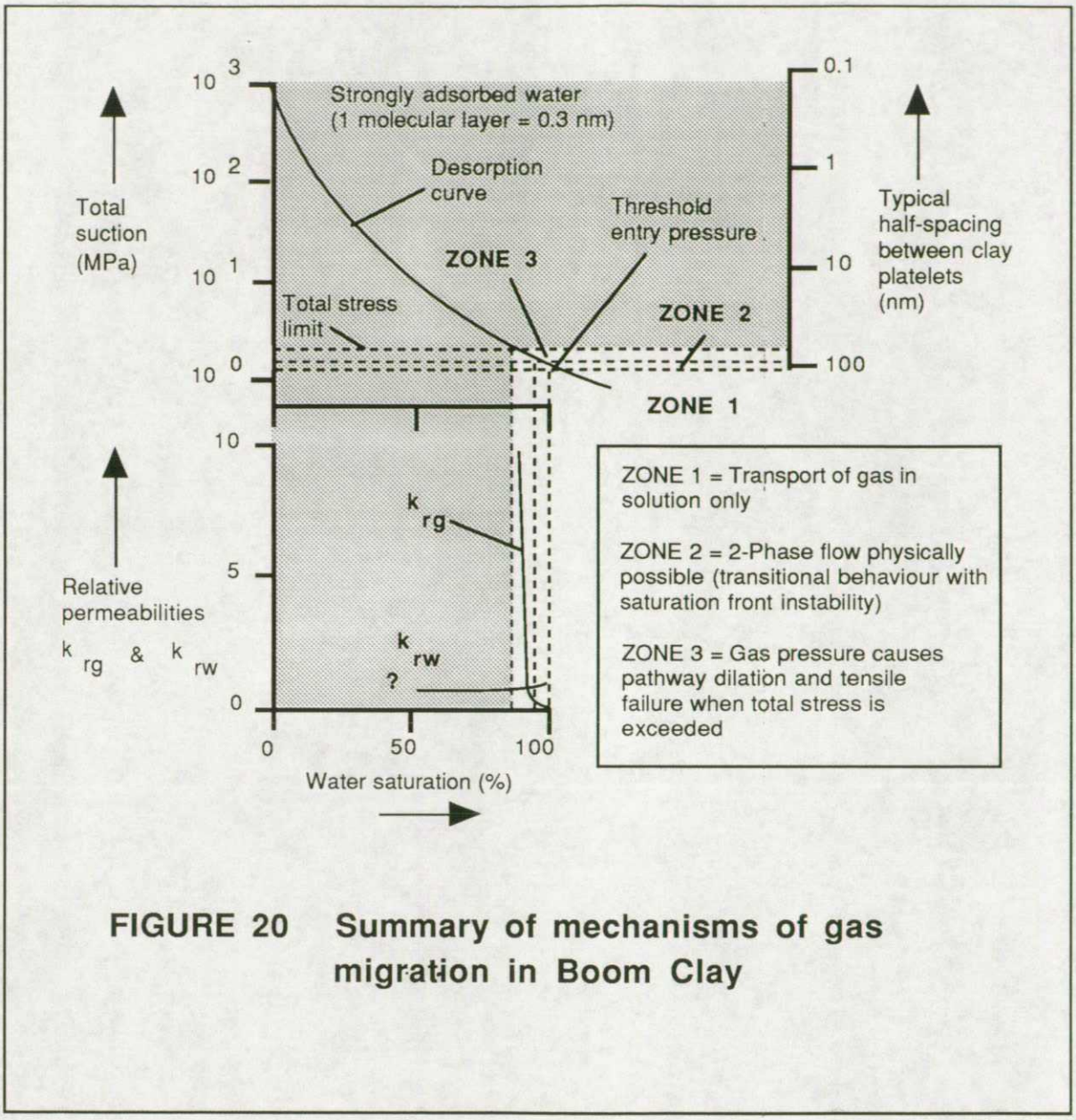

FIGURE 20 Summary of mechanisms of gas migration in Boom Clay